ISTANBUL TECHNICAL UNIVERSITY ★ GRADUATE SCHOOL OF SCIENCE ENGINEERING AND TECHNOLOGY

NUMERICAL AND EXPERIMENTAL INVESTIGATION OF CRASHING AND CRUSHING BEHAVIOUR OF AXIALLY IMPACTED NESTED TUBES

M.Sc. THESIS

Zana EREN

Department of Aeronautical and Astronautical Engineering

Aeronautical and Astronautical Engineering Programme

DECEMBER 2015

ISTANBUL TECHNICAL UNIVERSITY ★ GRADUATE SCHOOL OF SCIENCE ENGINEERING AND TECHNOLOGY

NUMERICAL AND EXPERIMENTAL INVESTIGATION OF CRASHING AND CRUSHING BEHAVIOUR OF AXIALLY IMPACTED NESTED TUBES

M.Sc. THESIS

Zana EREN
(511131171)

Department of Aeronautical and Astronautical Engineering

Aeronautical and Astronautical Engineering Programme

Thesis Advisor: Prof. Dr. Halit S. TÜRKMEN
Assoc. Prof. Dr. Zafer KAZANCI

DECEMBER 2015

İSTANBUL TEKNİK ÜNİVERSİTESİ ★ FEN BİLİMLERİ ENSTİTÜSÜ

EKSENEL DARBE YÜKÜ UYGULANAN İÇİÇE TÜPLERİN ÇARPIŞMA VE EZİLME DAVRANIŞININ SAYISAL VE DENEYSEL OLARAK İNCELENMESİ

YÜKSEK LİSANS TEZİ

Zana EREN
(511131171)

Uçak ve Uzay Mühendisliği Anabilim Dalı

Uçak ve Uzay Mühendisliği Programı

Tez Danışmanı: Prof. Dr. Halit S. TÜRKMEN
Doç. Dr. Zafer KAZANCI

ARALIK 2015

Zana EREN, a **M.Sc.** student of ITU **Graduate School of Science Engineering and Technology** student ID 511131171, successfully defended the **thesis/dissertation** entitled “**NUMERICAL AND EXPERIMENTAL INVESTIGATION OF CRASHING AND CRUSHING BEHAVIOUR OF AXIALLY IMPACTED NESTED TUBES**”, which he prepared after fulfilling the requirements specified in the associated legislations, before the jury whose signatures are below.

Thesis Advisor :	**Prof. Dr. Halit S. TÜRKMEN** İstanbul Technical University	....
Co-advisor :	**Assoc. Prof.Dr. Zafer KAZANCI** Turkish Air Force Academy	....
Jury Members :	**Prof. Dr. Zahit MECİTOĞLU** Istanbul Technical University	
	Prof. Dr. Vedat Z. DOĞAN Istanbul Technical University	
	Assoc. Prof. Dr. Hasan KURTARAN Gebze Technical University	

Date of Submission : 27 November 2015
Date of Defense : 25 December 2015

To my family,

FOREWORD

I would like to express my appreciation to my advisors Assoc. Prof. Dr. Zafer Kazancı and Prof. Dr. Halit S. Türkmen. Their valuable feedback, comments and suggestions contributed a lot to the present thesis study.

I would also like to thank my colleague Fatih Usta for his close collaboration and Prof. Dr. Zahit Mecitoğlu for his valuable advices.

I must express my very profound gratitude to my mother and father for providing me with unfailing support and continuous encouragement throughout my years of study. This accomplishment would not have been possible without them.

Finally, I would like to thank the TUBITAK that supported the thesis as a part of ARDEB 1001 Research Projects Programme (project code: 113M395).

December 2015 Zana EREN
(Engineer)

TABLE OF CONTENTS

Page

ABBREVIATIONS

ADINA	: Automatic Dynamic Incremental Nonlinear Analysis
AL	: Aluminium
CFE	: Crush Force Efficiency
DP	: Dual Phase
FEA	: Finite Element Analysis
kg	: Kilogram
LS-DYNA	: Livermore Software Dynamic
J	: Joule
m	: Meter
min	: Minute
N	: Newton
s	: Seconds
SEA	: Specific Energy Absorbation
St	: Steel

LIST OF TABLES

Page

LIST OF FIGURES

Page

NUMERICAL AND EXPERIMENTAL INVESTIGATION OF CRASHING AND CRUSHING BEHAVIOUR OF AXIALLY IMPACTED NESTED TUBES

SUMMARY

The crush and crashworthiness of a vehicle (airplane, automotive, ship, etc.) is today of great importance. Strict standards need to be adhered to in the industry, in particular to protect human life. In the aim for better performance, the design of vehicles has also evolved to improve protection capabilities. In order to decrease design times and ensure safe design standards regarding the crush and crashworthiness of vehicles, and their components, virtual tests are usually performed in numerical simulations. The virtual crush and crash test data are used throughout the entire development of a new design. These numerical simulations produce results without building a physical model, and can be performed relatively quickly and inexpensively. This permits optimization of the design before an actual prototype of the vehicle has to be built.

The most important phenomenon in a crush or crash situation is to absorb the kinetic energy. Crash tubes are designed for that purpose and are used in many practical situations. They have the ability to absorb and convert large amounts of kinetic energy into plastic strain energy under severe loading conditions. Therefore, there has been continued interest on the axial crushing and crashing behavior of tubes.

When a tube fails under progressive buckling, the initial peak force is much greater than the subsequent peak. In many instances, these tubes are used to absorb energy in cars and the high force peaks lead to high acceleration on the vehicle occupants during an accident/impact event. An ideal energy-absorbing device should therefore cause a uniform deceleration during the entire stroke. This ideal structure would absorb the shock first and then deform under progressive buckling to absorb the energy. Thus we considered a new geometric crash tube model which would be nested with different lengths. The longest tube would absorb the kinetic energy first, and they could act together with the other tube(s) after strong impact effect. This new tube would be lighter than bi tubular crash tubes and alignment of the tubes, geometric parameters would be important. Thus, we planned to investigate this event by experimentally and numerically, which was never investigated in te open literature before.

First of all, material tensile tests at elevated strain rates were carried out. For a constant thickness, different (cross-section, length, constant, etc.) specimens were produced. After producing specimens, some of them will be chosen for the experiment, and new specimens for experiments were produced. The tubes were be quasi-statically and dynamically crushed. The explicit non-linear finite element code (LS-DYNA, Abaqus were used to predict the response of the crash tubes subjected to axial crushing, and will be compared with experiments. The energy absorption capacity of a sheet metal structure depends on geometric and material parameters. Thus, it was investigated a different crash tube geometry which consist of nested tubes with different lengths. Important parameters such as arrangement, material, sheet thickness, flange width, spot-weld spacing and impact velocity will be optimized. There were no studies for

these kind of crash tubes in the literature. So, it would be interesting to observe final deformations and energy absorption characteristics of these kind of nested crash tubes. Optimum nested crash tubes were realized by numerical studies. These results were compared and validated by experiments.

EKSENEL DARBE YÜKÜ UYGULANAN İÇİÇE TÜPLERİN ÇARPIŞMA VE EZİLME DAVRANIŞININ SAYISAL VE DENEYSEL OLARAK İNCELENMESİ

ÖZET

Araçların (uçak, araba, raylı sistem araçları, gemi, vs.) darbelere dayanımı çok büyük önem teşkil etmektedir. Bu yüzden, insan hayatını korumak amacıyla bu konuda katı standartlar getirilmektedir. Daha iyi bir performans için, araçların yolcuları koruma kapasitelerini artırma yönündeki tasarımlar bir evrim geçirmektedir. Tasarım zamanını azaltmak, araçların ve bileşenlerinin çarpma ve ezilme tasarım standartlarını sağladığından emin olmak için çarpışma testleri genellikle sayısal olarak bilgisayarlarda yapılmaktadır. Elde edilen veriler yeni tasarımların geliştirilmesinde kullanılmaktadır. Sayısal simülasyonların bilgisayar ortamında yapılabilmesi her defasında fiziksel bir model üretme zorluğunu ortadan kaldırmakta, zaman ve maliyet açısından çok daha hızlı olmaktadır. Bu simülasyon süreci, gerçek bir araç prototipi üretilmeden önce en iyileştirmesinin yapılabilmesini sağlamaktadır. Ezilme veya çarpışma esnasında en önemli konu kinetik enerjinin nasıl emileceğidir. Bu amaçla tasarlanan ezilme kutuları birçok alanda kullanılmaktadır. Ezilme kutuları, araç çarpışmalarında ortaya çıkan büyük değerlerdeki kinetik enerjiyi plastik enerjiye dönüştürebilme kabiliyetlerine haizdir. Bu yüzden, ezilme kutularının çarpışma sonrası ezilme davranışları konusuna ilgi sürekli devam etmektedir.

Ezilen bir kutuda, ilk çarpmada meydana gelen pik kuvveti sonrakilerden çok daha fazladır. Çoğu zaman kaza esnasında, kutular araçlarda ve bileşenlerinde en fazla ivmelenmeye neden olan bu pik kuvvetlerini emmek için kullanılırlar. Aslında enerji emen ideal bir sönümleme yapısı tüm darbe süresince üniform bir yavaşlatma sağlamalıdır. Sürekli olmasa da kademeli olarak enerji yutma seviyeleri değiştirilen bir ezilme kutusu tasarımı ile pik kuvveti azaltarak mümkün olduğunca üniform bir yavaşlamayı sağlamak burada önerilen çalışmanın motivasyonunu oluşturmuştur. Ezilme kutusu önce ilk darbeyi şiddetli bir pik kuvveti oluşturmadan emmeli, daha sonra geri kalan enerjiyi yutabilmek için kademeli olarak deforme olmalıdır.

Belirlenen bu amaç doğrultusunda, iç içe geçen farklı uzunluktaki tüplerden oluşan yeni bir ezilme kutusu düşünülmektedir. İçteki en uzun tüp, ilk darbeyi emecek ve sonra diğer tüplerle birlikte deforme olacaktır. Yeni tüpün aynı boylarda olan iç içe tüplerden daha hafif olacağı ve tüplerin yerleşiminin, geometrik parametrelerinin sıralamasının önemli olacağı düşünülmektedir. Bu yüzden, daha önce hiç çalışılmamış olan, iç içe geçmiş farklı uzunluk ve geometrideki tüplerin deneysel ve sayısal olarak incelenmiştir.

Öncelikle, ezilme kutusunda kullanılacak olan metal malzemelerin çekme deneyleri farklı gerinim değişim hızlarında yapılarak gerilme-gerinim diyagramları elde edilmiştir. Çeşitli ezilme kutusu tasarımları geliştirilerek ve elde edilen malzeme test verileri kullanılarak sonlu elemanlar analizleri yapılmıştır. Doğrusal olmayan açık (explicit) sonlu eleman yazılımı (LS-DYNA/Explicit) ve kapalı (implicit) sonlu

eleman yazılımları (LS-DYNA/Implicit) kullanılarak tasarlanan ezilme kutularının çarpma sonrası ezilme davranışları analiz edilerek incelenmiştir. Farklı metallerin ve geometrilerin birleşimi olarak tasarlanan ezilme kutusu yapısının enerji emme kapasitesi geometri ve malzeme özelliklerine bağlıdır. Bu yüzden farklı boy ve kesitlerde iç içe geçen tüplerden oluşan farklı bir ezilme kutusu analizlere tabi tutulmuştur. Malzeme, cidar kalınlığı, flanş genişliği, çarpma hızı, iç içe tüplerin yerleşimi, uzunluğu ve çarpma hızı parametreleri için en iyileştirme yapılacaktır. Literatürde farklı uzunluklardaki tüplerin iç içe geçmesi ile meydana gelen ezilme kutuları ve parametrik analizleri mevcut olmadığından, bu tip tüplerin maksimum deformasyonları ve enerji emme kapasitelerinin analizinin yapılması ve değerlendirilmesi bu alanda önemli bir katkı sağlayacaktır. Sayısal modelleme çalışmaları sonucunda en iyi çarpışma kutusu tasarımları belirlenmiştir. Seçilen ezilme kutularının deneysel simülasyonları yapılarak analiz çalışmaları doğrulanmış. Bu duruma göre deneysel süreçler için farklı malzeme ve geometride ezilme kutuları üretttirilmiştir. Kutular, dinamik ve statik ezilme deneylerinde incelenmiştir. Testlerden elde edilen sonuçlar sayısal analiz sonuçları ile karşılaştırılarak değerlendirilmiştir.

Test çalışmaları neticesinde birtakım gözlemler yapılmıştır. Alüminyum 6063 ve Çelik AISI 304'ten üretilmiş numuneler ile deneyler gerçeklenmiştir. İç içe üç daireden oluşan AL 6063 tüpler, iç içe üç daireden oluşan AISI 304 çelik tüpler üretilmiştir. Ayrıca dairesel kesitlere ek olarak kare kesitli AL 6063 ve AISI 304 malzemeden iç içe tüpler üretilmiştir. Bunlara ek olarak içten dışa kare-daire-kare şeklinde alüminyum-çelik-alüminyum malzemeden sistem, kare-daire-kare şeklinde çelik-çelik-çelik malzemeden sistem, daire kesit alanlı alüminyum-çelik-alüminyum malzemeden sistem üretimi yapılmıştır. Bütün bu sistemler 2.69, 3.28, 3.77 ve 4.22 m/s gibi hızlarda çarpma testine tabi tutulmuştur. Kare kesitli tüplerde kenarlardan yırtılmalar gözlemlenmiş, bunların önüne geçilmesi için en dıştaki tüp duvar kalınlığını artırılabileceği, en dıştaki tüpün kenar uzunluklarının düşürülebileceği, en dışta kare kesit bulundurmama ve ya köşelerin yuvarlatılması gibi öneriler sunulmuştur. Alüminyum tüplerde gerçekleşen bu durumların benzeri çeliklerde de gözlemlenmiştir. Çelik tüplerde de köşelerin yuvarlatılmaması benzer sonuçlar doğurmuş ve köşelerde yırtılmalar meydana gelmiştir. Tüp çapları analizlerle global burkulma olmayacak şekilde seçildiğinden deneylerde de analizlerle uyumlu olarak global burkulmalar gözlemlenmemiştir. Lokal burkulmalar ile katlanmalar düzgün şekilde yaşanmıştır. Bu durum, yırtılma olan en dıştaki kare tüp içeren tasarımlar için içteki tüplerde de yaşanmıştır. Dairesel kesit alanlı tüplerde katlanmalar lokal burkulmalar şeklinde olsa da geometrik mükemmel olmayan durumlardan ötürü farklı katlanma şekilleri gözlemlenmiştir. Ancak farklı katlanma mekanizmaları benzer pik kuvvet değerleri üretmiştir. Farklı malzemeden tüplerin birarada olduğu sistemler kuvvet davranışı açısından verimli sistemler üretebilmiş ancak çelik içeren bu sistemlerin düşük ağırlık verimi de gözönüne alınmıştır. Sanki statik ezme testleri optimum geometri kararından sonra yapılmıştır. Dairesel kesit alanlı AL 6063 tüpler için 4 farklı statik ezme testi 2 mm/dakika hızlarda yürütülmüş ve kuvvet-zaman, kuvvet-ezilme eğrileri oluşturulmuştur. Bu grafikler, dinamik ezme test sonuçları ile karşılaştırılmış ve uyum gözlemlenmiştir. Gerinim hızlarının alüminyumda çok etkili olmadığı bu karşılaştırmalar ile görülmüştür.

Bu doğrultuda yapılan analiz, deney ve optimum tasarım için deney ve analiz uyumunun gözlemlenmesi çalışması tezin yapısını oluşturmaktadır. Analiz çalışmalarında Abaqus ve LS-DYNA sonlu eleman programları ve çözücüleri kullanılmıştır. Genel olarak benzer fikir verselerde programların farklı malzeme verileri ve değme durumlarında farklı kuvvet davranışlarını çıktı olarak verebilmektedir. Yine dikkat çeken bir unsur olarak, köpek kemiğ şeklinde oluşturulan ve çekme testi yapılan malzeme gerilme-gerinim eğrilerinin programlara girdi olarak verilmesi sonrasında deneylerle yeterli uyum gözlemlenmemiş ve statik ezme testlerine göre gerilme gerinim eğrilerinin modifiye edilmesi gerekmiştir. İncelendiğinde ezme hareketinde emze, çekme, burkulma birlikte olduğundan sadee çekme testinin yeterli olmaycağı görülmüştür.

Sonuç olarak optimum geometri olarak içiçe tüplerde kullanılmak üzere alüminyum 6063 malzemeden dairesel sistem tercih edilmiştir. Bunun yanısıra çelik ve alüminyum sistemlerin birlikte olduğu durumlarda pik kuvvetinin davranışının çarpma kuvvet verimi açısından çok iyi sonuçlar verebildiği görülmüş ancak sistem ağırlığı açısından sadece alüminyum sistem tercih edilmiştir.

1 INTRODUCTION

1.1 Purpose of Thesis

Impact and impact response of materials in the nature catch the attention of the researchers. On the grounds that impact cause damage and survival limitation of engineering structures, researchers have tried to investigate harmfull effect of this phenomenon with the aim of developing more efficient materials and structures.

In space, vehicles might be subjected to impact of meteoroids and debris particles or loads acting during landing. Design of spacecraft shield gains more importance for protection of spacecraft's structural integrity and crews' health. Researchers generally focus on hypervelocity impact phenomenon due to being more common encountered problem.

To mention about the automobile industry, over one million people are killed and 20-50 million people are injured during traffic accidents per a year. According to WHO, 1.24 million people were killed in 2010 (World Health Organization, n.d.). For this reason, raising safety level of a car is an important scientific research subject. Crash tubes are used to reduce the harm of the accidents on passengers and equipped generally in front of the cars. They have an important role to reduce harmful effects of accidents. Numerous studies have been done to enhance the crashworthiness characteristics of crash tubes at dynamic and quasi-static velocities.

The main targets of crash tube design are peak load should be lower and amount of energy absorption should be higher at the same time despite being adverse processes. Researchers aim to obtain its better crashworthiness characteristics.

In this study, firstly, numerical models were constructed by verifying the models from the literature. After that, better cross sections were decided via computer analysis and new designs were analyzed if they would be suitable to manufacture for experimental procedures. In the experimental stage, different type of materials were used to construct nested tube design. Square and circular cross sections, are made of steel and aluminium tubes were used to in the experiments. Results were presented in addition to decision of optimum design. With the decision of optimum design, numerical models and experimental analyses were conducted to compare to see capability of finite element analysis programs. In addition to dynamic tests, quasi-static crushing tests were conducted to see effect of impact velocity and strain rate of materials.

It is known that due to the complexity and time intensity, the analyses leading to those recommendations cannot be carried out on the basis of a simulation of a whole car. So attempts to find consistent numerical models and measuring consistency of numerical analysis programs are important to create certification procedures without experimental procedures in near 10-20 years.

1.2 Literature Review

Thin-walled metal tubes are widely used in the automotive industry as safety components for the protection of the passengers, drivers and electronic devices of vehicles based on relatively less price and higher energy absorption capability. It is located in the front of automobiles due to collusion damages generally was occured frontal area of the cars. It serves the purpose of converting some amount of kinetic energy during collusion to the plastic energy, which prevents passengers and devices from squeezing. Besides, inertial loads, which occur at the beginning of the collusion, can be harmful for passengers during dynamic crash. Accordingly, main target of design and fabrication of crash tubes is considered that the peak load should be lower and the amount of absorbed energy should be higher simultaneously in spite of being adverse processes. Therefore, the design of crash tubes gains more importance.

There are several studies on configuration types of crash tubes such as foam-filled, multi-cell and geometrical parameters of crash tubes such as tube length, cross section, wall thickness. Qiao et al.(Qiao, Chen, & Che, 2006) examined the crash response of square tubes made of AA6063 considering the damage evaluation. They evaluated that crash response of aluminum tubes depends on microstructure of the material, boundary conditions, wall thickness and length of tube and impact velocity. Ghamarian et al. investigated the difference between foam filled and empty end-capped conical and cylindrical tubes numerically and experimentally. SEA (specific energy absorption) values of conical tubes was found to be 18.4% higher than those of cylindrical tubes (Ghamarian, Zarei, & Abadi, 2011). Li et al. performed multiobjective robust optimization to improve crashworthiness properties of the foam filled tubes, where the

SEA and the peak force are defined as objectives and the mean crush force as constraint (Li, Sun, Huang, Rong, & Li, 2015). Zhang et al. conducted aluminum multi-cell tubes, which were divided into 3 parts: corner, crisscross and T-shape numerically and analytically under axial loading. Crisscross part gave higher energy absorption than the others (X. Zhang, Cheng, & Zhang, 2006). Tang et al. investigated the non-convex multi-corner crash tubes to increase energy absorption (Tang, Liu, & Zhang, 2012). Results showed that multi-corner tubes, including 12 and 20 corners, have 1.18 and 2.54 times higher SEA values than a conventional square tube due to shorter wavelength.

Chen and Wierzbicki studied hollow empty and foam filled multi-cell tubes by using numerical and analytical methods under axial loading. Energy absorption characteristics of single, double and triple cell tubes were calculated according to Super Folding Element theory and validated with the numerical results. SEA values of double and triple cell tubes were found to be higher than those of single tubes (Chen & Wierzbicki, 2001). Yamashita et al. investigated crashing performance of various types of polygonal crash tubes. Number of corners were defined from 4 to 12 and 96. Consequences, increase of the number of corners improved crush strength, tubes with less than six corners were not proper to obtain better collapse modes and higher plastic hardening rate could lead to symmetric collapse pattern (Yamashita, Gotoh, & Sawairi, 2003). Fan et al. examined concave and convex polygonal crash tubes: hexagon, octagon, 12-sided and 16-sided star. 12 sided tubes were more efficient in terms of the absorbed energy when the nominal diameter and the wall thickness ratio is less than 50 (Fan, Lu, & Liu, 2013).

Kim investigated different types of triggered and multi-cell square tubes made of aluminum numerically and analytically. Multi-cell tubes had advantages in respect to SEA and weight efficiency in comparison with traditional square tubes (Kim, 2002). Nagel and Thambiratnam analyzed straight and tapered square crash tubes in terms of number of tapered tubes and taper angle subjected to axial dynamic loads. Crash force efficiency of tapered tubes was higher than that of straight tubes because of their stable crash loads and collapse modes. However, increasing the number of taper reduced energy absorption capability per unit mass (Nagel & Thambiratnam, 2006)(Nagel & Thambiratnam, 2005). Chiandussi and Avalle performed an optimization study to obtain better crash performance for the tapered crash tubes. Load uniformity, parameter of study and ratio of peak force and mean crash force, was preferred higher as much as possible because of being less sensitive to young modulus and thickness (Chiandussi & Avalle, 2002). Liu et al. investigated buckling behaviors of a special cross sectional aluminum alloy columns subjected to quasi static loads and presented ultimate strength and failure modes (Liu, Zhang, Wang, & Chang, 2015).

Nested tubes were studied by a few researcherd up to now. Zhang et al investigated crashworthiness of bitubal hexagonal structures with honeycomb core under dynamic loading. External volume and total mass was defined same for each specimen, otherwise thickness of wall and side length of inner tube were defined as variable parameters. Honeycomb core improved SEA due to its lower density . (X. Zhang, Cheng, Wang, & Zhang, 2008). Zhang et al. conducted an optimization study of foam filled bitubal structures according to SEA, peak force and crashing length. It improved efficiency of crashworthiness in comparison with foam-filled monotubal structures (Y. Zhang, Sun, Li, Luo, & Li, 2012). Olabi et al. analyzed the quasi-static lateral compression of nested systems that was different from multi cell profiles, numerically and experimentally (Olabi, Morris, & Hashmi, 2007). Usta et al. examined the effect of the number of tubes for stepped and concentric circular crash tubes under axial impact loading, numerically (Usta, Eren, Türkmen, Kazancı, & Mecitoğlu, 2015). Eren et al. analyzed square and circular stepped and concentric crash tubes made of aluminum and steel by using LS-DYNA and Abaqus (Eren, Usta, Kazancı, Türkmen, & Mecitoğlu, 2015).

According to Kazancı and Bathe, the results of numerical analysis using ADINA (based on implicit time integration method) integration method) was in good agreement with the experimental results at quasi static crush speeds which meant that an implicit time integration method (Bathe Method) could be a good alternative because of having shorter solution time. Besides, changing velocity of impact mass affected the crashworthiness characteristics of crash boxes (Kazancı & Bathe, 2012). Ince et al. searched the energy absorption characteristics of hybrid crash tubes providing to save 17.5% of total weight (İnce et al., 2011).

Impact phenomena can be seen in many field such as debris impact on spacecraft vehicle, bird strike on aircraft wing etc., so energy absorbers are used as structural components of aerospace vehicles.

2 NUMERICAL MODELLING

2.1 Implicit and Explicit Methods

It is known that engineers doing finite element analyses in programs strive to construct the model right. For instance, boundary conditions, element types, shapes, the method of meshing and integration method etc. Specific conditions are generally chosen without exactly knowing what they effect. Because of too long solution durations, it is desirable to finally be able to give recommendations about which settings of FEA programs to get accurate results under which specific conditions. It is important to know that the mesh issue and time integration must be known. These will be compromises substantially influenced by the computation time, which should be minimized as far as possible without losing too much of accuracy.

Abaqus/Explicit and LS-DYNA FEA solvers are generally used for dynamical phenomena. Dynamical situations, especially, fast occurred ones need to artificial methods like explicit time integration scheme. Mesh element length, time step size and data recording steps are important to reach correct force-time and force-deformation curves in crash analyses.

Having less velocities in dynamical cases allow using implicit time integration scheme. Normally for the fast occurred cases, it is not true to use implicit scheme because of its nature to try solve all stiffness matrix in the finite element method.

Mathematical backgrounds of implicit and explicit time integration schemes are summarized. The basic equations used in the time integration scheme have been known for a long time. In the method of Bathe, the complete time step Δt is subdivided into two equal sub-steps. For the first sub-step the trapezoidal rule is used and for the second sub-step the 3-point Euler backward method is employed with the resulting equations. This method is named as modified implicit time integration scheme or with other name, Bathe method (Bathe, 2007).

The implicit method is unconditionally stable, hence the time step to be used in the time integration can be chosen with respect to accuracy considerations only. Implicit time integration scheme was used for crash analysis in the literature before (Kazancı & Bathe, 2012). While explicit time integration is now widely used for crush and crash analyses, it is well known that the use of such integration scheme to solve certain problems, notably low speed dynamic or almost static problems, can lead to difficulties. According the results of Kazancıand Bathe’s research, in such cases, an implicit time integration solution may well be more suitable or might at least provide a valuable alternative in the solution approach (Kazancı & Bathe, 2012). Figure 2.1 and 2.2 are quite useful schematics to give general motion of equation of a system.

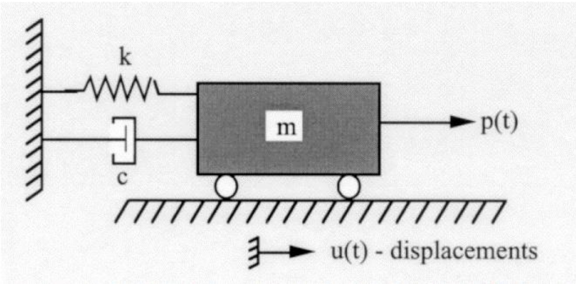

Figure 2.1 : Single degree of freedom damped system (Livermore Software Technology Corporation, 2006).

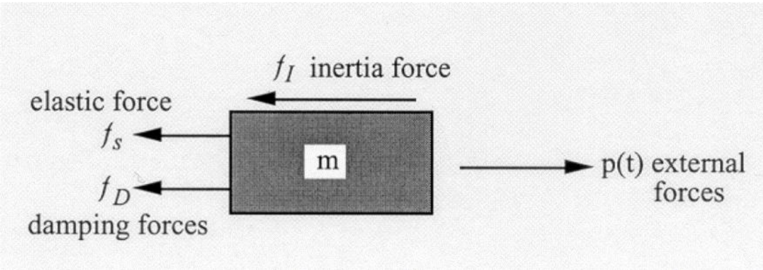

Figure 2.2 : Forces acting on mass (m) (Livermore Software Technology Corporation, 2006).

Equation 2.1 to 2.4 define force function terms of a dynamical beviour. General representations are seen from the Equation 2.5 and 2.6.

$$f_I + f_D + f_{int} = p(t) \tag{2.1}$$

$$f_I = m\ddot{u}; \qquad \ddot{u} = \frac{d^2u}{dt^2} \quad acceleration \tag{2.2}$$

$$f_D = c\dot{u}; \qquad \dot{u} = \frac{du}{dt} \quad velocity \tag{2.3}$$

$$f_{int} = ku; \qquad u \quad displacement \tag{2.4}$$

Where c is the damping coefficient, and k is the linear stiffness. For criticial damping $c = c_{cr}$. The equations of motion for the linear behaviour lead to a linear ordinary differential equation. But for the nonlinear case, the internal force varies as a nonlinear function of the displacement.

$$m\ddot{u} + c\dot{u} + ku = p(t) \qquad \textbf{(2.5)}$$

$$m\ddot{u} + c\dot{u} + f_{int}(u) = p(t) \qquad \textbf{(2.6)}$$

In addition to the dynamic response of linear system subjected to a harmonic loading, it is useful to define some commonly used terms. Loading function is represented in the Equation 2.7 and natural frequency term is seen from the Equation 2.8 and 2.9. These terms are used to construct finite element model of the dynamic behaviour of the systems.

Harmonic loading: $$p(t) = p_0 sin\omega t \qquad \textbf{(2.7)}$$

Circular frequency: $$\omega = \sqrt{\frac{k}{m}} \text{ for single degree of freedom} \qquad \textbf{(2.8)}$$

Natural frequency: $$f = \frac{\omega}{2\pi} = \frac{1}{T} \quad T = period \qquad \textbf{(2.9)}$$

Damping ratio: $$\xi = \frac{c}{c_{cr}} = \frac{c}{2m\omega} \qquad \textbf{(2.10)}$$

According the explicit computation logic, time step performing is very important tool. When stifness and mass matrices is calculated, time step decision process should be decided via following formulas.

During the solution, it is fond a new time step size by taking the minimum value over all elements.

$$\Delta t^{n+1} = a.\min\{\Delta t_1, \Delta t_2, \ldots\ldots, \Delta t_N\} \qquad \textbf{(2.11)}$$

where N is the number of element. For stability reasons the scale factor a is typically set to a value of 0.9 in the LS-DYNA (or a smaller value).

A critical time step size, Δt_c is computed for solid elements from

$$\Delta t_c = \frac{L_s}{\{[Q + (Q^2 + c^2)^{1/2}]\}} \tag{2.12}$$

where Q is a function of bulk viscosity coefficients C_0 and C_1:

$$Q = \begin{cases} C_1 c + C_0 L_c |\dot{\varepsilon}_{kk}|, & \dot{\varepsilon}_{kk} < 0 \\ 0, & \dot{\varepsilon}_{kk} \geq 0 \end{cases} \tag{2.13}$$

L_c is characteristic length :

8 node solids : $L_c = \frac{\vartheta_c}{A_{cmax}}$

4 nodes tetrahedras : $L_s = minimum\ altitude$

ϑ_c is element volume, A_{cmax} is the area of the largest side, and c is the adiabatic sound speed:

$$c = \left[\frac{4G}{3\rho_0} + \left.\frac{\partial p}{\partial \rho}\right)_s\right]^{1/2} \tag{2.14}$$

where ρ is the specific mass density. Brief definitions of all terms can be found in the LS-DYNA Theory Manual (Livermore Software Technology Corporation, 2006). c has a final equation for elastic materials with a constant bulk modulus as that:

$$\sqrt{\frac{E(1-\vartheta)}{(1+\vartheta)(1-2\vartheta)\rho}} \tag{2.15}$$

where E is the Young's modulus, and ϑ is the Poisson' ratio. Time step calculations for the shell element is conducted with the following time step definitions:

$$\Delta t_c = \frac{L_s}{c} \tag{2.16}$$

where L_s is the characteristic length and c is the sound of speed:

$$c = \sqrt{\frac{E}{\rho(1-\vartheta^2)}} \tag{2.17}$$

$$L_s = \frac{(1+\beta)}{\max(L_1, L_2, L_3, (1-\beta)L_4)} \quad \textbf{(2.18)}$$

where $\beta = 0$ for quadrilateral and 1 for triangular shell elements, A_s is the area, and $L_i, (i = 1,2,3,4)$ is the length of the sides defining the shell elements. There are two other options two calculate characteristic length but LS-DYNA theory sources. can be examined for further details (Livermore Software Technology Corporation, 2006).

2.2 Definitions on Low Velocity Impact

2.2.1 Total energy absorption

When an energy absorber component absorbs the energy (mostly kinetic energy), the absorbed energy can be easily calculated via crush force and crush distance (deflection). Total absorbed energy (kJ) can be calculated as in the equation:

$$E = \int_0^{deflection} P d\delta \quad \textbf{(2.19)}$$

P (kN) is the axial crush force per distance. And δ (mm) is the crush distance in the axial direction. This relation is represented as the area under the force-deformation curve. The figure 2.3 represents a typical force-deflection curve of an absorber.

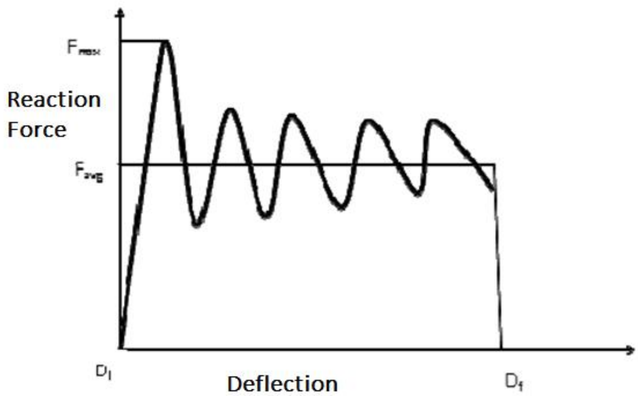

Figure 2.3 : Force-deflection (deformation) curve representation.

2.2.2 Maximum crush force

As it is seen in the Figure 2.3, F_{max} means maximum crush force value. Maximum crush force means that it is the highest initial load required to initiate collapse, which start the energy absorption process. A larger peak force will result in the device transferring significantly large forces to the body until the load required to initiate collapse is reached. Otherwise, a small peak force will result in the device collapsing under load which will not cause any signicant damage to a body being proected.

Another crush force indicator is the mean crushing force which is an indicator of the energy absorbing capability of a structure when compared to the displacement required to absorb the energy. The mean crushing force is the average force for a given deformation, which can be defined as the total energy absorbed divided by the total deformation in the direction of the force as the

$$F_{mean} = \frac{\int_0^{deflection} P d\delta}{deflection} \quad \textbf{(2.20)}$$

2.2.3 Crush force efficiency

Apart from the mean crushing force and peak crushing force, there are other two ways to measure the energy absorbing capability.

The one of them is the crush force efficiency which is based on the mean crushing force and can be expressed as the following equation.

$$n_c = \frac{P_m}{P_p} \quad \textbf{(2.21)}$$

n_c indicates that the average forces in the system is comparable to the peak force required to initiate crushing. Under such conditions, it is evident from equation that the energy absorbed, given by the area ander the force displacement curve, is increased and the higher n_c means the better performance of the energy.

2.2.4 Specific energy absorption

The other way is the specific energy absorption (SEA), which is the most important and common parameter used to estimate the capability of the energy absorption. It can be defined as the following equation.

$$SEA = \frac{E_{total}}{m} \quad \textbf{(2.22)}$$

Where, E_{total} is the total absorbed energy and m is the mass. Therefore, the SEA is the absorbed energy per uit mass so that it is usually used as an indicator of the weight efficiency of an energy absorber.

2.3 Abaqus Modelling

Abaqus CAE is capable for static, quasi-static and dynamic simualtions. In this section, Crushing behaviour of tubes are modelled using explicit solver of Abaqus. It is important to decide to units due to there is no ready set like in Ansys. Table 2.1 is an unit relation table and is used to understand the conversion issue.

Table 2.1 : The units used in Abaqus FEA Program.

Abaqus units	Mass	Lenght	Time	Velocity	Stress (Elasticity-Yield)	Density
Thickness (mm)	2	2	2	mm/s	N/mm^2 (MPa)	Tonne/mm^3

Some tips need to be highlighted:

- Between tubes and cross surfaces, instead of geometrical surface definitons, mesh surface definitions are preferred.
- **Surface-Surface Contact:**
  Master surface:Impactor (surface mesh element)
  Slave surface:tubes' all surfaces
- **General Contact:**
  Tube-self contact is defined via this method.
- Impactor mass is modelled as shell elements and rigid.,
- 1 mm above the tube's upper line, is used to model impactor mass.
- A nodal mass is added to the center point of Impactor mass. Rotary inertia information is input.
- Rotary inertia: $M \times \frac{A^2+B^2}{12}$
- "Predefined Field" is defined for nodal mass as velocity vector.
- To read reaction forces, from the reference point of rigid base plate is used.

- For the velocity output impactor mas’s reference point is used in History-output section.

For the energy value, from the sytem history output section, option is defined. Contact algorithms and an example problem model could be find in the Abaqus User Manual (Abaqus, n.d.-a). Method information in the boxes above should be known while analysis is being done. Especially, differences between general contact and surface to surface contact make difference in some type of analyses. Additionaly, slave surface and master surface selections are another important point.

2.3.1 Verification of Abaqus model from the literature

For ensuring that the analysis model were constructed right, verification analysis is run. Firstly; impactor, tube and base plate below the tube is constructed for the analysis setup. Each of modelled elements of tubes are a type of shell (S4R). Verification study is conducted via a model of a study from the literature (Marzbanrad, Mehdikhanlo, & Saeedi Pour, 2009) (Table 2.2).

Table 2.2 : Verification input.

Lenght(mm)	A (mm)	B (mm)	Thickness (mm)	Impact velocity (mm/s)	Mass of impactor (tonne)
150	30	30	1.25	9396	0.1

Marzbanrad’s work’s material data was used to correlate the analysis (Table 2.3) (Marzbanrad et al., 2009). Units are important to reach true results. Shell elements are used to construct mesh. Element information was given in the Table 2.4. Inertial effects and mass information is input. The Figure 2.4 represents the Abaqus model of the problem.

Table 2.3 : Material data for verification study (Marzbanrad et al., 2009).

Material	Density	Elasticity Modulus	Yield Stress	Poisson ratio
Steel	7830x10^{-12} $\frac{tonne}{mm^3}$	207000 MPa	280 MPa	0.3

Table 2.4 : Element length for analysis program.

	Tube
Element mesh length	2 mm

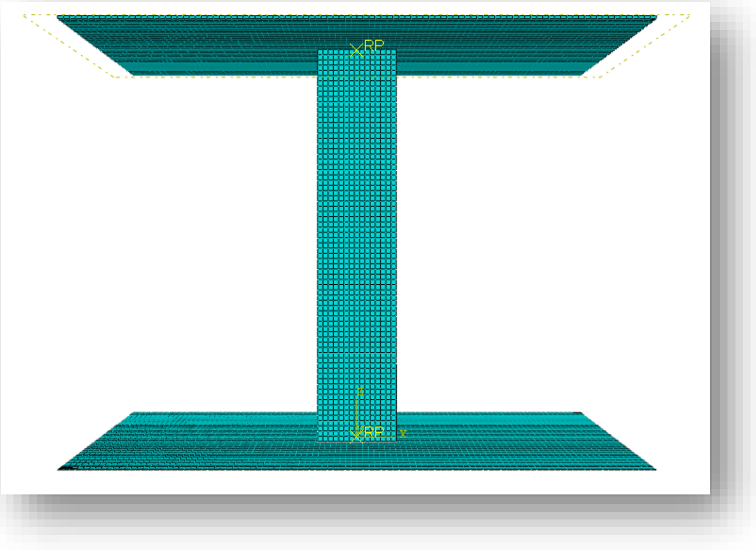

Figure 2.4: Abaqus mesh model.

2.3.2 Results

Steel tube having 1.25 mm thickness was analysed and force-deformation curve is given in the Figure 2.5. And it was compared with Marzbanrad's work.

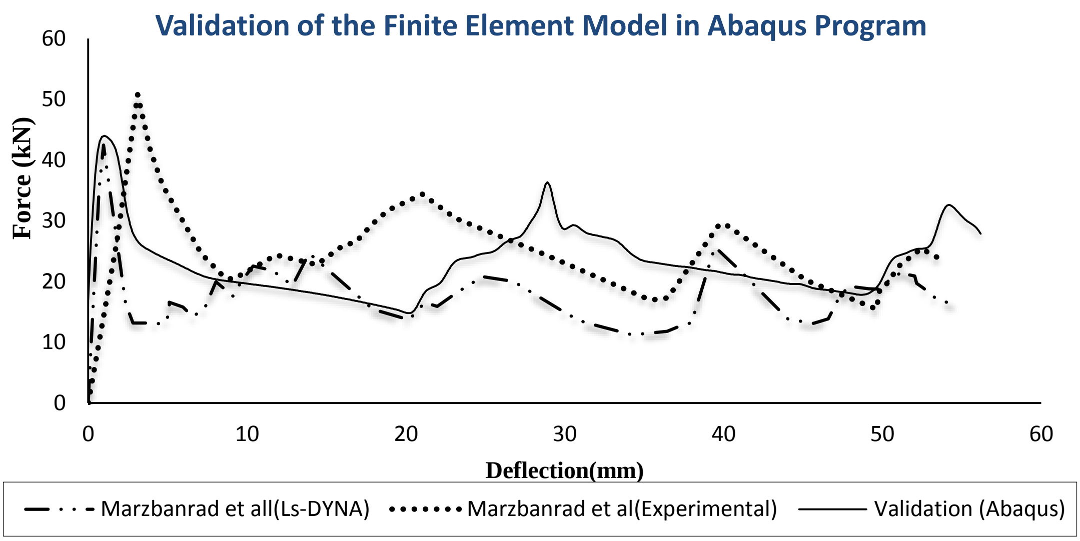

Figure 2.5 : Verification of analysis from the literature via Abaqus (Marzbanrad et al., 2009).

Efficient correlation was estimated from the Figure 2.5. In the Figure 2.6, first and last instant of crushing was showed.

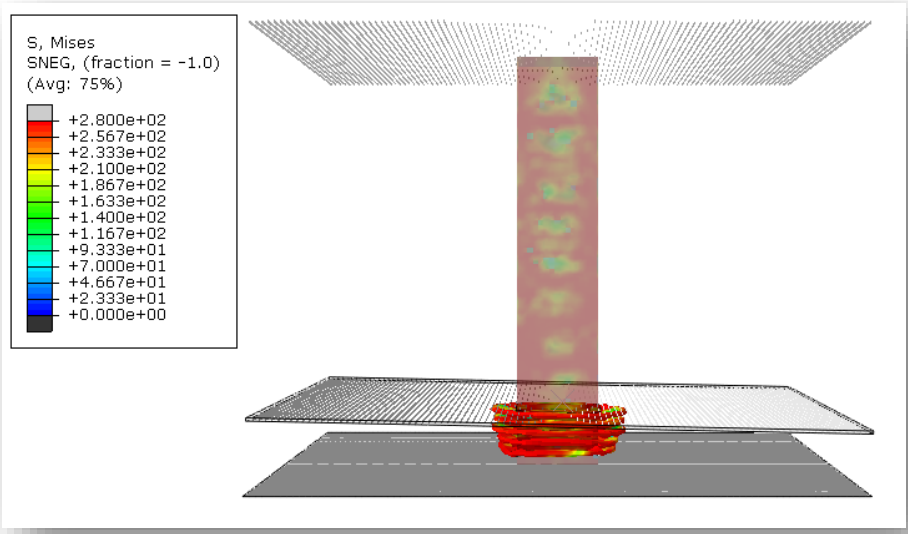

Figure 2.6 : Crushed tubes with initial and last instant.

End time of the crushing and conversion of kinetic to internal energy is seen from the Figure 2.7. When energy data become constant, velocity becomes zero.

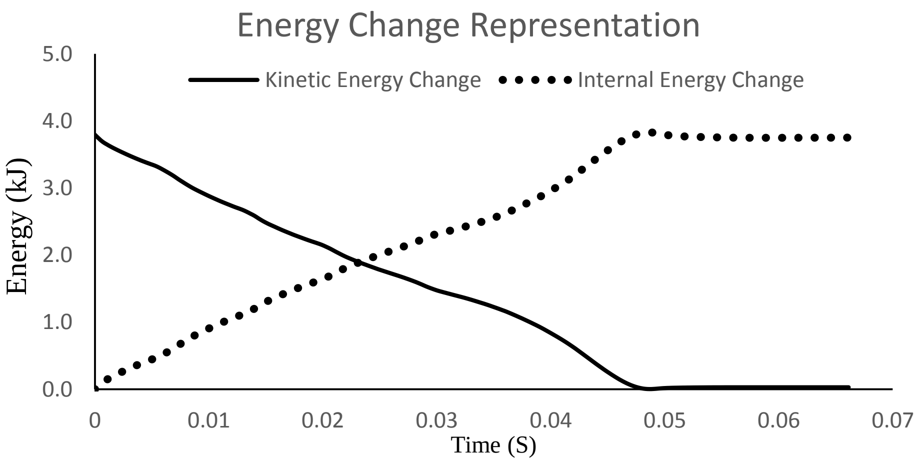

Figure 2.7 : Change of energy in Marzbanrad's work.

2.3.3 New models in Abaqus

2.3.3.1 Model setup

After the verification study, nested tubes having square and circular cross sections were modelled. AL 6063 and St DP600 materials were used for simulations as in the experimental production. Information about the system, material properties and plastic stress-straim curve were given below (Table 2.5, 2.6, 2.7, 2.8).

Table 2.5 : Model lengths constructed in Abaqus.

Material	Tube 1	Tube 2	Tube 3
Thickness (mm)	2	2	2
Tube length (mm)	200	180	160

Table 2.6 : Model information constructed in Abaqus.

Cross Section	AL 6063	St DP600
Square	A1	A2
Circular	B1	B2

Two different cross sections were used to model nested tube design. Totally, with the AL 6063 and St DP600 usage, 4 different models were constructed. Top view of models are seen in the Figure 2.8.

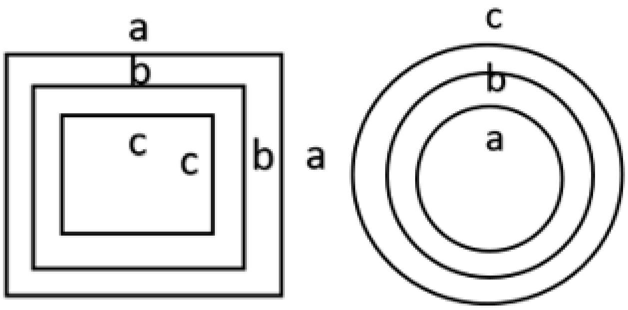

Figure 2.8 : Concentric tube system having square and circular cross sections.

Table 2.7 : Impactor information.

Impactor mass	Impact velocity
1.130 tonne (1130 kg)	4221 mm/s (4.221 m/s)

Table 2.8 : Spesifications.

Material	Aluminium 6063	Advanced High Strenght Steel DP600
Density	$2.7x10^{-9}$	$7.8x10^{-9}$
Poisson’s ratio	0.33	0.3
Material	68000 MPa	205000 MPa
Yied Stress	60 MPa	400 MPa

Abaqus model is comprised of nested 3 tubes which each of them has 2 mm thickness and different lengths. In addition, base plate and impactor plate were modelled. Impactor mass has inertial and mass information (Impactor mass is 1130 kg). All elements were modelled as shell. Abaqus model of the circular system is represented in the Figure 2.11.

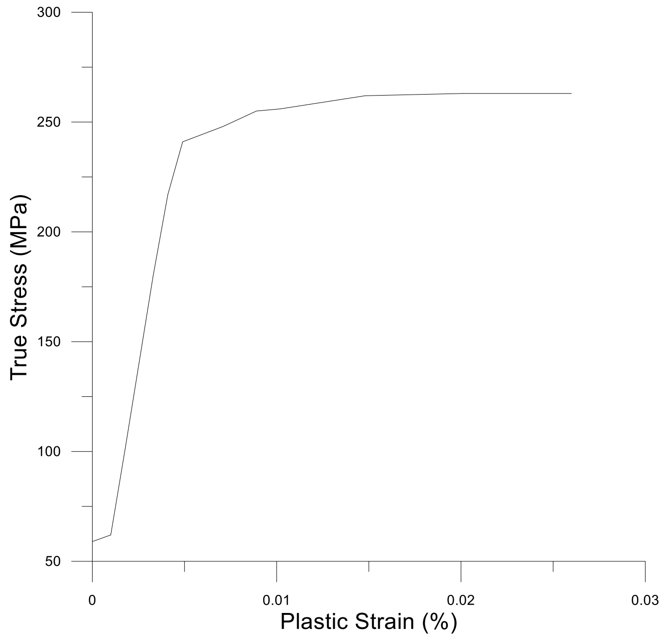

Figure 2.9 : AL6063 material true stress-plastic strain curve taken from suppliers' database (Key to Metals AG, 2015).

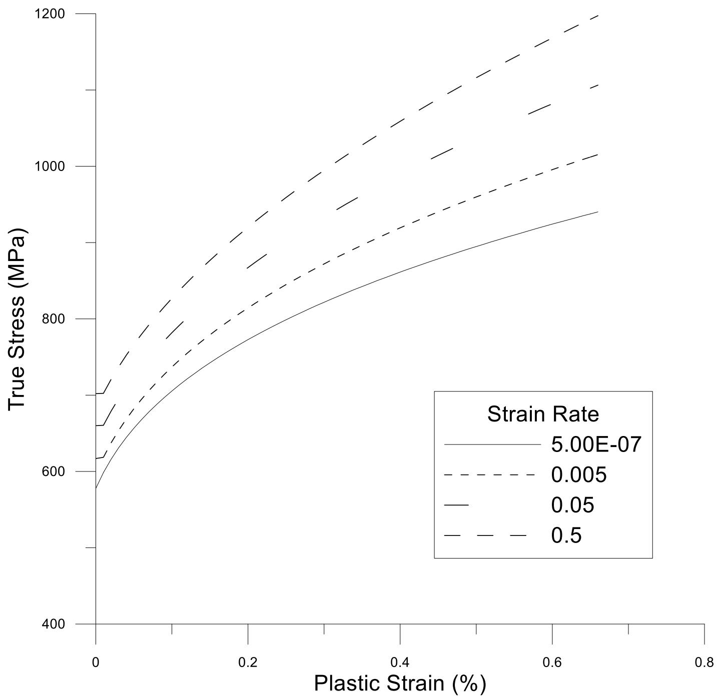

Figure 2.10 : St DP 600 material true stress-plastic strain curve (Key to Metals AG, 2015).

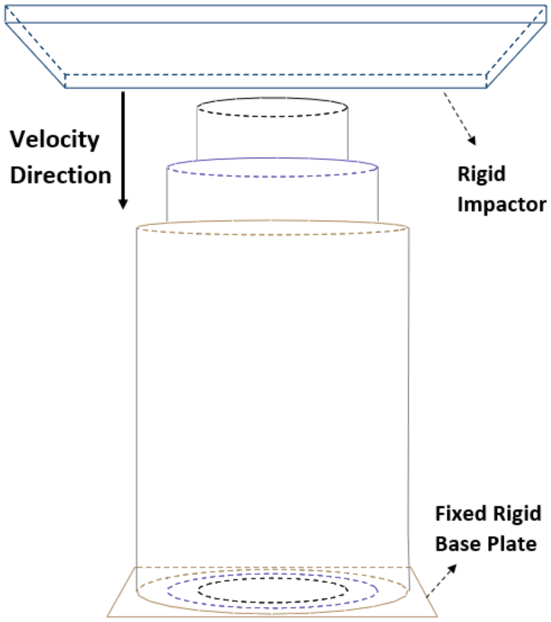

Figure 2.11 : Problem definition with nested tube having gradually decresing lengths.

2.3.3.2 Results

Table 2.9 : Abaqus analysis results.

Material	Model A1(AL square cross section)	Model A2(St square cross section)	Model B1(AL circular cross section)	Model B2(St circular cross section)
Deformation	84.6 mm	39.8 mm	81.4 mm	63.9 mm
Peak forces	0.33	207-405-678 kN	80-163-211 kN	150-290-425 kN
Deformation time	29 ms	26 ms	48 ms	21.4 ms

Abaqus analysis results were summarized in the Table 2.9. In the Figure 2.12 and 2.13, undeformed and deformed tubes are seen. Colorful representation provide different von Mises stresses.

The 2000 Hz SAE filtering was decided so that filtering cases was resulted according the experience. For the circular design, crushed tubes was showed in the Figure 2.13. The information about the topic can be find from the Abaqus and LS-DYNA User Manuals (Abaqus, n.d.-b). Kinetic energy and internal energy has cross-ratio; when kinetic energy decreases, internal energy increases.

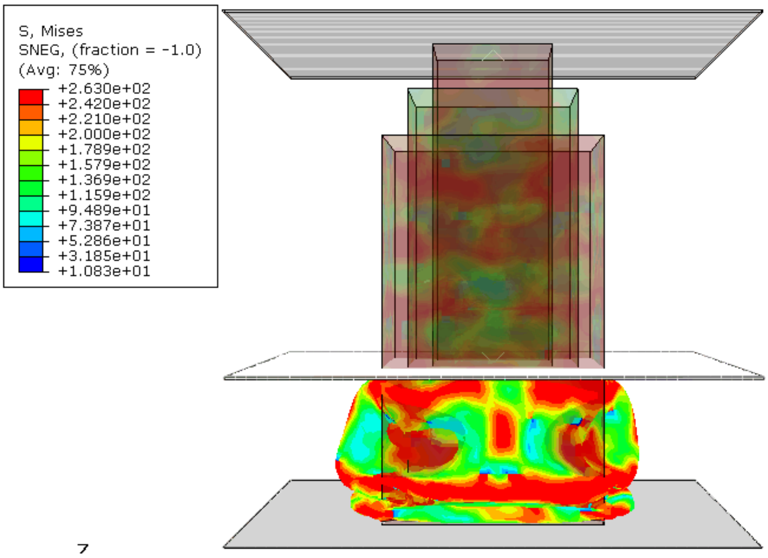

Figure 2.12 : Model A1 (AL6063 Square cross section)–crushed tubes representation.

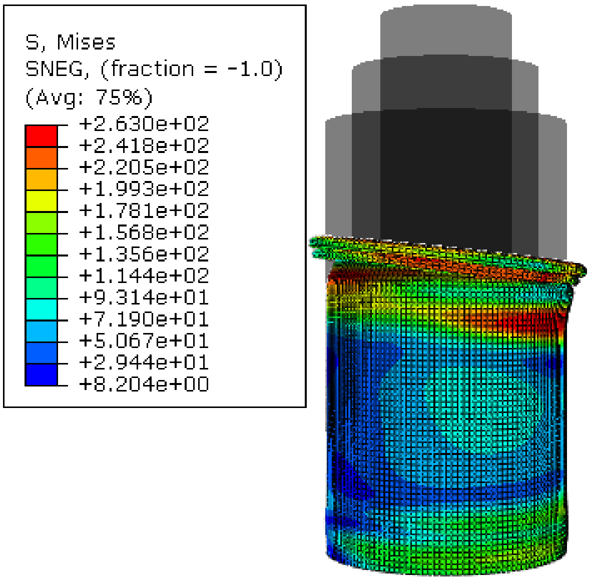

Figure 2.13 : Model B1 (AL6063 circular cross section)–crushed tubes representation.

The Figure 2.14 gives force-deflection behaviours of square and circular cross section AL 6063 tubes. It is obvious that square cross section tubes had more deflection than circular ones. In addition to that, 3 of peak forces are seen higher than circular ones too. Differently from AL 6063 systems, it is seen from the Figure 2.14 that force-deflection curves of tube systems made of St DP 600 has high differences. The circular system had far higher deflection than square one.

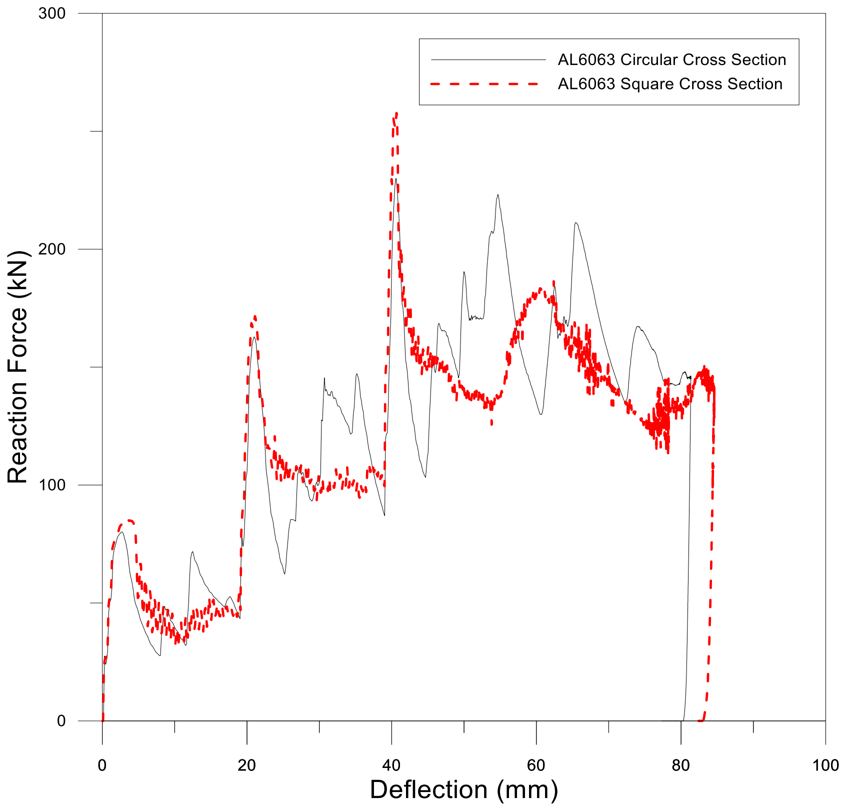

Figure 2.14 : Reaction force deformation curves for the systems having different cross sections and made of AL6063.

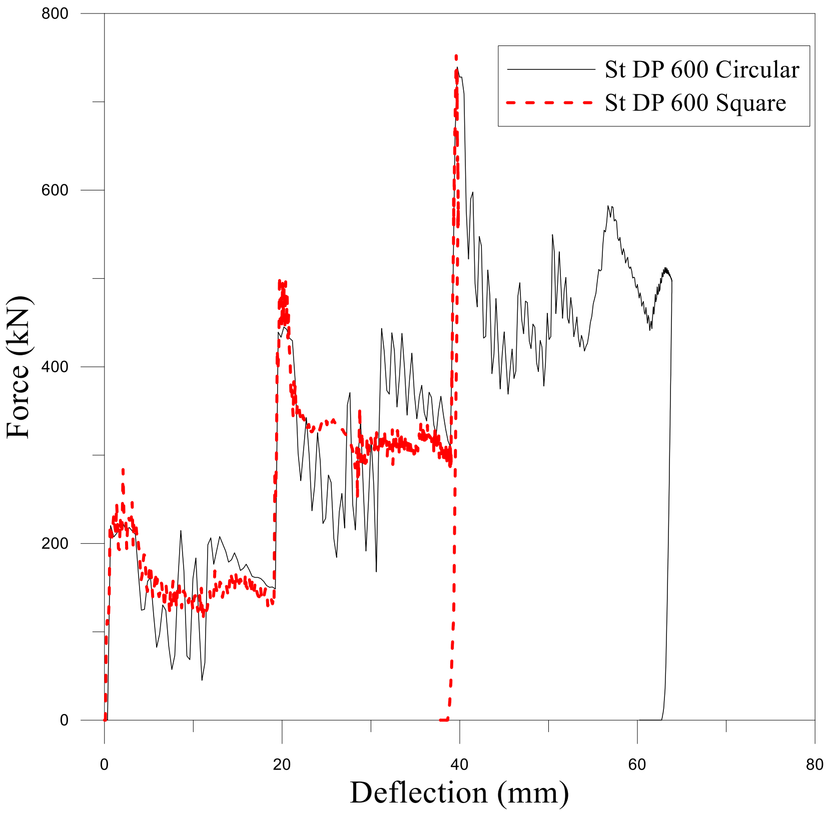

Figure 2.15 : Reaction force deformation curves for the systems having different cross sections and made of St DP600.

2.4 LS-DYNA modelling

2.4.1 Verification of LS-DYNA model

LS-DYNA presents explicit solver to run dynamic impact, crash phenomenas. Implicit solver feature has been added later to it. In explicit solver, time steps should be more smaller than implicit one. For the measurement issue, critical time step is measured according the mesh length and speed of sound.

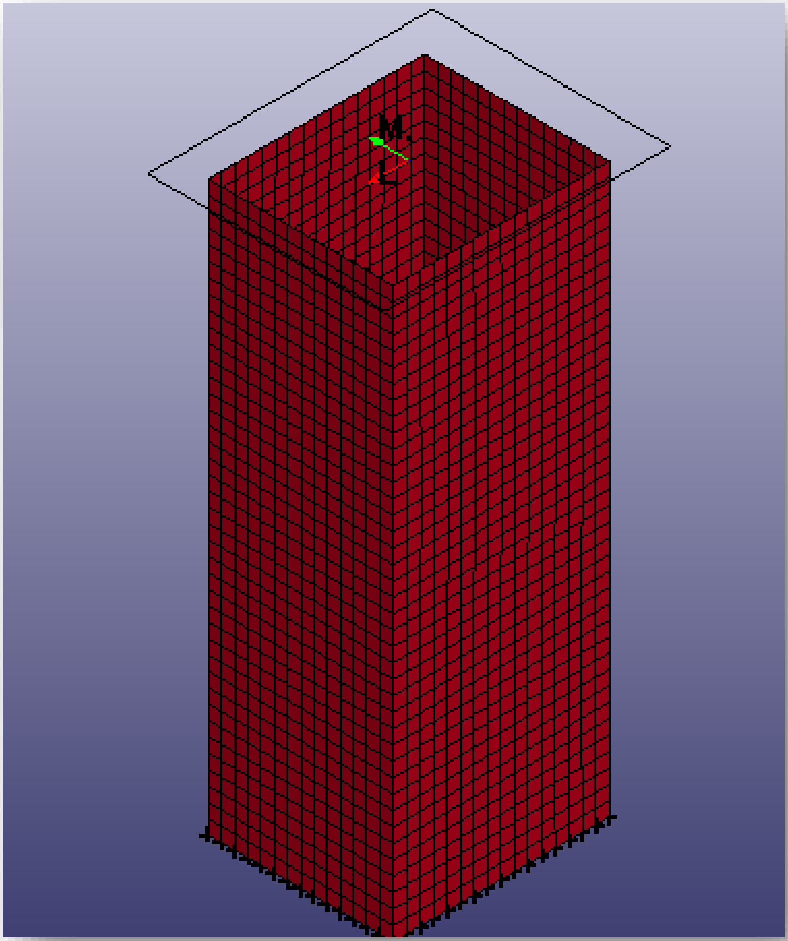

Figure 2.16 : Tube and rigid wall-impactor.

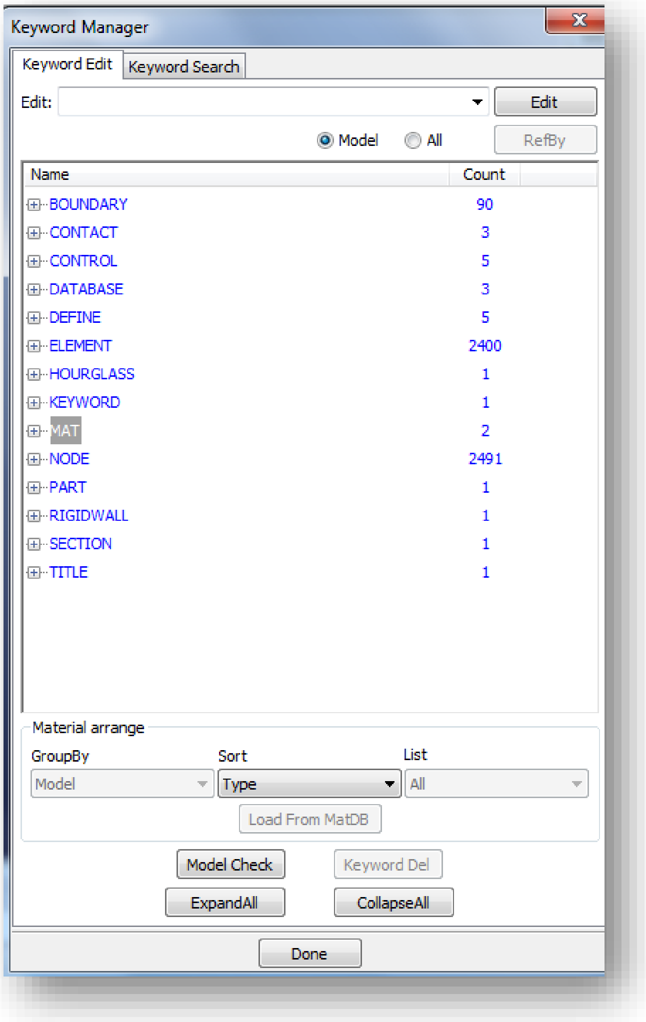

Figure 2.17 : LS-DYNA keyword input interface.

Material selection: Experimental data is used as stress-strain curve and 024-*PIECEWISE_LINEAR_PLASTICITY is suitable one as LS-DYNA material card input. Mesh unit length is 4 mm and SHELL element is used. Impactor is modelled via LS-DYNA library keyword *RIGIDWALL_PLANAR_MOVING_FORCES.

LS-DYNA and Abaqus units relations are important to understand unit input method of programs. So the Figure 2.18 is generally used in the pre-processor environment to be able to construct right unit system. An experimental and numerical work comparison from the literature for tube crash response was given in the Figure 2.19.

MASS	LENGTH	TIME	FORCE	STRESS	ENERGY	DENSITY	YOUNG's	35MPH 56.33KMPH	GRAVITY
kg	m	s	N	Pa	J	7.83e+03	2.07e+11	15.65	9.806
kg	cm	s	1.0e-02 N			7.83e-03	2.07e+09	1.56e+03	9.806e+02
kg	cm	ms	1.0e+04 N			7.83e-03	2.07e+03	1.56	9.806e-04
kg	cm	us	1.0e+10 N			7.83e-03	2.07e-03	1.56e-03	9.806e-10
kg	mm	ms	kN	GPa	kN-mm	7.83e-06	2.07e+02	15.65	9.806e-03
g	cm	s	dyne	dyne/cm²	erg	7.83e+00	2.07e+12	1.56e+03	9.806e+02
g	cm	us	1.0e+07 N	Mbar	1.0e+07 Ncm	7.83e+00	2.07e+00	1.56e-03	9.806e-10
g	mm	s	1.0e-06 N	Pa		7.83e-03	2.07e+11	1.56e+04	9.806e+03
g	mm	ms	N	MPa	N-mm	7.83e-03	2.07e+05	15.65	9.806e-03
ton	mm	s	N	MPa	N-mm	7.83e-09	2.07e+05	1.56e+04	9.806e+03
lbf-s²/in	in	s	lbf	psi	lbf-in	7.33e-04	3.00e+07	6.16e+02	386
slug	ft	s	lbf	psf	lbf-ft	1.52e+01	4.32e+09	51.33	32.17
kgf-s²/mm	mm	s	kgf	kgf/mm²	kgf-mm	7.98e-10	2.11e+04	1.56e+04	9.806e+03
kg	mm	s	mN	1.0e+03 Pa		7.83e-06	2.07e+08		9.806e+03
g	cm	ms	1.0e+1 N	1.0e+05 Pa		7.83e+00	2.07e+06		9.806e-04

Figure 2.18 : LS-DYNA analysis unit relations (LS DYNA, 2015).

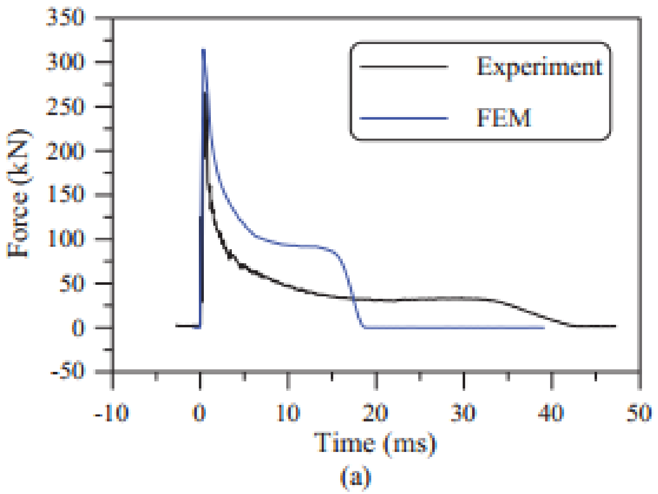

Figure 2.19 : Steel material FEA and experimental results (İnce et al., 2011).

2.4.2 Analysis and results

After the construction of the model, the results are taken via “ASCII” output card. For understanding if there is noise in data, time step choice must be suitable. While doing filtering it should be paid attention curve’ general shape. In this situations, peak forces generally change but general line stays in same level.

It is provided that LS-DYNA takes time stepping automatically. In theoratically background of that is related with numerical calculation algorithm of explicit time stepping. Critical time step is decided by the program. From the aspect of the user, it is only important post-processing section’s using rightly by selecting data writing option enough small. Deleting noise by this filtering takes us the right results.

2.4.3 Element lengths and time step

Filtering is applied when starting point seen at zeo point. According the issue, SAE 500 or SAE 600 filter was applied (Figure 2.20-2.21) (Livermore Software Technology Corporation, 2015).

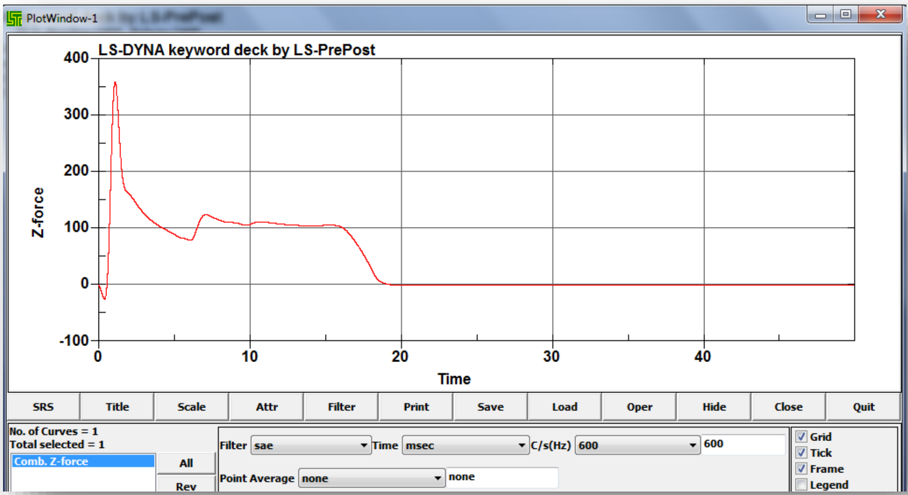

Figure 2.20 : Force time curve which SAE 600 filter is applied to.

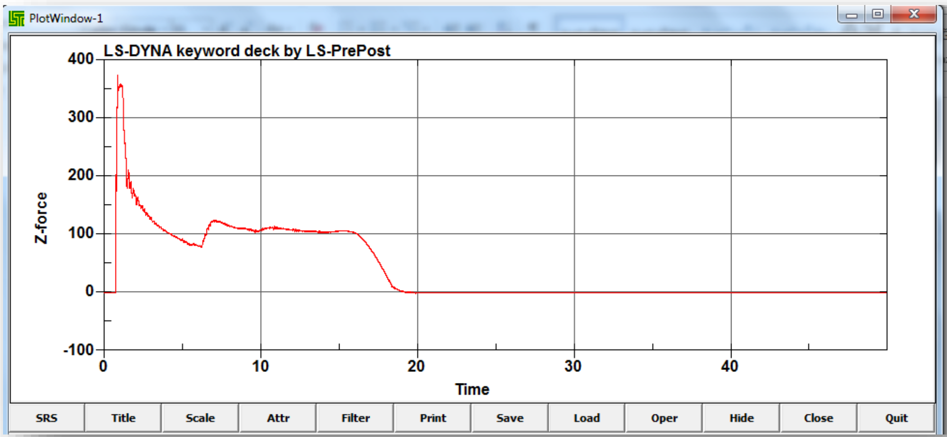

Figure 2.21 : Unfiltered force time curve

2.4.4 Reading energy value

Energy values is read drom the RGWall section. This section covers:

1) ASCII-GLSTAT provide kinetic, internal energy data.
2) History output option provide “Global”, “Part”, “Nod”, “Element” sourced output.

2.4.5 New model construction in LS-DYNA

Model information was shown in the Table 2.10. The tubes made of AL6063 and St DP 600 were modelled both in Abaqus and LS-DYNA. The model names in the Table 2.11 were used in all of other parts of the thesis.

Table 2.10 : Model lengths constructed in LS-DYNA.

Material	Tube 1	Tube 2	Tube 3
Thickness (mm)	2	2	2
Tube length (mm)	200	180	160

Table 2.11 : Model information constructed in LS-DYNA.

Cross Section	AL 6063	St DP600
Square	A1	A2
Circular	B1	B2

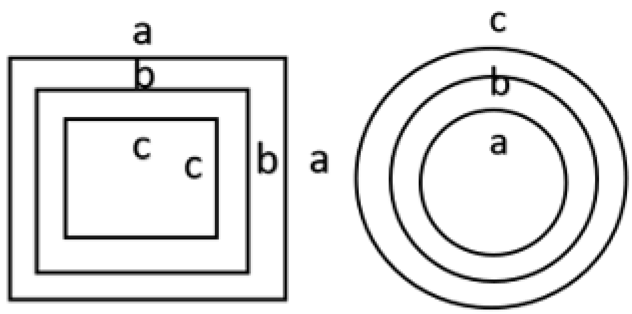

Figure 2.22 : Concentric tube system having square and circular cross sections.

2.4.6 Definitions

Contact between tubes are defined to simulate the analysis in real-like conditions. For this aim, *SET_SHELL command is isued. For all tubes, we should define it. Figure 2.23 represents shell definition in LS-Prepost environment to define contact relation between tubes.

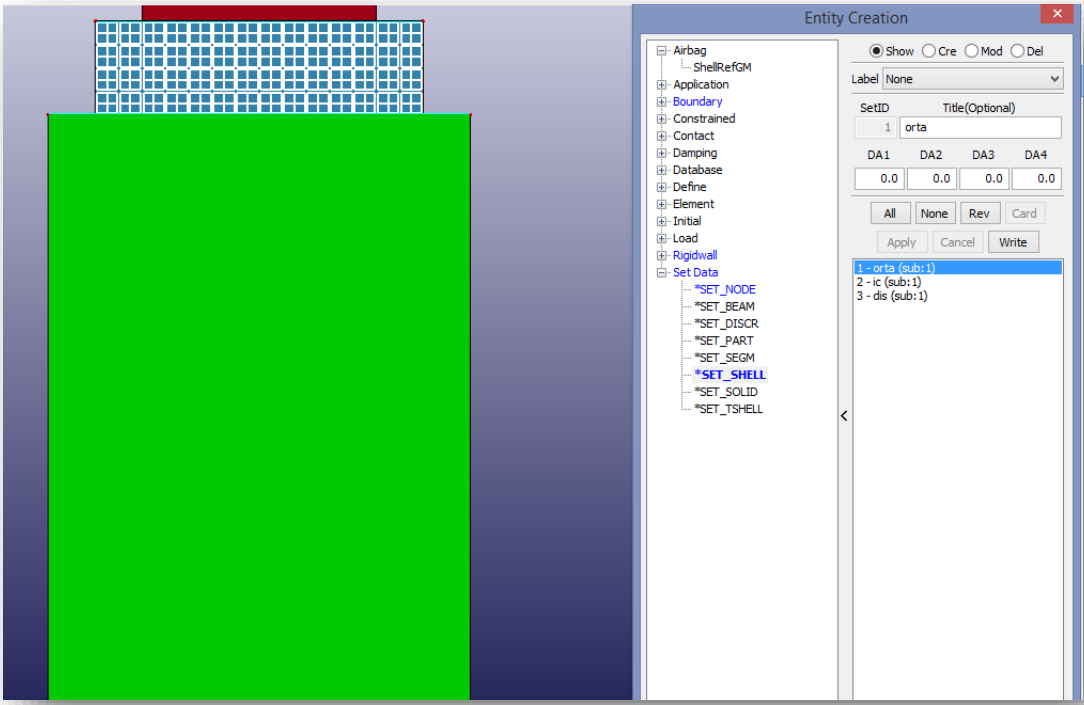

Figure 2.23 : Model A and SET_SHELL usage for middle tube.

2.4.7 Contact methods

LS-DYNA's different contact algorithms create different results so it is important to use right contact algorithm. Rigid wall contact algorithm as impactor is automatically provided by LS-DYNA. Self-contact of tubes are provided by *SURFACE_TO_SURFACE contact algorithm. Detailed explanations were showed in the Table 2.12, 2.13 and 2.14.

Table 2.12 : Contact definition between tubes.

*AUTOMATIC_SURFACE_TO_SURFACE
SSID:3 MSID:1 SSTYP:1 MSTYP:1
SSID:2 MSID:1 SSTYP:1 MSTYP:1
The innermost contacts middle tube, tube in the middle contacts the outermost one. This is defined via shell element groups. To define shell elements, 3 SET_SHELL were defined. For this purpose, SSTYP and MSTYP were selected type of 1.

Table 2.13 : Contact definition between tubes and rigid wall (optional).

*AUTOMATIC_NODE_TO_SURFACE

SSID:0 MSID:1 SSTYP:0 MSTYP:3

SSID:0 MSID:2 SSTYP:0 MSTYP:3

SSID:0 MSID:3 SSTYP:0 MSTYP:3

Explanation:

- SSTYP:EQ.0: segment set ID "surface to surface contact",
- MSTYP:EQ.3: part ID,
- MSID numbers 1,2 and 3 3 ayrı tüp partlarını ifade etmektedir.
- SSID is made 0. Rigid wall already contacts without definition of the contact.

Table 2.14 : Contact definition of self-contact of tubes (optional).

*AUTOMATIC_SINGLE_SURFACE

SSID:0 MSID:0 SSTYP:5 MSTYP:5

Self contact of tubes are provided by this command.
MSID definition is not necessary because only one tube is folded itself. SSTYP amd MSTYP is chosen as "5" (EQ.5: includes all for single surface definition).

2.4.8 Model setup

When the results are requested, ***DATABASE, *GLSTAT and *SPCFORC cards are selected by using enough small time steps.

Steps means when data would be saved in. Mesh size, impact velocity specify critical time step. ***GLSTAT provide energy output and velocity of impactor. Reactions forces in boundary condition nodes is take via *SPCFORC.

Outputs can be taken:

1. Reaction force on rigid wall
2. Velocity-time graphics on rigid wall
3. Reaction forces output at tubes' bottom nodes
4. Energy converted to plastic energy

5. Total energy behavior

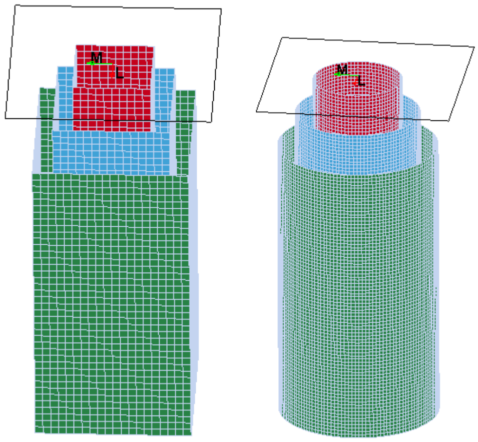

Figure 2.24 : A1 and A2 models at 0 milliseconds.

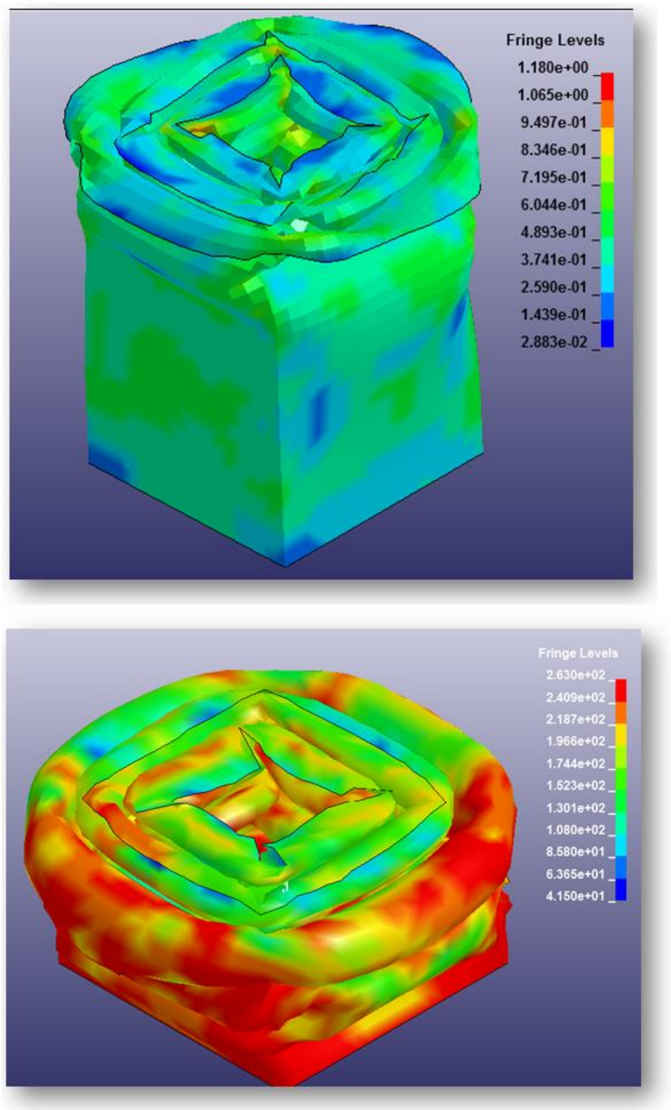

Figure 2.25 : A1 ve A2 models at 20 miliseconds**.**

2.4.9 Results

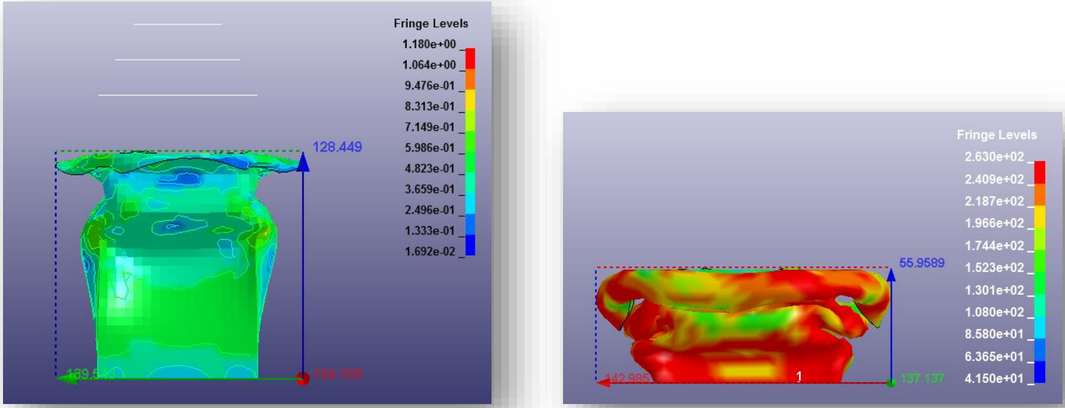

Figure 2.26 : Deformed Model A (A1:DP 600 and A2:AL 6063).

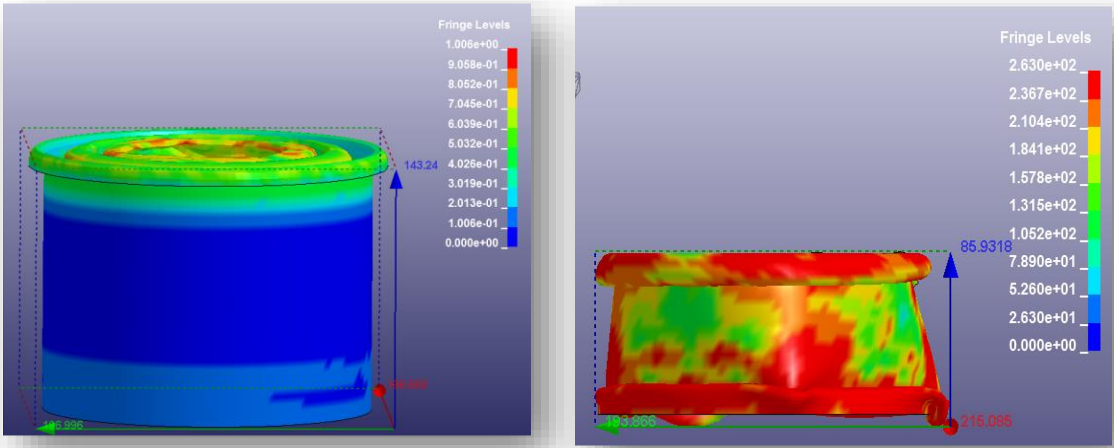

Figure 2.27 : Deformed Model B (B1: DP 600 and B2: AL 6063).

The Figure 2.26 shows that aluminium tubes have more deflection than steel ones. Colorful representation of the aluminium tube is different from the steel tube in consequence of yield point of aluminium tubes is lower than aluminium ones. Figure 2.27 is another good representation to predict physical test results before the tests. In general manner, tubes made of steel have lower deflections than aluminium ones for both cross sections.

Comparison for circular cross section of tubes between made of AL 6063 and St DP 600 was presented in the Figure 2.28. Before the tests, it was inferred that peak force regime would be higher for steel tubes comparing to aluminium ones. Surely, if the deflection issue make a important sense of the design consideration, then aluminium tubes' high deflection should be taken into the account.

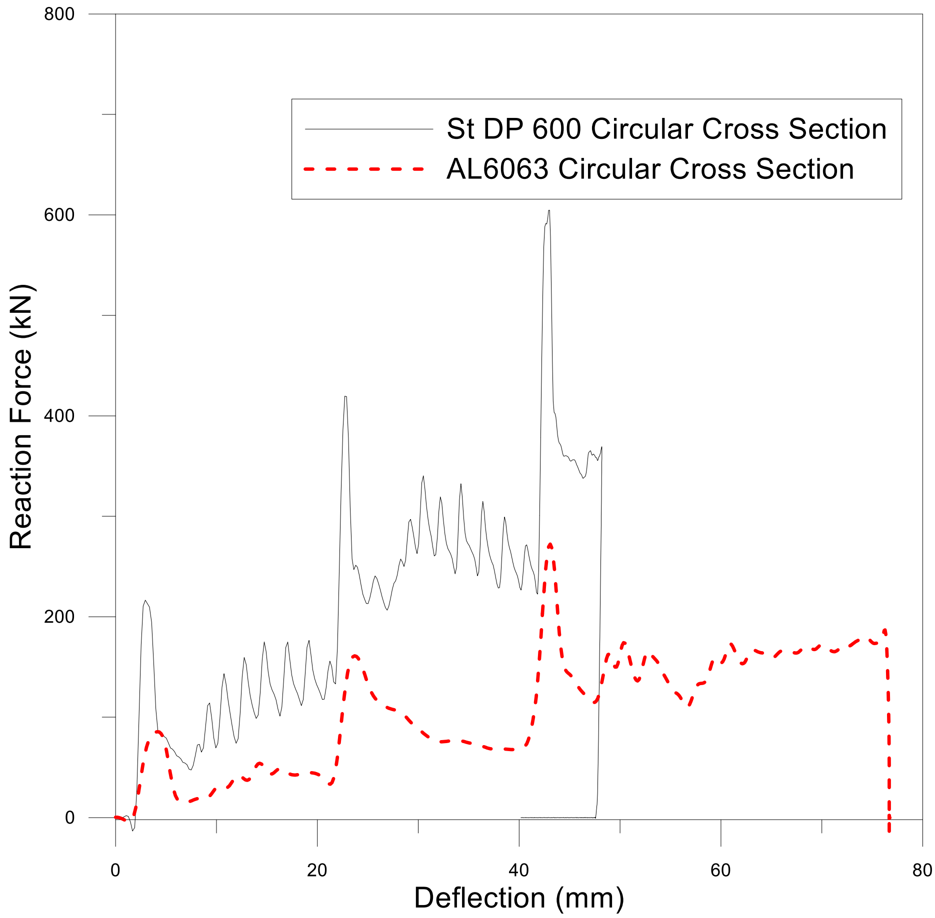

Figure 2.28 : Force-deflection curve of 2 different systems.

For energy calculation, kinetic energy conversion to internal energy is taken into the account. Total energy must be constant in global, kinetic energy is stored by conversion to the internal energy. For this type of processes, LS-DYNA's history-global card option is used as in the Figure 2.29. Outputs were recorded from *RIGIDWALL by *DATABASE_ASCII_option_GLSTAT.

Table 2.15 : Model A1, A2, B1, B2 peak forces.

Peak forces	DP600 (A1 and B1)	AL6063 (A2 and B2)
Model A (Square)	255-475-600 kN	100-185-225 kN
Model B (Circular)	300-640-830 kN	156-324-417 kN

Table 2.16 : Model lengths.

Material	Tube 1	Tube 2	Tube 3
Thickness (mm)	2	2	2
Tube length (mm)	200	180	160

Table 2.17 : Model A1, A2, B1, B2 deflections.

Deflections	DP 600	AL 6063
Model A1→A2	71,51 mm	158.9959 mm
Model B1→B2	55.943 mm	114 mm

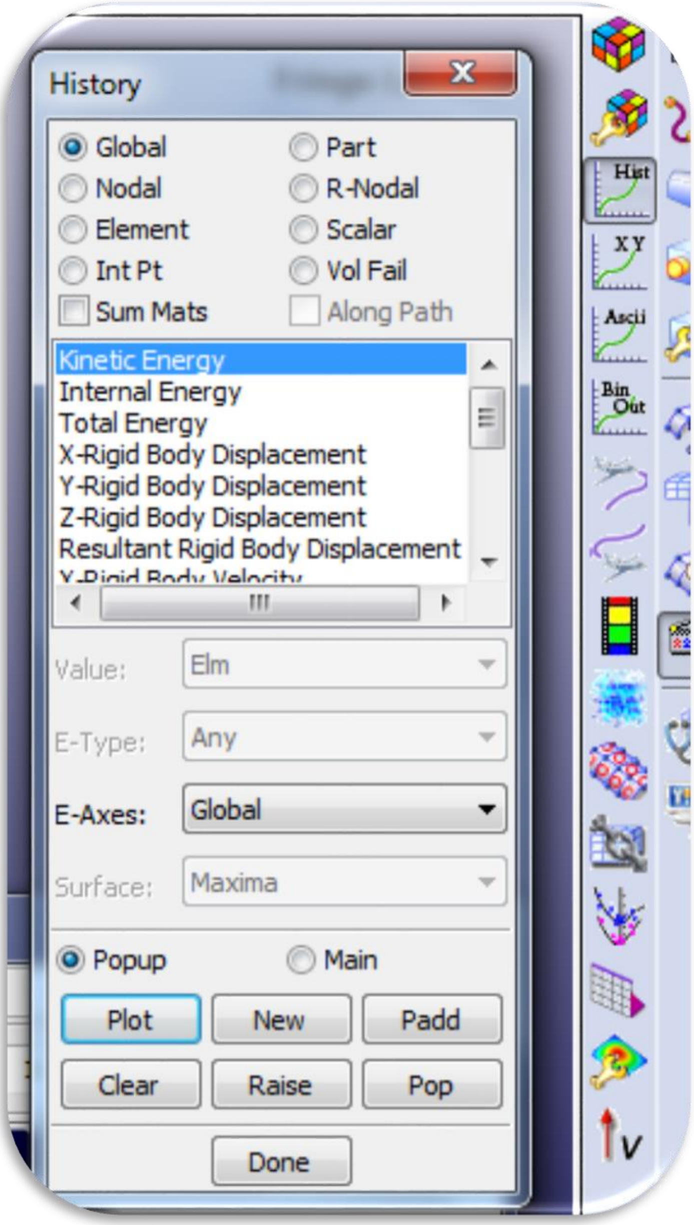

Figure 2.29 : Post-process screen of History Card.

Table 2.18 : Internal energy behaviour.

Internal energy change	DP 600	AL 6063
Model A1→A2	21.3 kJ	21.3 kJ
Model B1→B2	21.3 kJ	21.3 kJ

Table 2.19 : Model A1, A2, B1, B2 crushing times

Rigid wall movement duration	DP 600	AL 6063
Model A1→A2	15.3 ms	28.9 ms
Model B1→B2	10.6 ms	25.7 ms

2.5 Comparison of Numerical Analysis

The reaction force-deflection curves that Abaqus/Explicit and LS-DYNA/Explicit Solvers gave were used to make comment in same figure. Figure 2.30 shows square and circular cross section comparison.

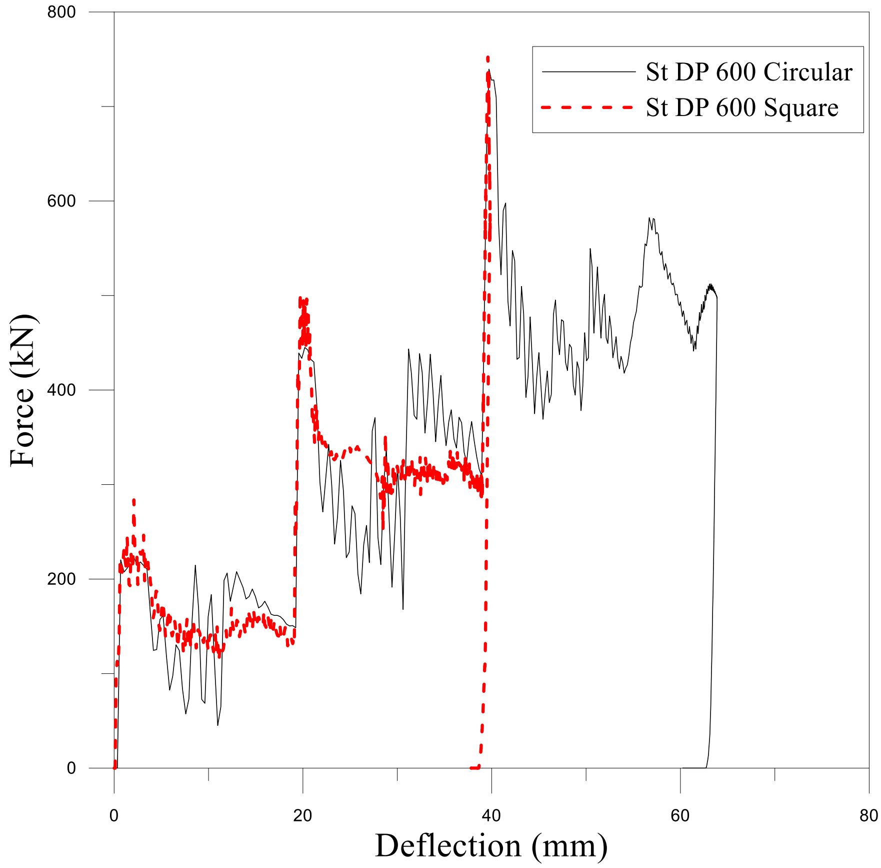

Figure 2.30 : Abaqus force-deflection comparison for St DP600 tubes (square-circular).

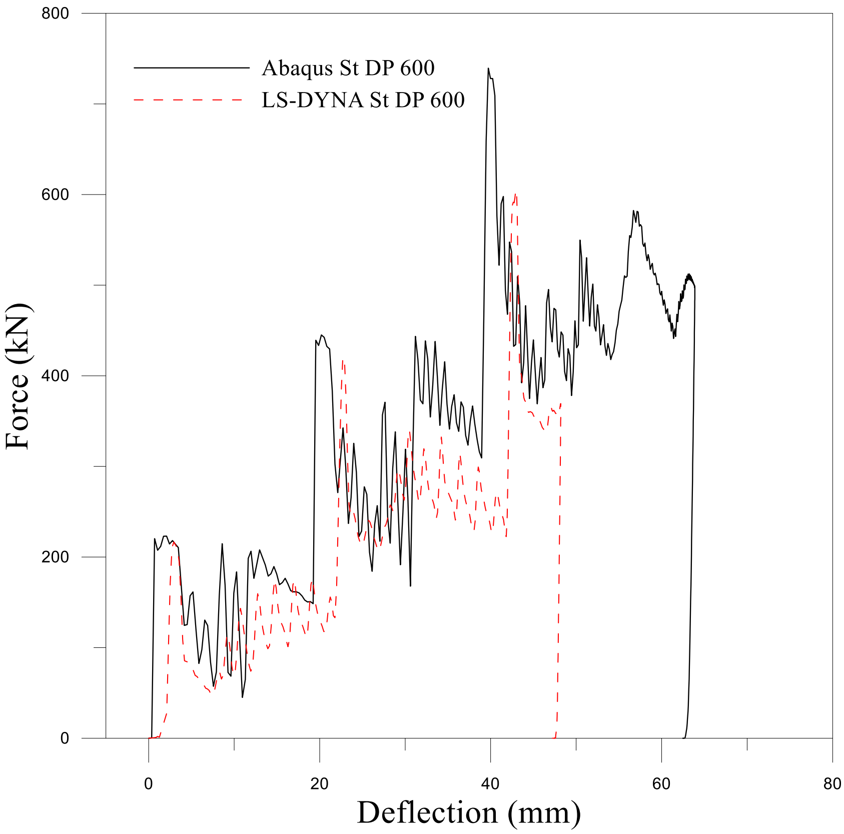

Figure 2.31 : Abaqus and LS-DYNA force-deflection comparison for St DP600 tubes (circular tubes).

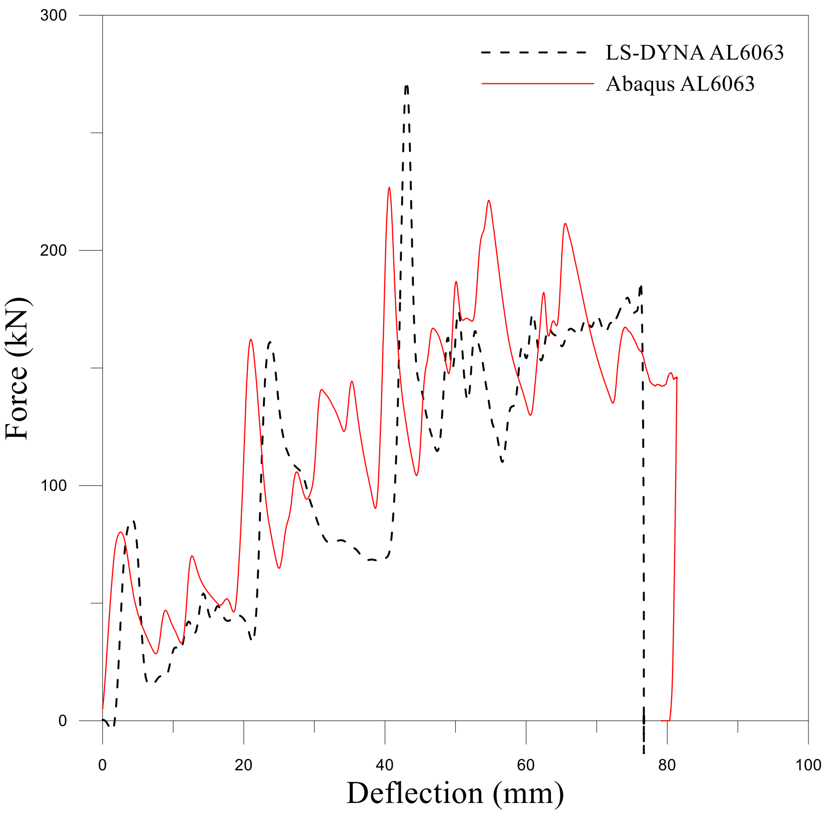

Figure 2.32 : Abaqus and LS-DYNA force-deflection comparison for AL 6063 tubes (circular).

The Figure 2.31 gives an idea for circular cross section comparison of DP 600 materials in Abaqus and LS-DYNA solvers, and the Figure 2.32 shows similar comparison for AL 6063 tubes. The Figure 2.33 shows mesh dependency of AL 6063 circular cross section tubes. According the figure first peaks of rection forces are seen close to each other. With the developing contacts second and third peaks are changed but smaller mesh elements do not make curve line low level. For instance, after the third peak, 1 mm mesh length' curve acts in higher level. However, in general manner, 1 and 2 mm mesh lengths shows similar behaviour including similar deflections.

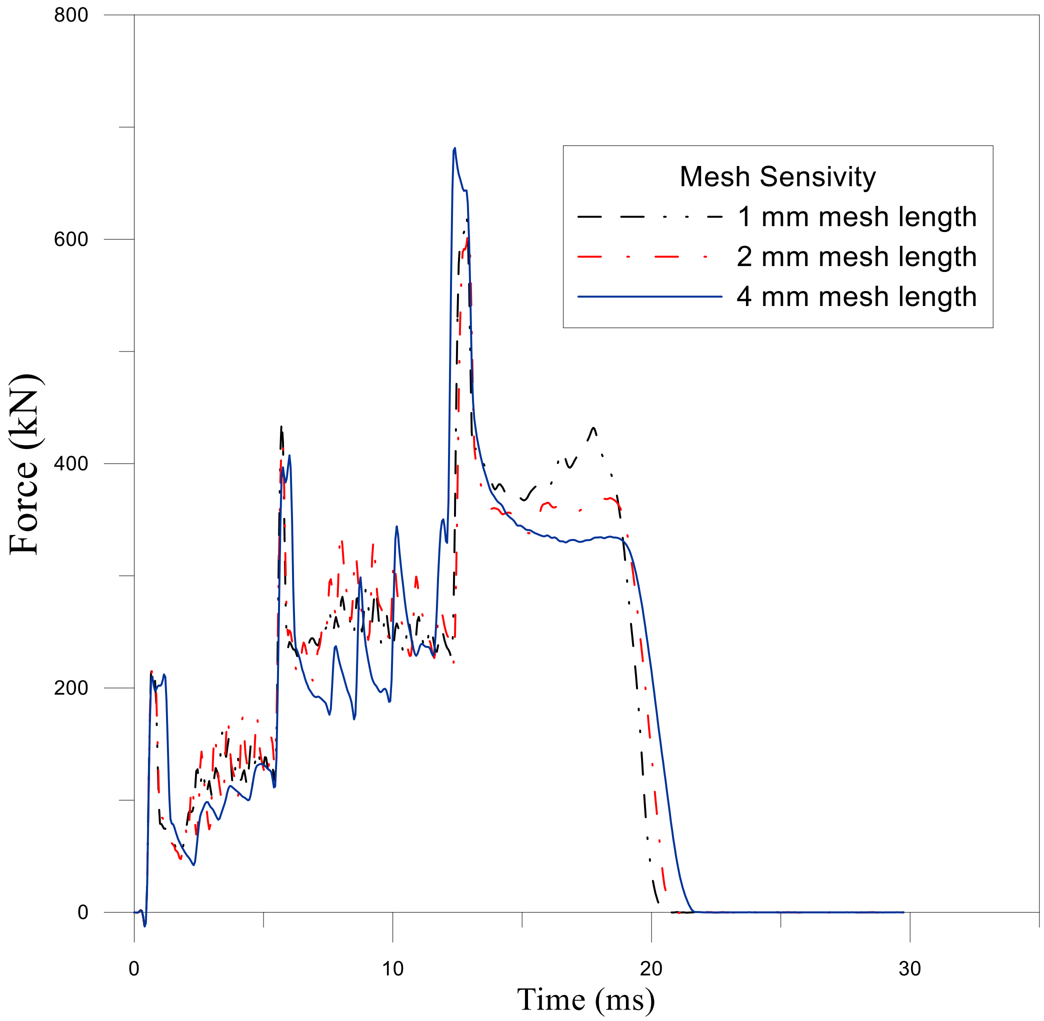

Figure 2.33 : Mesh sensitivity analysis of circular cross section AL 6063 tube sytem.

3 EXPERIMENTAL STUDIES

The experimental studies were conducted for samples that it could be fond in the steel and aluminium tube market. So, AISI 304 steel and aluminium 6063 tubes are used for the tests.

3.1 Dynamic Tests

3.1.1 AL 6063 circular tubes

Dynamics tests were conducted at 4.22, 3.77 and 3.28 m/s for the circular design. Produced three were showed in the Figure 3.1. The first sample loaded with 4.22 m/s has 112 mm deflection. The second sample loaded with 3.77 m/s has 97 mm and the third one loaded with 3.28 m/s has 77 mm deflection, respectively. Loading mass, impactor, had a mass of 1130 kg. Force-time, energy-time curves are shown in the Figure 3.7 and Figure 3.8. Peak forces are about 30, 75 and 140 kN. Different velocities did not make much sense.

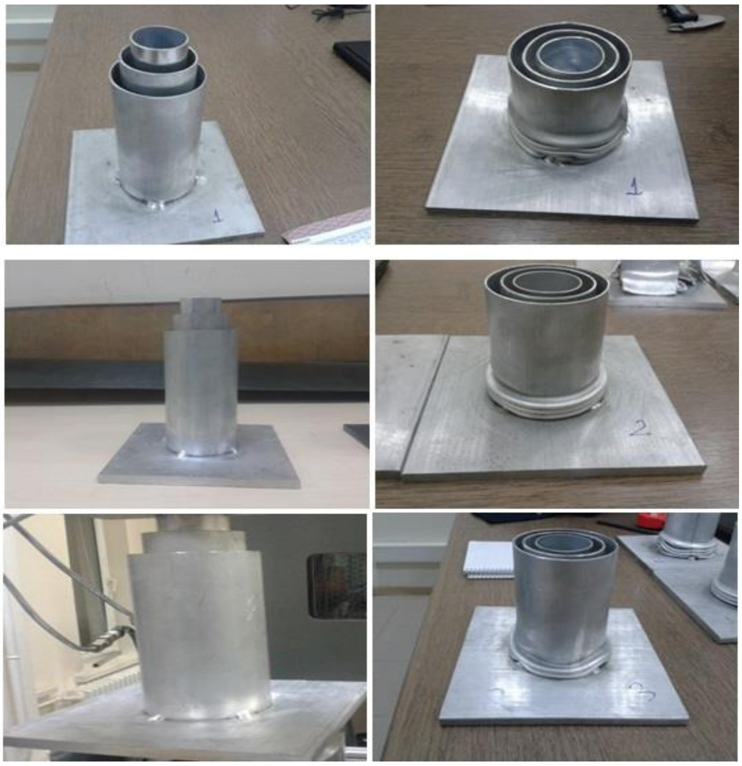

Figure 3.1 : AL 6063 samples before and after the tests

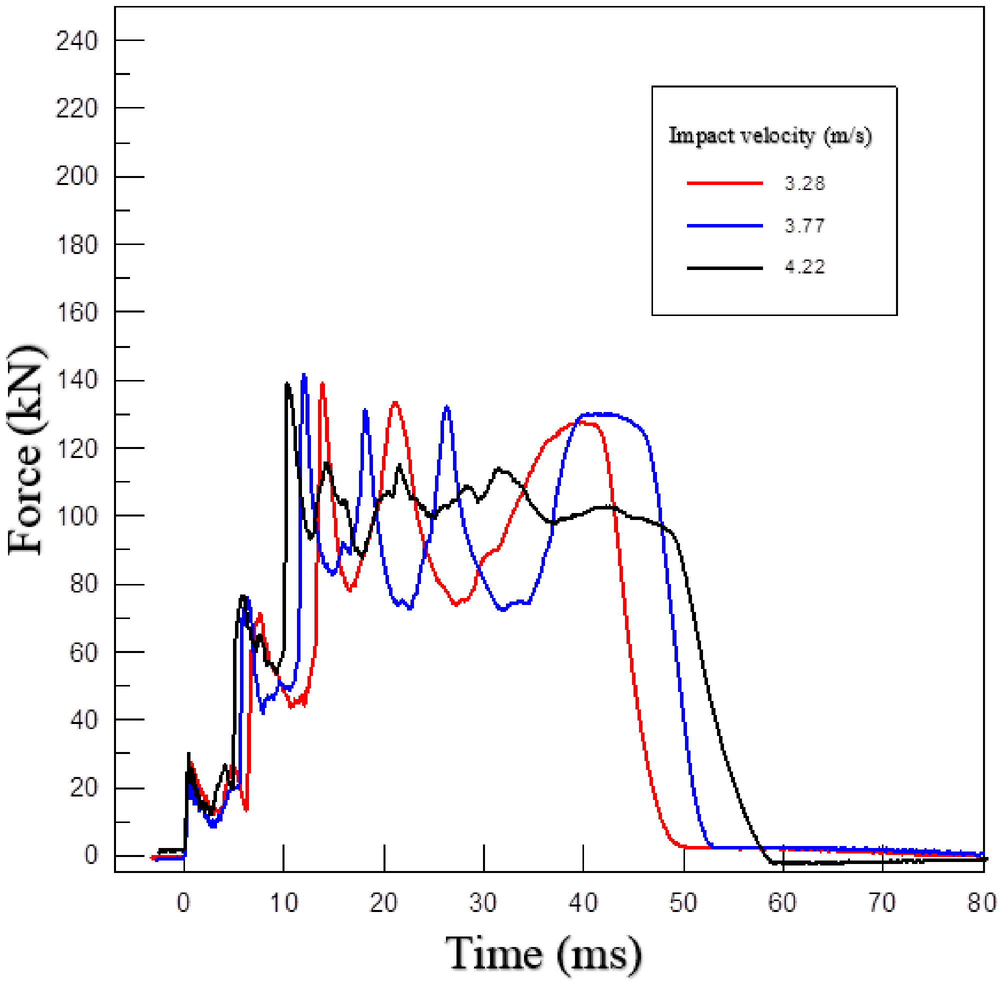

Figure 3.2 : Force-time curves of circular cross section tubes, made of AL 6063.

3.1.2 St 304 circular tubes

As in the Figure 3.3, tests were conducted for 4 different velocities; 2.69, 3.28, 3.77 and 4.22 m/s. It is obvious that there is no exact classification from the peak force and impact velocity side. Non-linear behaviour of material caused developing of new contacts between the tubes and some imperfections of the tubes, caused different folding mechanisms and foldings caused different contacts and as a result, different reaction force behaviours are occurred while under the area of force-deflection (deformation) curve is giving absorbed energy.

As in the Figure 3.3, according the different impact velocities, different deformation shapes were occurred. Most deflection was occurred in the case of the highest velocity 4.22 m/s. Increasing impact velocities; 2.69 m/s, 3.28 m/s, 3.77 m/s and 4.22 m/s respectively did not provide similar deformation and buckling mechanisms. 2.69 m/s impact velocity folded generally bottom side of tubes and additionaly, some crushing from the upper side. 3.28 m/s impact velocity’s effect on the upper side of tubes was seen in significant manner. Higher velocities developed foldings and contacts ın the bottom side of tubes.

Figure 3.3 : St AISI 304 samples before and after the tests

As in the Figure 3.4, 2.69 m/s impact case gives the highest peak force among the all tubes while 4.22 m/s impact case gives the lowest peak force response interestingly. However, the highest impact velocity cause to absorb the highest energy, as a result, force curve stays in higher level. This behaviour makes AISI304 more effective in higher impact velocities.

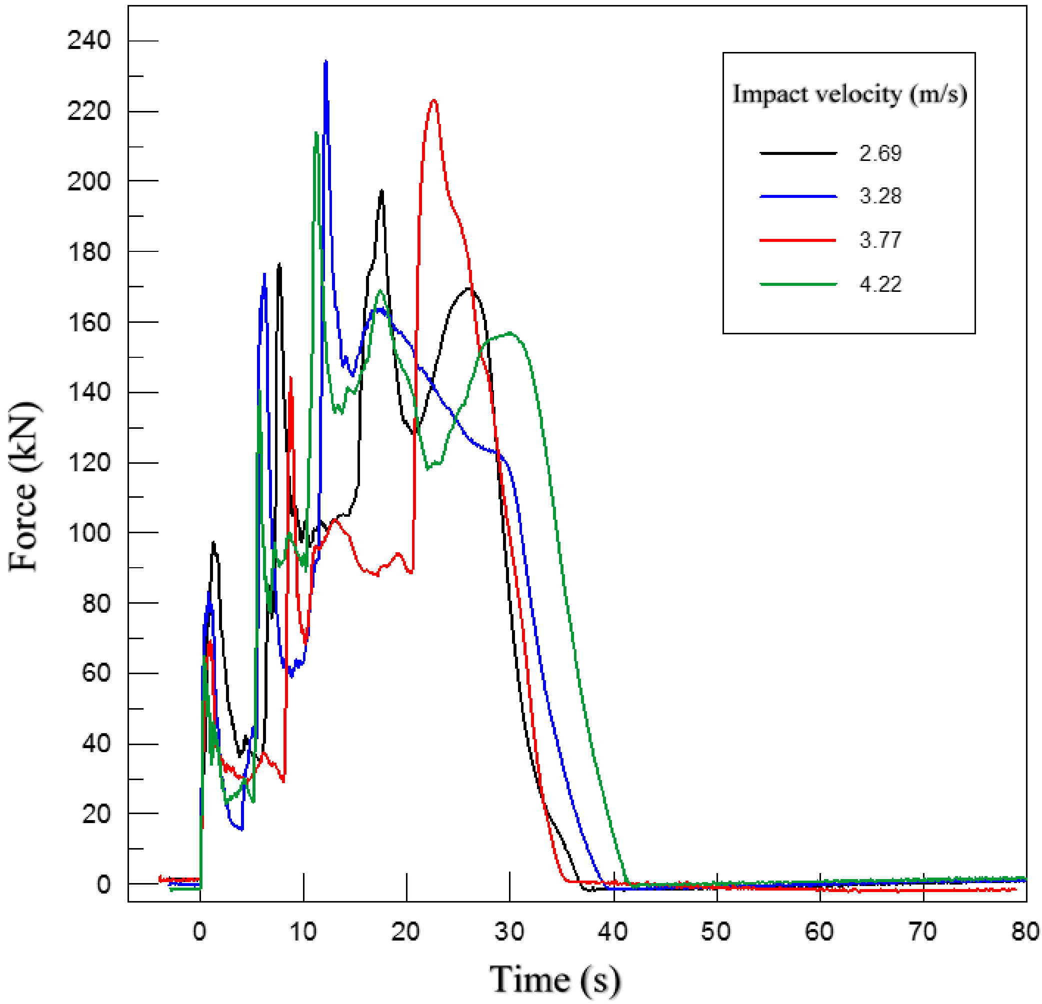

Figure 3.4 : Force-time curves of circular cross section tubes, made of St AISI 304

Figure 3.5 shows internal energies of systems. In practics; heat and friction losses do not change the total energy level signally. Kinetic energy is calculated by $\frac{1}{2}mV^2$ formulation and 4.22, 3.77, 3.28 and 2.69 m/s velocities are used to calculate differences between internal energy and kinetic energy.

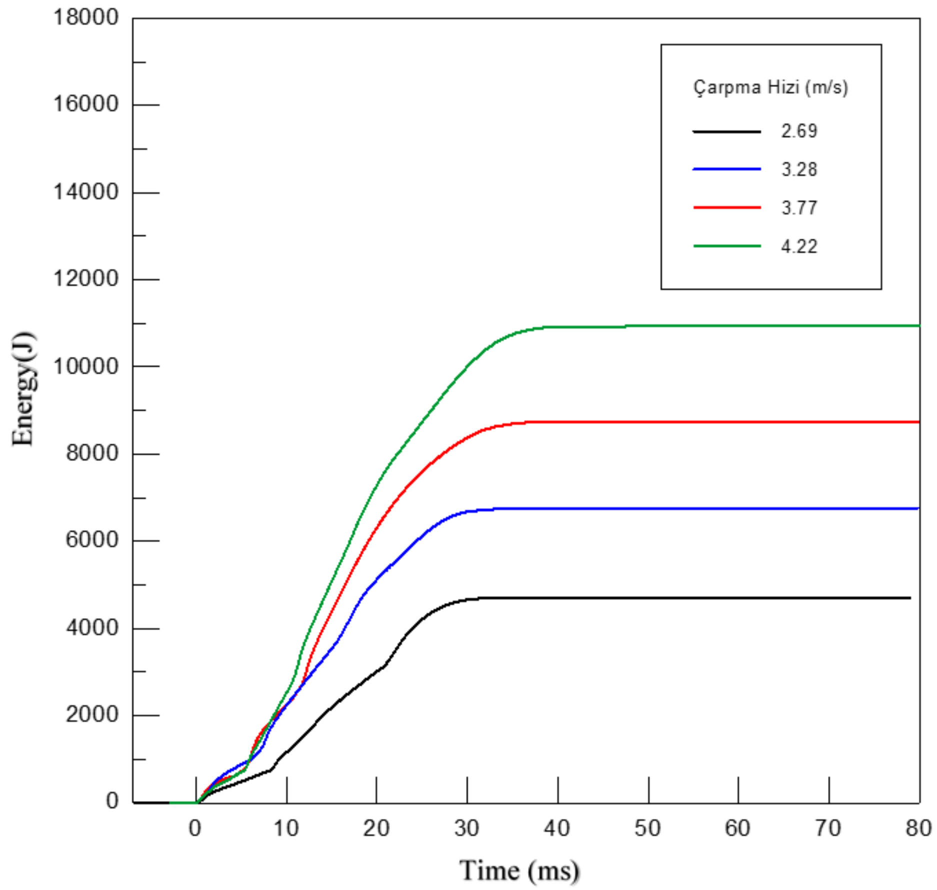

Figure 3.5 : Energy-time curves of circular cross section tubes, made of St AISI 304

3.1.3 AL 6063 square tubes

Square tubes that are made of aluminium showed edge failures because of sharp edges. Inner tubes shows progressively folding inspite of contact and pressure between eachself related with folding onto each other. The outmost tube did not resist horizontal pressure of the inner tube. While there was no difference between first peak forces in spite of different impact velocities, subsequent peaks were changed with the effect of interaction between tubes. For instance, the lowest impact velocity cause the highest 3rd peak force because of non-linear contact issues.

First two experiments were done with 4.22 m/s impact. The reason of difference between two experiments is that impactor of drop tower was impacted to tubes by rotating sample on the table. Deflections were measured as 123, 95 and 68 mm, respectively. 4.22 m/s impact caused 171 mm deflection. Unfortunately, the sensor could not recorded data that can be used to observe the effect of rotating the sample which was suitable to the impactor’s cross section. The outmost square tube that the side length of was 80 mm was teared. If it had thicker walls or smaller side lengths, it would be progressive buckling (Figure 3.6-3.7)

Figure 3.6 : AL6063 samples before and after the tests

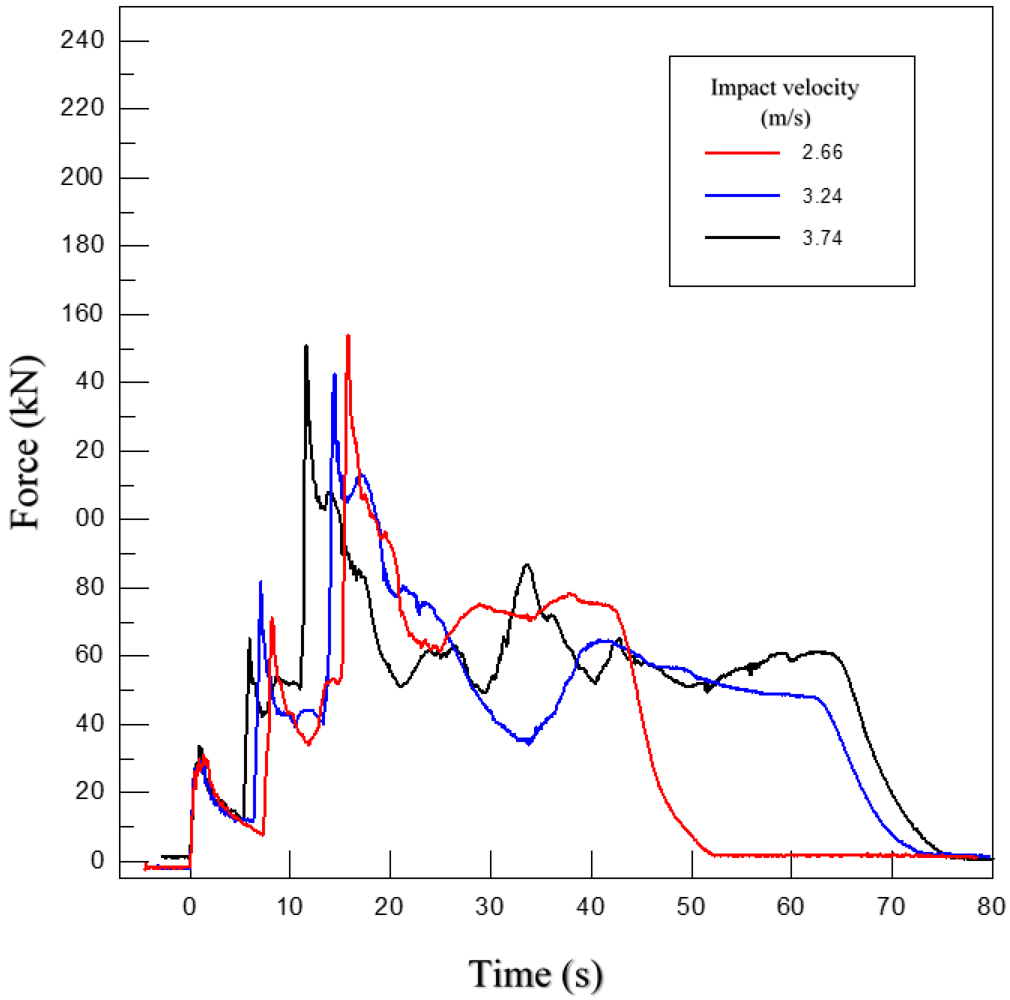

Figure 3.7 : Force-time curves of square cross section tubes, made of AL 6063

3.1.4 Innermost AL 6063 square, middle St AISI 304 circular outermost AL 6063 square

First attempt to construct the nested system in mixed geometry, was made by square-circular-square cross sections placement from in to out. 2 samples were tested in 3.77 m/s impact velocity. The first test was experimented and it was seen that outmost tube did not overlap with crasher surface because of the tube's larger dimensions than crasher. The second attempt was conducted to overcome the issue and as it is seen in the Figure 3.8, to change the orientation of the tube by turning it 45 degrees, did not give a different value. The outmost tube had 100 mm edge dimensions with 2 mm thickness. The middle tube had 78 diameter with 1.5 thickness, the innermost tube had 40 mm edge length with 2 mm thickness.

Figure 3.8 : The systems having from in to out: square AL6063, circular St AISI 304 and square AL 6063 tubes.

The innermost tube because of its short edge length, was folded progressively. Another reason of its folding progressively was middle tube’s being in blocker position. Middle tube did not give any fracture behavior thanks to its being circular, small diameter and made of steel. When the Figure 3.9 was investigated, because of the third tube’s non regular tearing as a result of its large dimensions, the peak force was not developed efficiently.

It is seen from the Figure 3.9 that 2 tests were conducted for 3.77 m/s velocity impact. According the observations for the first test, impactor surface did not match the sample’s top cross section in enough width. So sample was converted to suit it impactor shape, however, it has been concluded that outmost tubes had too large dimensions when tearings and impactor’s entering the outmost tube were observed.

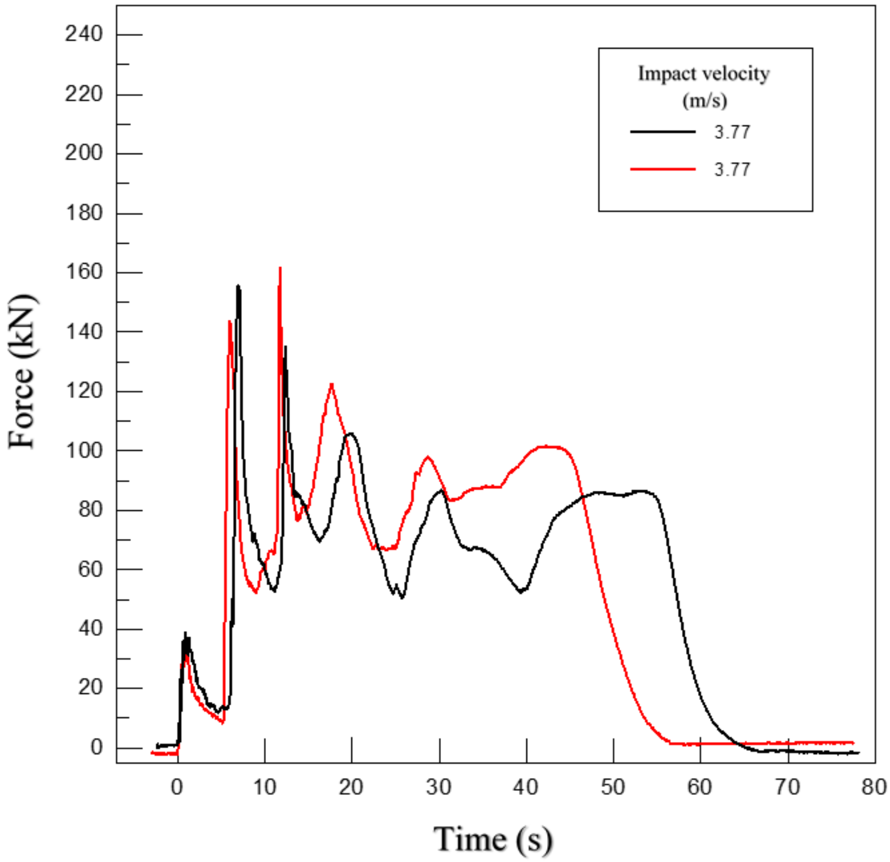

Figure 3.9 : Force-time curve of the systems having from in to out: square AL6063, circular St AISI 304, square AL 6063 tubes

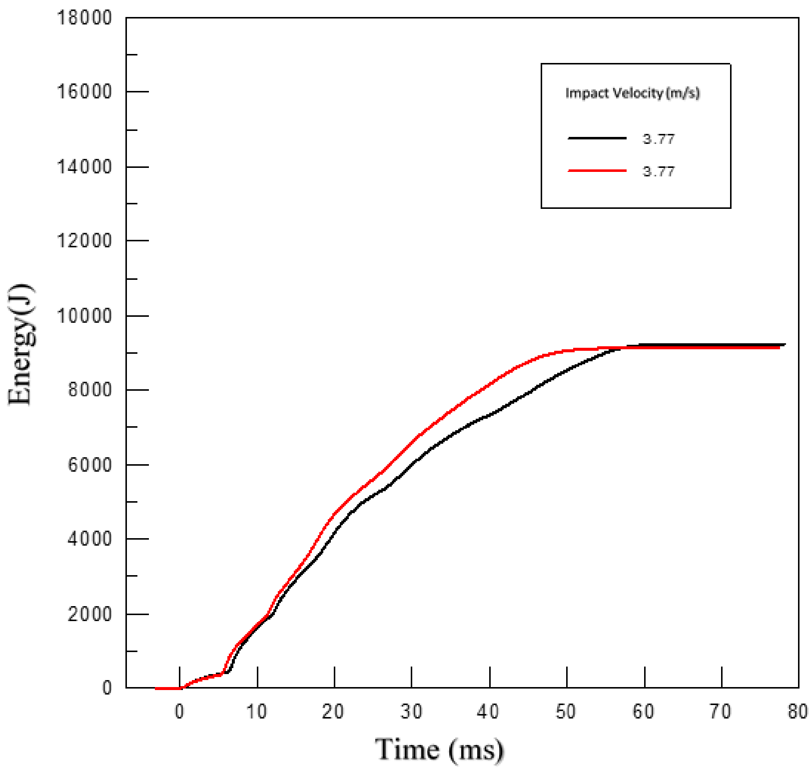

Figure 3.10 : Energy-time curves of the systems having from in to out: square AL6063, circular St AISI 304, square AL 6063 tubes

To provide progressively folding of the outermost tube, tube dimensions have been changed for that, outermost square tube was selected as 80 mmx80 mm cross section. The middle tube which is made of AISI 304 steel was selected as 51 mm diameter. The innermost tube has 30 mm*30 mm square cross-sections dimensions. Lastly, 4 samples were tested in 3 different velocities. The sample images before and after the tests were presented in the Figure 3.9. As it is seen in the Figure 3.9, tearing was again occurred. It was decided that tearing is closely related with the sharp edge design so soft edge turns should be provided for square cross sections. In addition to sharp edge issue, inner tubes' pressure on the outmost tube cause tearing. If the outermost tube has higher stiffness or thickness, it can be reached regular folding mechanisms without tearing. Dynamic tests were conducted in 2.69, 2.69, 3.22 and 3.77 m/ velocities, and the force-time and energy-time results were plotted in the Figure 3.12 and 3.13, respectively. Deflection distances of the samples were measured as 65, 65, 84 and 104 mm, respectively.

According the initial experience on the dimension issue, the outmost tube' dimensions was chanced to 80x80 mm cross section. The tube in the middle was decided as AISI 304 steel tube with 51 mm diameter, the innermost tube was decided as AL 6063 with 30x30 mm dimensions. 4 samples were produced and tested in 3 different impact velocity conditions (2.69 m/s twice, 3.22 m/s, 4.22 m/s). Figure 3.12 and 3.13 were obtained from these tests. Deflections were measured as 65, 65, 84 and 104 mm, respectively. As a similar behaviour with previous test samples, the outmost tube teared from the edges. The reason of that was thought to have too thin thickness and sharp edges.

Figure 3.11 : The systems having from in to out: square St AISI 304, circular St AISI 304, square St AISI 304 tubes

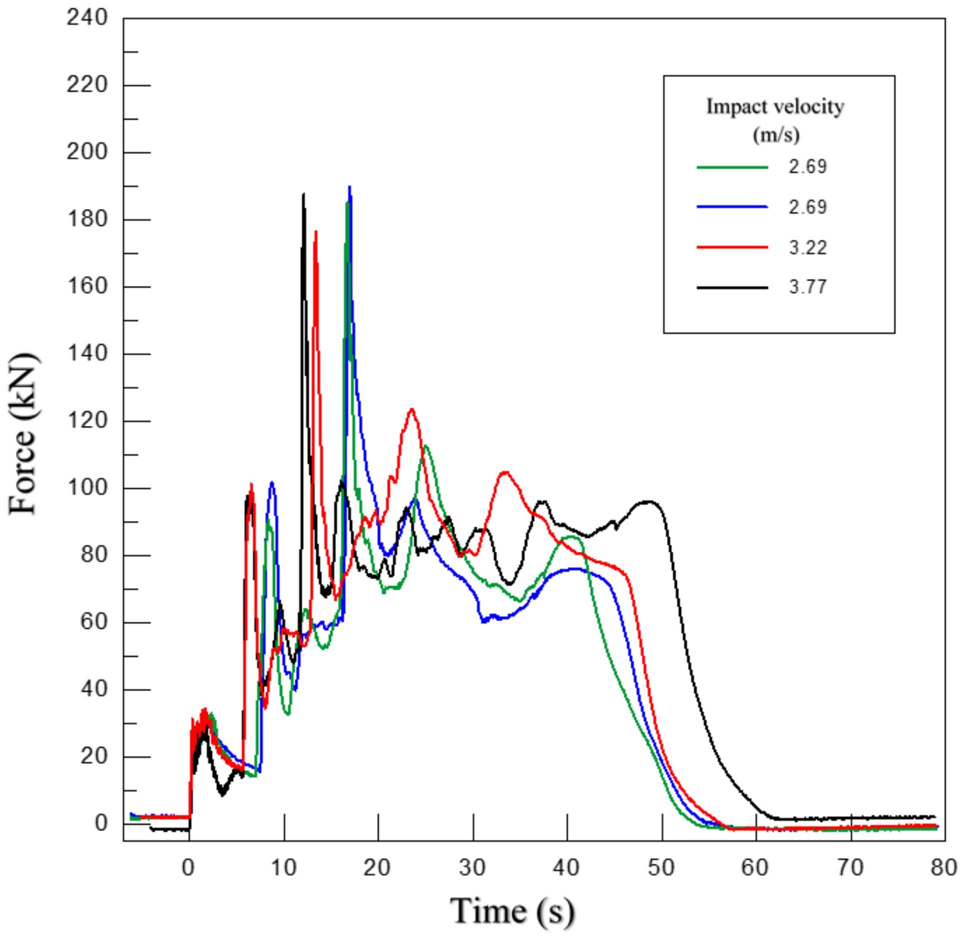

Figure 3.12 : Force-time curve of the systems having from in to out: square St AISI 304, circular St AISI 304, square St AISI 304 tubes

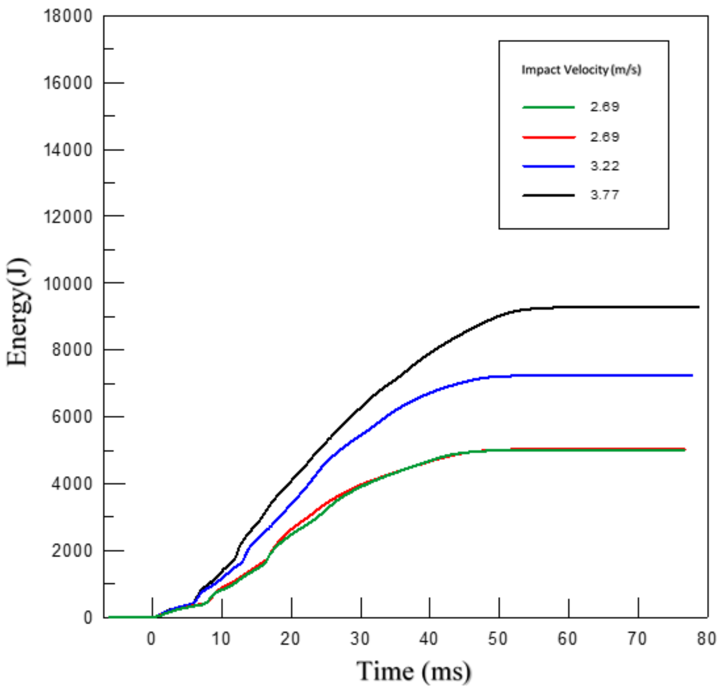

Figure 3.13 : Energy-time curve of the systems having from in to out: square St AISI 304, circular St AISI 304, square St AISI 304 tubes

Figure 3.14 : The systems having from in to out: square AL 6063, square St AISI 304, square AL 6063 tubes

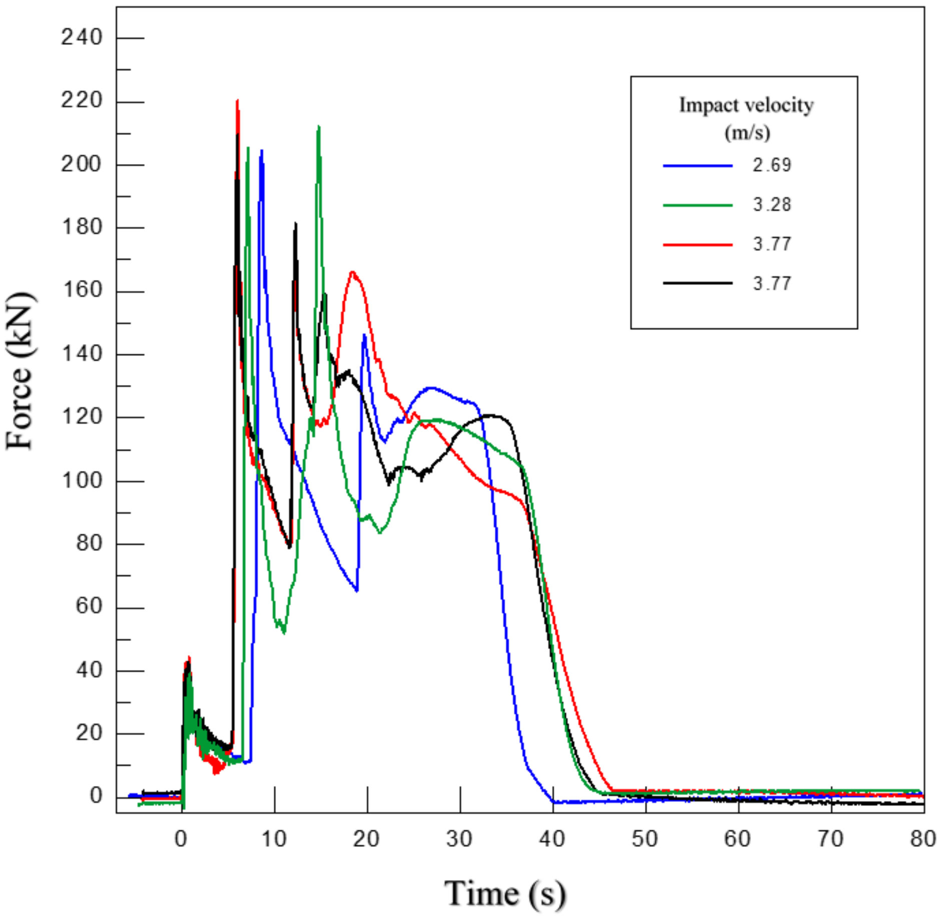

Figure 3.15 : Force-time curve of the systems having from in to out: square AL 6063, square St AISI 304 and square AL 6063 tubes

System that inner and outest tubes are made of AL 6063 and square cross section and the middle tube is square cross section and made of St AISI 304 was produced as 4 samples and tested. Tests are conducted in 3.77, 3.77 (twice), 3.22 and 2.69 m/s. Crushing distances are 73, 75, 64 and 48 mm progressively. Figures representing before the tests and after test cases are shown in the Figure 3.12. Data from the force-time and energy-time graphics were drawn in Figure 3.15 and 3.16.

At the lowest impact velocity, tearings did not occur at the outmost tube. 3.28 m/s velocity impact caused tearings at the top section which can be thought related with imperfections. According the Figure 3.15, it was seen that AISI 304 steel tube in the middle increased peak force so much than aluminium ones. It can be inferred initially that first tube can be constructed as made of steel while other ones made of aluminium.

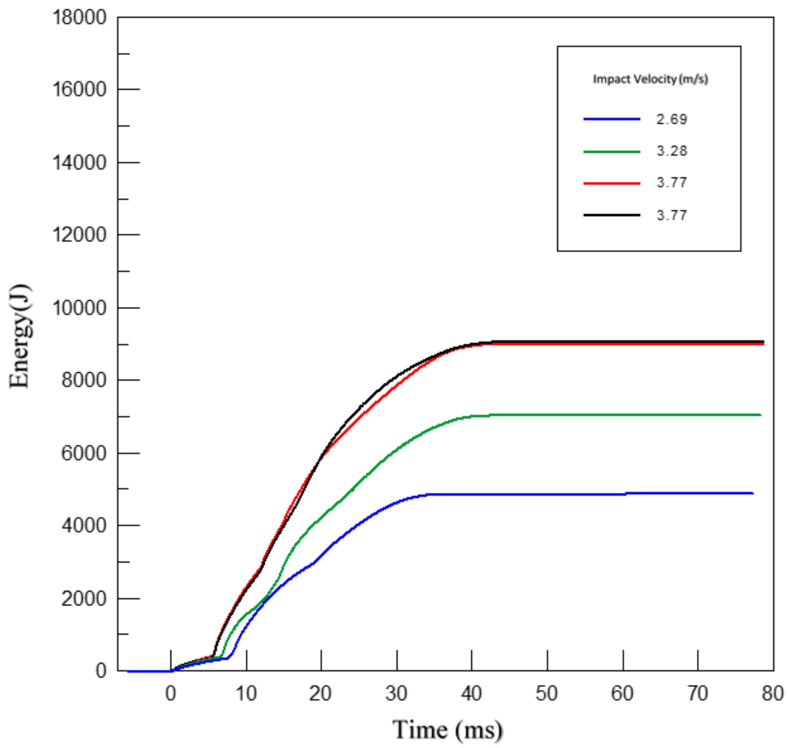

Figure 3.16 : Energy-time curves of the systems having from in to out: square AL 6063, square St AISI 304 and square AL 6063 tubes.

3.1.5 Innermost St AISI304 square, middle St AISI304 circular outermost St AISI304 Square

The Innermost and outermost tubes which are of square cross section and made of AISI 304 Steel, were manufactured as 4 samples and tested in dynamical impact conditions. Tests were conducted at 3.77, 3.22, 2.69 and again 2.69 m/s velocities. Deflections are 83, 69, 50, 45 mm, respectively. Images before and after the tests are represented in the Figure 3.17.

Figure 3.17 : The systems having from in to out: square, circular and square St AISI 304 tubes.

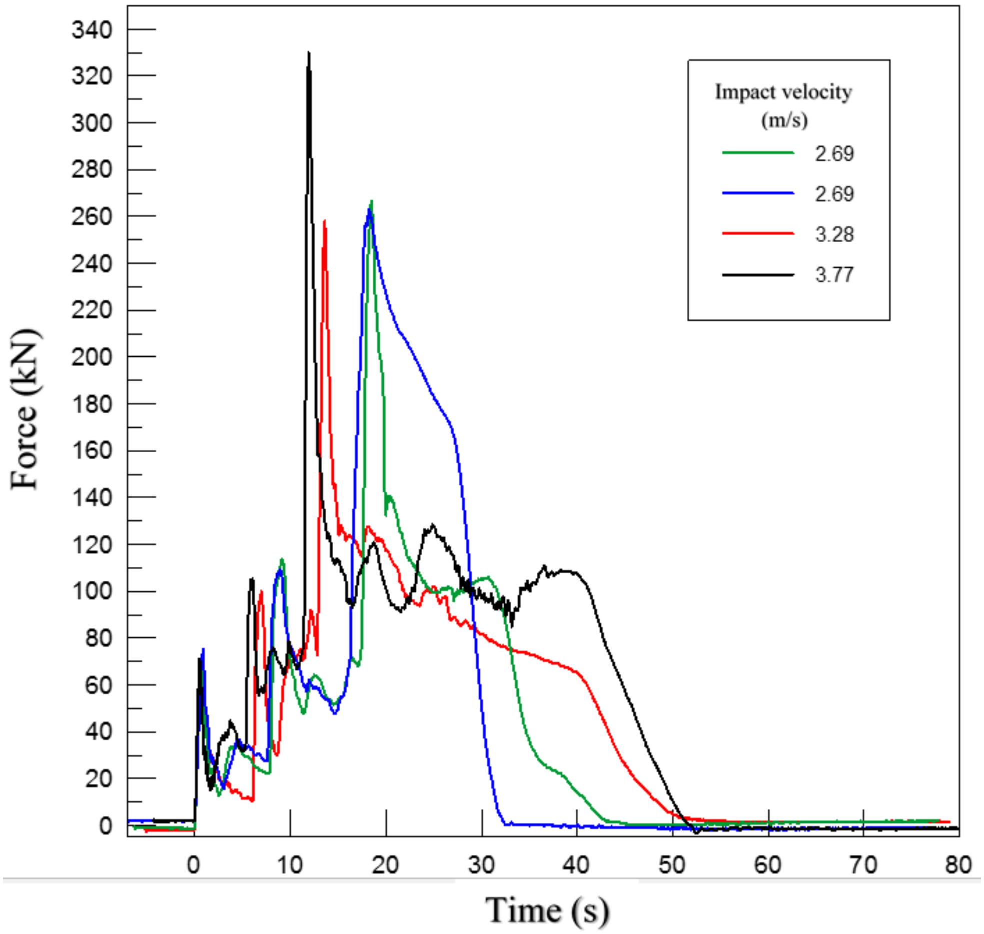

Figure 3.18 : Force-time curves of the systems having from in to out: square , circular and square St AISI 304.

The highest impact cases, 3.77 m/s and 3.28 m/s caused similar tearings as in the Figure 3.17. The lowest impact velocity, 2.69 m/s was obtained twice to see effect of rotaing the tube system, and it was seen that impactor's close-fitting on the top cross section of tubes provided different bucklings of the outmost tube. Progressive buckling developed on the innermost tube without global bucklings even it had small cross section. The tube in the middle was buckled easily thanks to its having circular cross section. The outmost tube showed tearing behaviour similar to aluminium tubes. It was concluded that stress concentration at the edges must be removed via chambered tubes' placement in design consideration. The Figure 3.18 represents the peak force behaviour of the systems loaded with different impact velocities. The Figure 3.19 was drawn for energy behaviour.

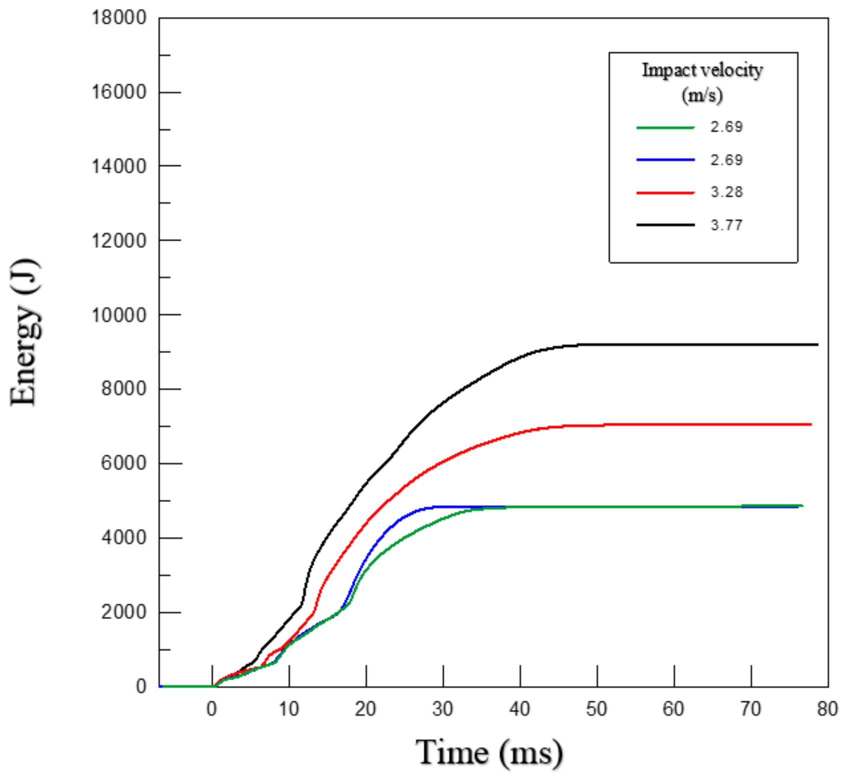

Figure 3.19 : Energy-time curves of the systems having from in to out: square, circular and square St AISI 304 tubes.

3.1.6 Innermost AL 6063 circular, middle St AISI 304 circular outermost AL 6063 circular

The system that the innermost and outmost tubes which are of square cross section and made of AISI 304 Steel and the middle tube which is of circular cross section and made of AISI 304 steel were manufactured as 4 samples and tested in dynamical impact conditions. Tests were conducted at 3.77, 3.22, 2.69 m/s velocities. Deflections are 74, 62, 50 mm, respectively. Images before and after the tests are represented in the Figure 3.20. And the force-time curves and energy-time curves of different samples which were tested in different velocities are presented in the Figure 3.21 and 3.22.

The most valuable result in this system test setup is that different type of materials combinations provided becoming close each self for the second and the last peak forces. It is inferred that steel and aluminum combination can provide higher mean crush force to have higher crush force efficiency.

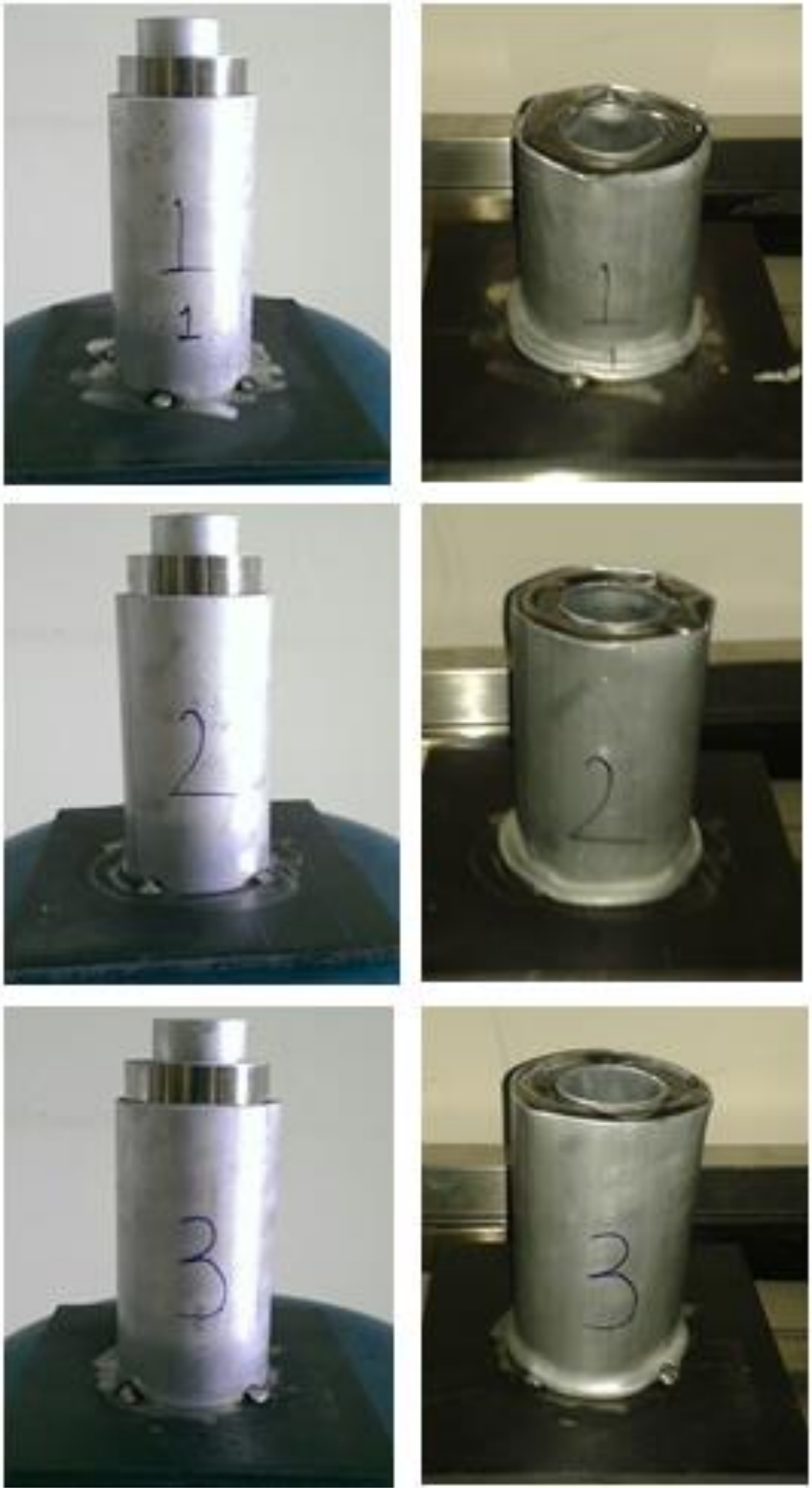

Figure 3.20 : The systems having circular St AISI 304 tubes from in to out.

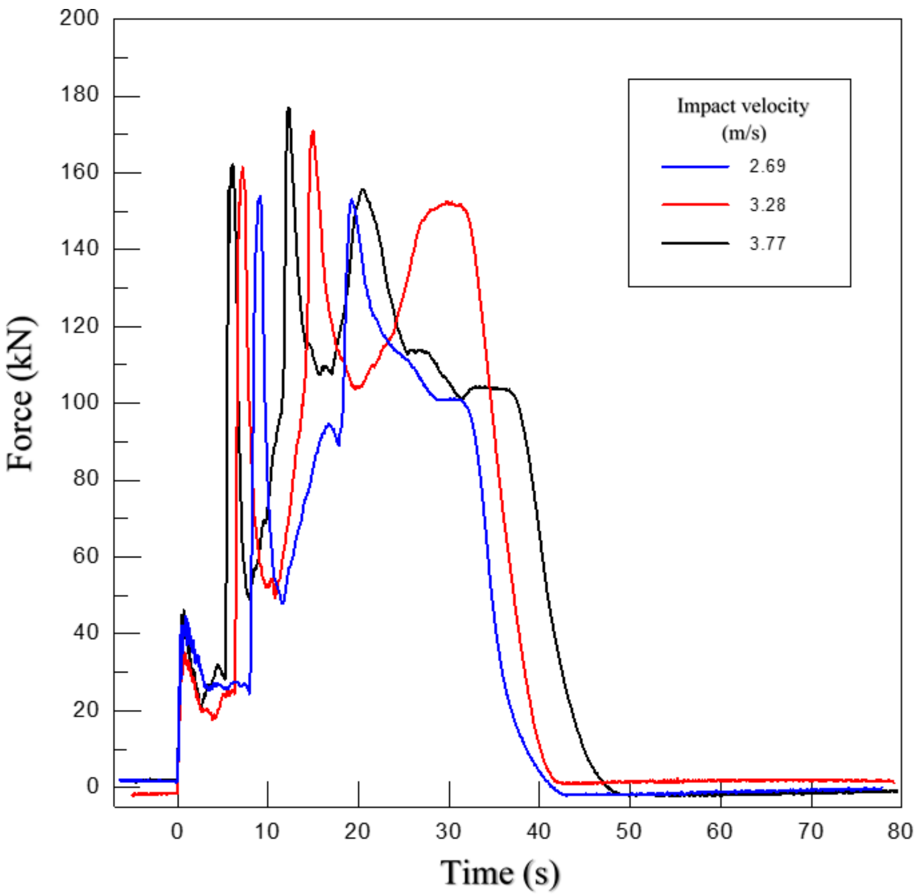

Figure 3.21 : Force-time curves of the systems having from in to out: circular AL 6063, St AISI 304 and AL 6063 tubes.

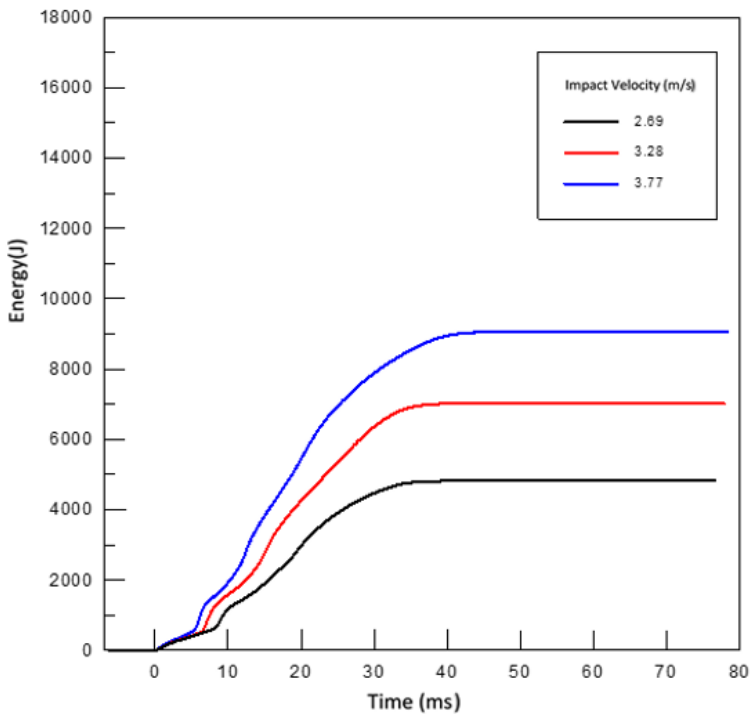

Figure 3.22 : Systems' energy behaviour having inside AL6063 Circular, Middle St AISI304 Circular, Outside AL6063 Circular Tube

The Figure 3.21 showing the system having AL6063 circular tube inside, St AISI304 circular tube in the middle, AL6063 circular tube outside means that the tube in the middle could be placed as innermost tube to reach same level peaks for better CFE value. The Figure 3.22 was placed to show internal energy behaviour of axially loaded tubes for different impact velocities.

3.2 Discussion About the Dynamic Test

3.2.1 2.69 m/s impact case

In the tests which are done in 2.69 m/s; the samples number 10 and 14 have shown better specific energy absorbing capability (SEA) than others. The issue is shown in the comparison in the Figure 3.20. Sample number 10, 17 and 23 have shown less maximum peak force than others. Number 6, 20 and 23 samples have shown better Mean crush force ability than others. Lastly, crush force efficiency is seen the highest at samples 17 and 23.

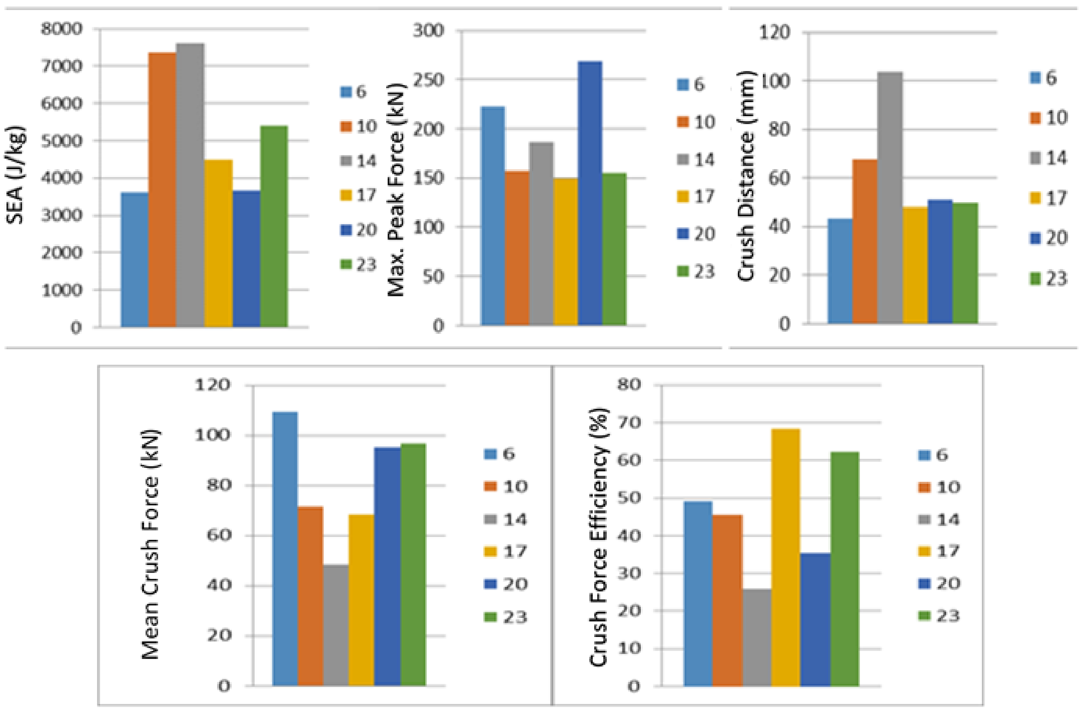

Figure 3.23: Test efficiency comparisons for loaded with impact velocity 2.69 m/s

3.2.2 3.28 m/s impact case

In the tests which are done in 2.69 m/s; the samples number 3, 9 and 13 have shown better specific energy absorbing capability (SEA) than others. The issue is shown in the comparison in the Figure 3.24. Sample number 9 having square cross section and has more deflection than others, Samples 3 and 9 have less peak forces values. Sample number 4 provides more mean crush force value than others and sample 3, 4 and 22 provide more crush force efficiency.

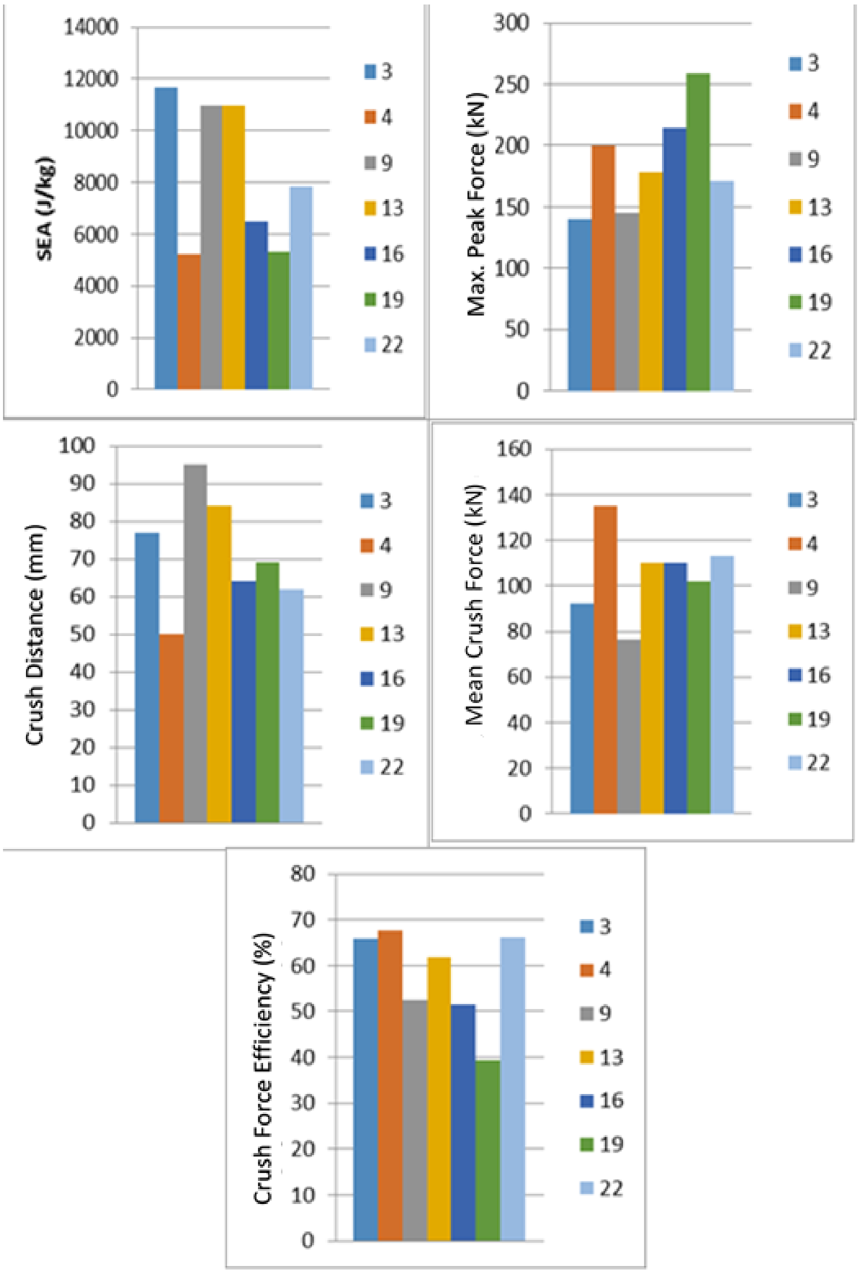

Figure 3.24: Test efficiency comparisons for loaded with impact velocity 3.58 m/s

3.2.3 3.77 m/s impact case

In the tests which were done in 3.77 m/s; the samples number 2, 8 and 12 have shown better specific energy absorbing capability (SEA) and crush force efficiency than others (Figure 3.25). The longest crush distance was observed at sample 8 (AL6063 square tubes) Maximum peak force value is seen at samples 5 and 18. Mean crush force efficiency is higher at the sample 5 (AISI 304 circular tubes) than others. Samples 8, 12 and 18 shows lower crush force efficiency than others.

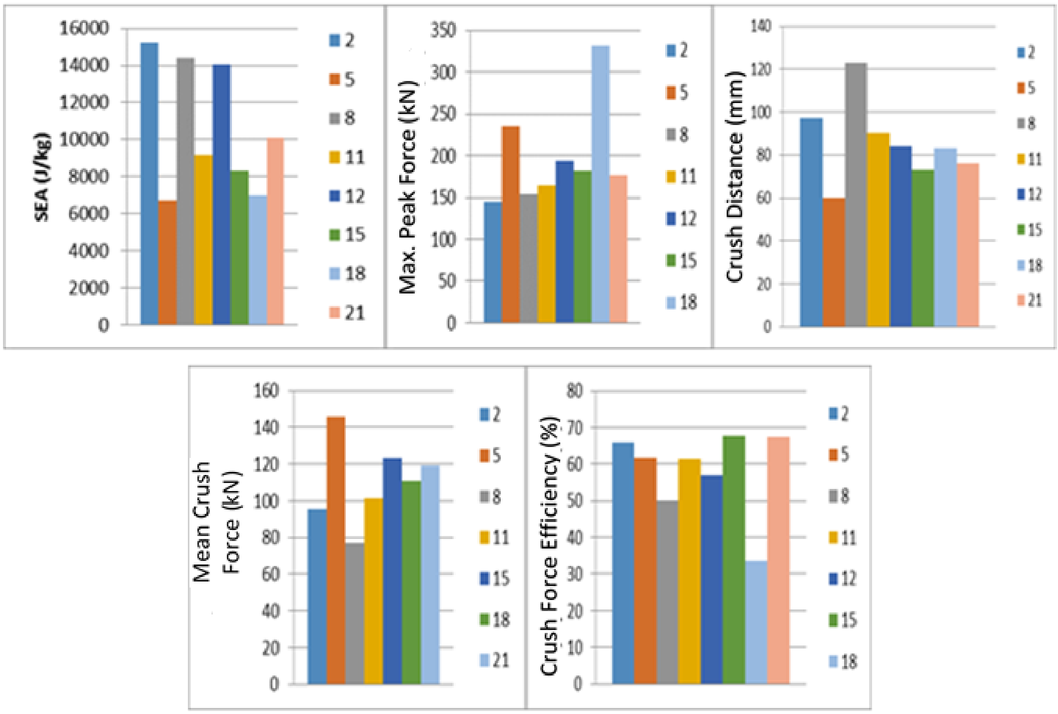

Figure 3.25: Test efficiency comparisons for loaded with impact velocity 3.77 m/s

3.2.4 4.22 m/s impact case

In the tests which were done in 4.22 m/s; the samples number 1 and 7 were compared and the design made of AL 6063 and having circular cross section have shown better specific energy absorbing capability (SEA) and crush force efficiency than other (Figure 3.26). It means that aluminium and circular design shows better efficiency that the steel and circular one.

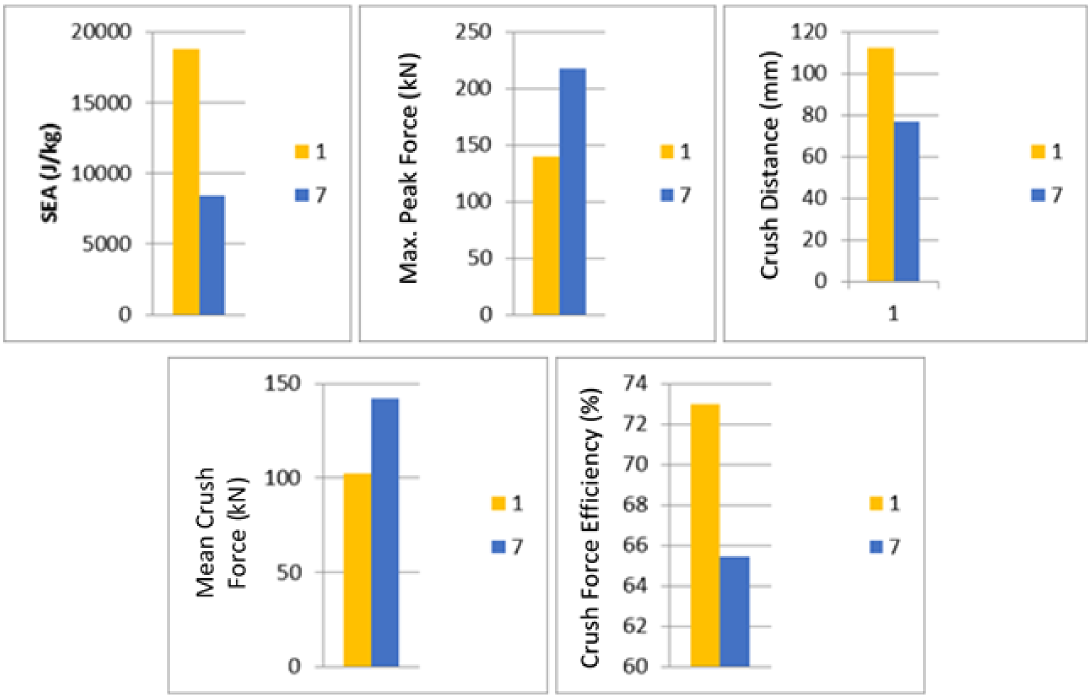

Figure 3.26 : Test efficiency comparisons for loaded with impact velocity 4.22 m/s

As a result of comparisons, the circular cross section design made of AL 6063 has been selected as the most suitable one from the point of crush force efficiency (CFE). Later, with the results of the experiments, the optimum design was analyzed in LS-DYNA (Explicit) Solver.

Table 3.1 : Comparison table

Sample Number	Materials and Dimensions W=width					Impact Velocity (m/s)	SEA (J/kg)	Crush Distance (mm)	Peak Force (kN)
1	**Innermost**	Circular AL6063	D=50 mm	Length=200 mm	Thickness=2 mm	4.22	18775	112	30-76-140
	Middle	Circular AL6063	D=70 mm	Length=180 mm	Thickness=2 mm				
	Outermost	Circular AL6063	D=90 mm	Length =160 mm	Thickness=2 mm				
2	**Innermost**	Circular AL6063	D=50 mm	Length =200 mm	Thickness=2 mm	3.77	15223	97	24-77-145
	Middle	Circular AL6063	D=70 mm	Length =180 mm	Thickness=2 mm				
	Outermost	Circular AL6063	D=90 mm	Length =160 mm	Thickness=2 mm				
	Innermost	Circular AL6063	D=50 mm	Length =200 mm	Thickness =2 mm				

3	**Middle**	Circular AL6063	D=70 mm	Length =180 mm	Thickness =2 mm	3.28	11662	77	28-72-140
	Outermost	Circular AL6063	D=90 mm	Length =160 mm	Thickness =2 mm				
4	**Innermost**	Circular AISI304	D=50 mm	Length =200 mm	Thickness =1.2 mm	3.28	5207	50	98-178-200
	Middle	Circular AISI304	D=76 mm	Length =180 mm	Thickness =1.5 mm				
	Outermost	Circular AISI304	D=89 mm	Length =160 mm	Thickness =1.5 mm				
5	**Innermost**	Circular AISI304	D=50 mm	Length =200 mm	Thickness =1.2 mm	3.77	6728	60	84-176-236
	Middle	Circular AISI304	D=76 mm	Length =180 mm	Thickness =1.5 mm				
	Outermost	Circular AISI304	D=89 mm	Length =160 mm	Thickness =1.5 mm				
6	**Innermost**	Circular AISI304	D=50 mm	Length =200 mm	Thickness =1.2 mm	2.69	3620	43	70-144-223
	Middle	Circular AISI304	D=76 mm	Length =180 mm	Thickness =1.5 mm				
	Outermost	Circular AISI304	D=89 mm	Length =160 mm	Thickness =1.5 mm				
7	**Innermost**	Circular AISI304	D=50 mm	Length =200 mm	Thickness =1.2 mm	4.22	8413	77	73-143-217
	Middle	Circular AISI304	D=76 mm	Length =180 mm	Thickness =1.5 mm				
	Outermost	Circular AISI304	D=89 mm	Length =160 mm	Thickness =1.5 mm				
8	**Innermost**	Square AL6063	D=80 mm	Length=200 mm	Thickness =2 mm	3.77	14384	123	34-66-154
	Middle	Square AL6063	W=60 mm	Length=180 mm	Thickness =2 mm				
	Outermost	Square AL6063	W=40 mm	Length=160 mm	Thickness =2 mm				
9	**Innermost**	Square AL6063	W=80 mm	Length=200 mm	Thickness =2 mm	3.28	10991	95	33-84-145
	Middle	Square AL6063	W=60 mm	Length=180 mm	Thickness =2 mm				
	Outermost	Square AL6063	W=40 mm	Length=160 mm	Thickness =2 mm				
	Innermost	Square AL6063	W=80 mm	Length=200 mm	Thickness =2 mm				

10	**Middle**	Square AL6063	W=60 mm	Length=180 mm	Thickness =2 mm	2.69	7369	68	34-74-157
	Outermost	Square AL6063	W=40 mm	Length=160 mm	Thickness =2 mm				
11	**Innermost**	Square AL6063	W=40 mm	Length=200 mm	Thickness =2 mm	3.77	9167	90	36-146-165
	Middle	Daire AISI304	D=76 mm	Length=180 mm	Thickness =1.5 mm				
	Outermost	Square AL6063	W=100 mm	Length=160 mm	Thickness =2 mm				
12	**Innermost**	Square AL6063	W=30 mm	Length=200 mm	Thickness =1 mm	3.77	14077	65	33-100-194
	Middle	Daire AISI304	D=51 mm	Length=180 mm	Thickness =1,5 mm				
	Outermost	Square AL6063	W=80 mm	Length=160 mm	Thickness =2 mm				
13	**Innermost**	Square AL6063	W=30 mm	Length=200 mm	Thickness =1 mm	3.28	10974	84	34-101-178
	Middle	Daire AISI304	D=51 mm	Length=180 mm	Thickness =1,5 mm				
	Outermost	Square AL6063	W=80 mm	Length=160 mm	Thickness =2 mm				
14	**Innermost**	Square AL6063	W=30 mm	Length=200 mm	Thickness =1 mm	2.69	7610	104	33-91-186
	Middle	Daire AISI304	D=51 mm	Length=180 mm	Thickness =1,5 mm				
	Dış Tüp	Square AL6063	W=80 mm	Length=160 mm	Thickness =2 mm				
15	**Innermost**	Square AL6063	W=40 mm	Length=200 mm	Thickness =2 mm	3.77	8306	73	42-211-182
	Middle	Square AISI304	W=60 mm	Length=180 mm	Thickness =2 mm				
	Outermost	Square AL6063	W=80 mm	Length=160 mm	Thickness =2 mm				
16	**Innermost**	Square AL6063	W=40 mm	Length=200 mm	Thickness =2 mm	3.28	6493	64	42-208-214
	Middle	Square AISI304	W=60 mm	Length=180 mm	Thickness =2 mm				
	Outermost	Square AL6063	W=80 mm	Length=160 mm	Thickness =2 mm				
17	**Innermost**	Square AL6063	W=40 mm	Length=200 mm	Thickness =2 mm	2.69	4496	48	33-207-149
	Middle	Square AISI304	W=60 mm	Length=180 mm	Thickness =2 mm				
	Outermost	Square AL6063	W=80 mm	Length=160 mm	Et kalınlığı=2 mm				

18	**Innermost**	Square AISI304	W=30 mm	Length=200 mm	Thickness=1,2 mm	3.77	6974	83	70-105-331
	Middle	Circular AISI304	D=51 mm	Length=180 mm	Thickness=1,5 mm				
	Outermost	Square AISI304	W=80 mm	Length=160 mm	Thickness=2 mm				
19	**Innermost**	Square AISI304	En=30 mm	Length=200 mm	Thickness=1,2 mm	3.28	5324	69	75-103-259
	Middle	Circular AISI304	D=51 mm	Length=180 mm	Thickness=1,5 mm				
	Outermost	Square AISI304	En=80 mm	Length=160 mm	Thickness=2 mm				
20	**Innermost**	Square AISI304	En=30 mm	Length=200 mm	Thickness=1,2 mm	2.69	3676	51	71-117-269
	Middle	Circular AISI304	D=51 mm	Length=180 mm	Thickness=1,5 mm				
	Outermost	Square AISI304	En=80 mm	Length=160 mm	Thickness=2 mm				
21	**Innermost**	Square AL6063	D=50 mm	Length=200 mm	Thickness=2 mm	3.77	10128	76	46-165-177
	Middle	Circular AISI304	D=76 mm	Length=180 mm	Thickness=1,5 mm				
	Outermost	Square AL6063	D=90 mm	Length=160 mm	Thickness=2 mm				
22	**Innermost**	Square AL6063	D=50 mm	Length=200 mm	Thickness=2 mm	3.28	7844	62	38-163-171
	Middle	Circular AISI304	D=76 mm	Length=180 mm	Thickness=1,5 mm				
	Outermost	Square AL6063	D=90 mm	Length=160 mm	Thickness=2 mm				
23	**Innermost**	Square AL6063	D=50 mm	Length=200 mm	Thickness=2 mm	2.69	5393	50	47-155-155
	Middle	Circular AISI304	D=76 mm	Length=180 mm	Thickness=1,5 mm				
	Outermost	Square AL6063	D=90 mm	Length=160 mm	Thickness=2 mm				

4 OPTIMUM DESIGN

4.1 Numerical Results for Optimum Design

As a result of numerical analyses, supremacy of circular cross section against square cross section was shown. Tubes having circular cross section were found easily in the market so they were continued to use in the analysis. In the literature, it was seen that plastic stress-strain curves of AL6063 T1, T4, T5 which were generally used can differ and these can cause the differences at force-time and force-deflection curves.

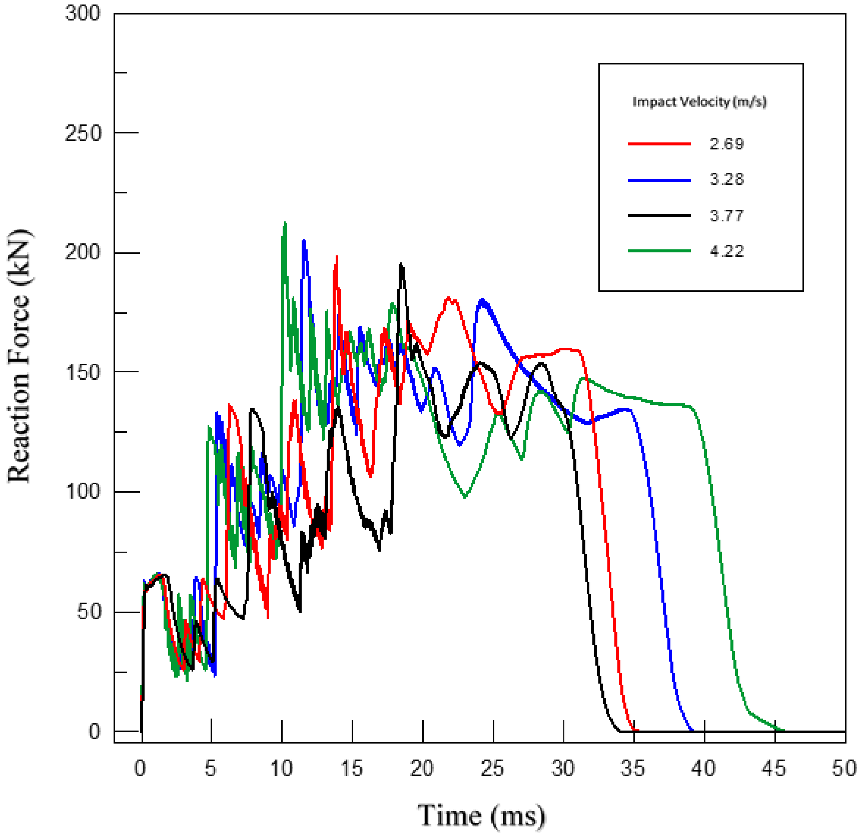

Figure 4.1 : Abaqus program force-time curve for the optimum design (circular cross section) in 4 different velocities

In this context, tensile test and static crush tests were used to find plastic stress-strain curves. Later, peak force curves were found in LS-DYNA via the plastic stress-strain curves. In the the Figure 4.1 and 4.2, force response of 4 different velocity impact cases in LS-DYNA and Abaqus were showed.

As in the experiments, first peak force values are not seen different between them but there is disintegration for second and third peak forces.

Abaqus and LS-DYNA comparison can be made via Figure 4.1, 4.2 and 4.3. It is obvious that peak forces of different programs gave similar results to compare with the experiments. Surely, it should not be expected to reach same force curve results from different programs. In the modelling phase, it was seen that we can reach different result according if force was read from the top nodes of tubes or was read from the bottom nodes or rigid base plate. So, for the constant mesh size and element types mesh sensitivity comparison is given.

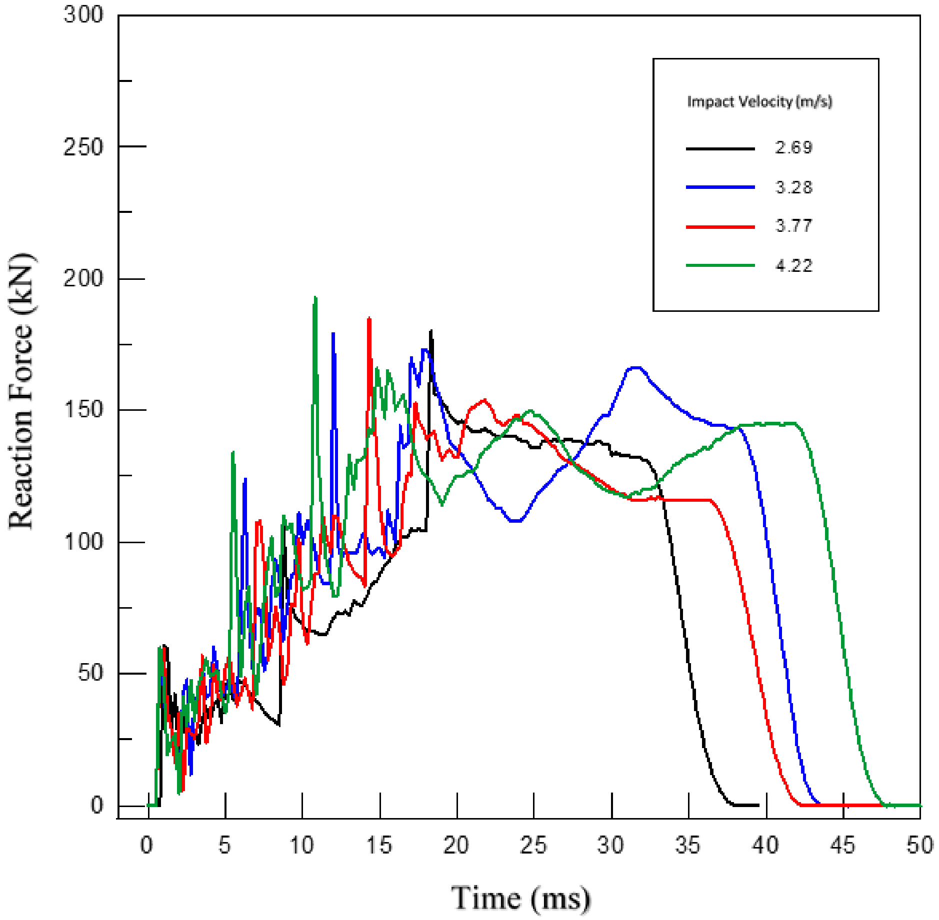

Figure 4.2 : LS-DYNA program force-time curve for the optimum design (circular cross section) in 4 different velocities.

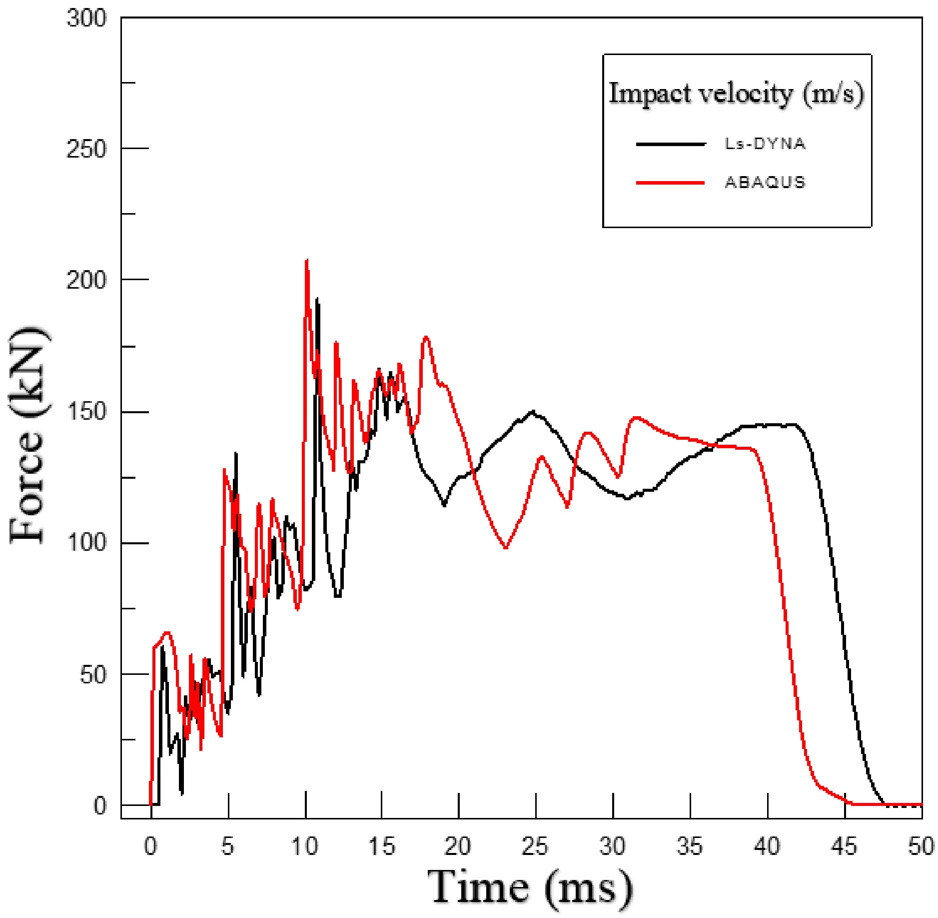

Figure 4.3 : LS-DYNA and Abaqus force-time curve comparison for the optimum design (circular cross section) in 4. 22 m/s.

The Figure 4.4, 4.5, 4.6 and 4.7 were given to comment about folding mechanism of tubes in diffrent impact velocity conditions. AL 6063 tubes were loaded by 1.130 tonnes impactor using diffrent impact velocities and it was seen that different folding mechanisms were shown. Experimental processes showed us that material and production imperfections effect folding mechanisms. Even top nodes were constrained in numerical analyses, folding shapes can be different from the experimantal ones. Contact algorithms of Abaqus solver can be main reason of that. Contact forces are important becasue of its nature to be open to get the reaction force curve upper level.

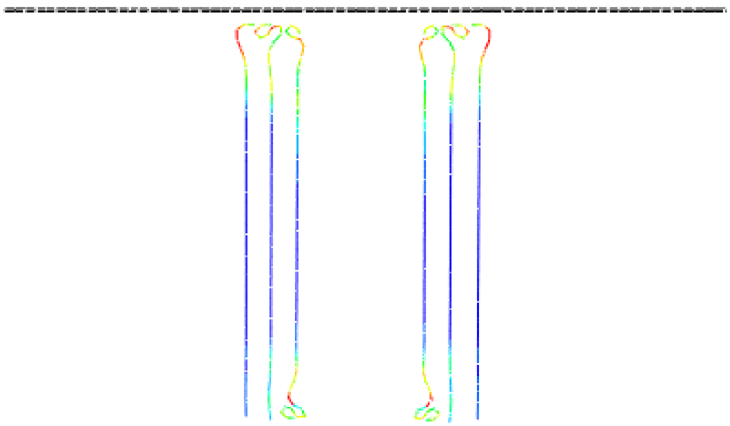

Figure 4.4 : 2D crushed tube representation of 4 kJ impact load.

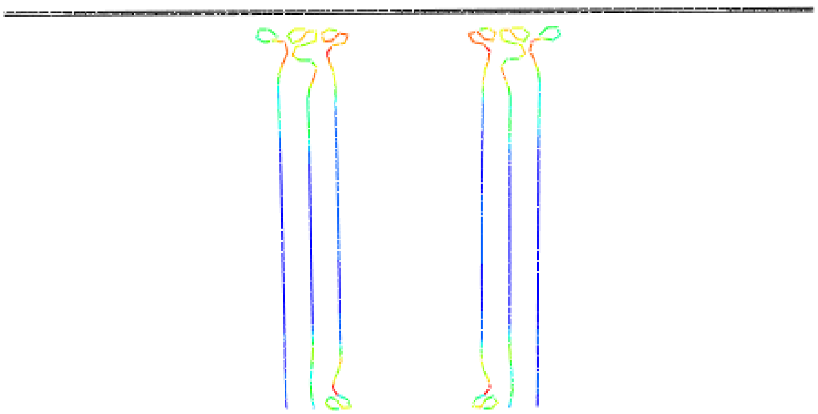

Figure 4.5 : 2D crushed tube representation of 6 kJ impact load.

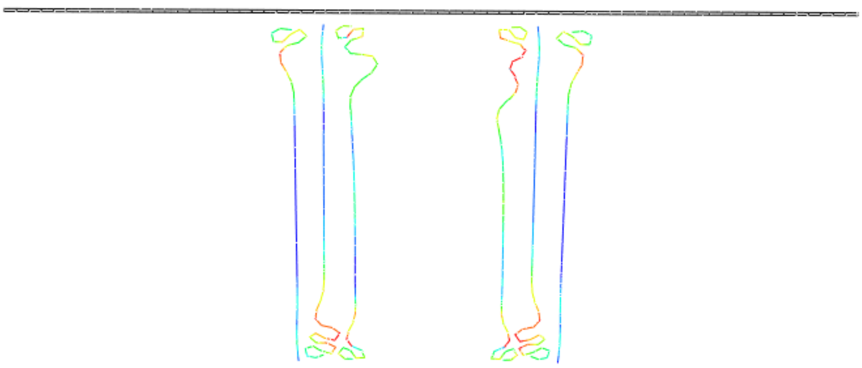

Figure 4.6 : 2D crushed tube representation of 8 kJ impact load.

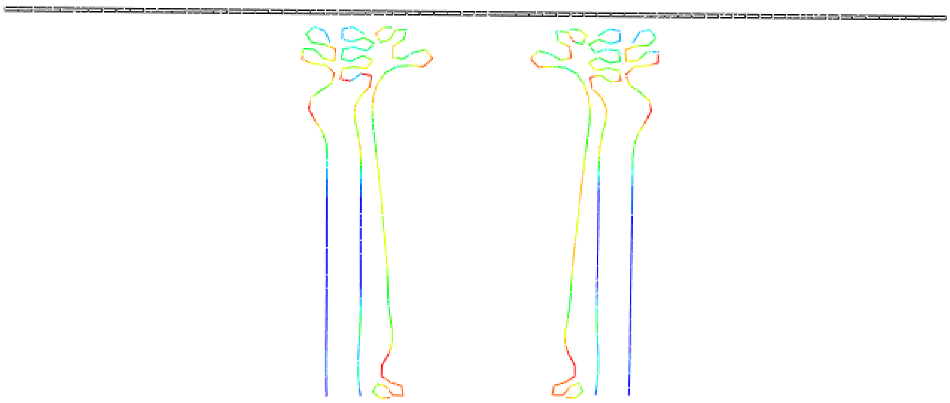

Figure 4.7 : 2D crushed tube representation of 10 kJ impact load.

4.2 Quasi-static Tests for Optimum Design

For the optimum design, 600 kN static crushing test machine was used to crush system with 2 mm/min.velocity. Crushing behaviour of the nested tubes were plotted in the Figure 4.8 and 4.9. Four different crushing tests were conducted with the 2 $\frac{mm}{min}$ crushing velocity. As it is seen in the Figure 4.8, folding mechanisms had developed differently at each other. The sample 1 and 3 showed proper foldings while the sample 2 and 4 showed different foldings. For further details, at different time points, images were recorded to see foldings at the sample 1. Imperfections are important indicator effecting folding mechanisms, and it is seen from the Figure 4.8 that different folding shapes could mean related with the imperfections.

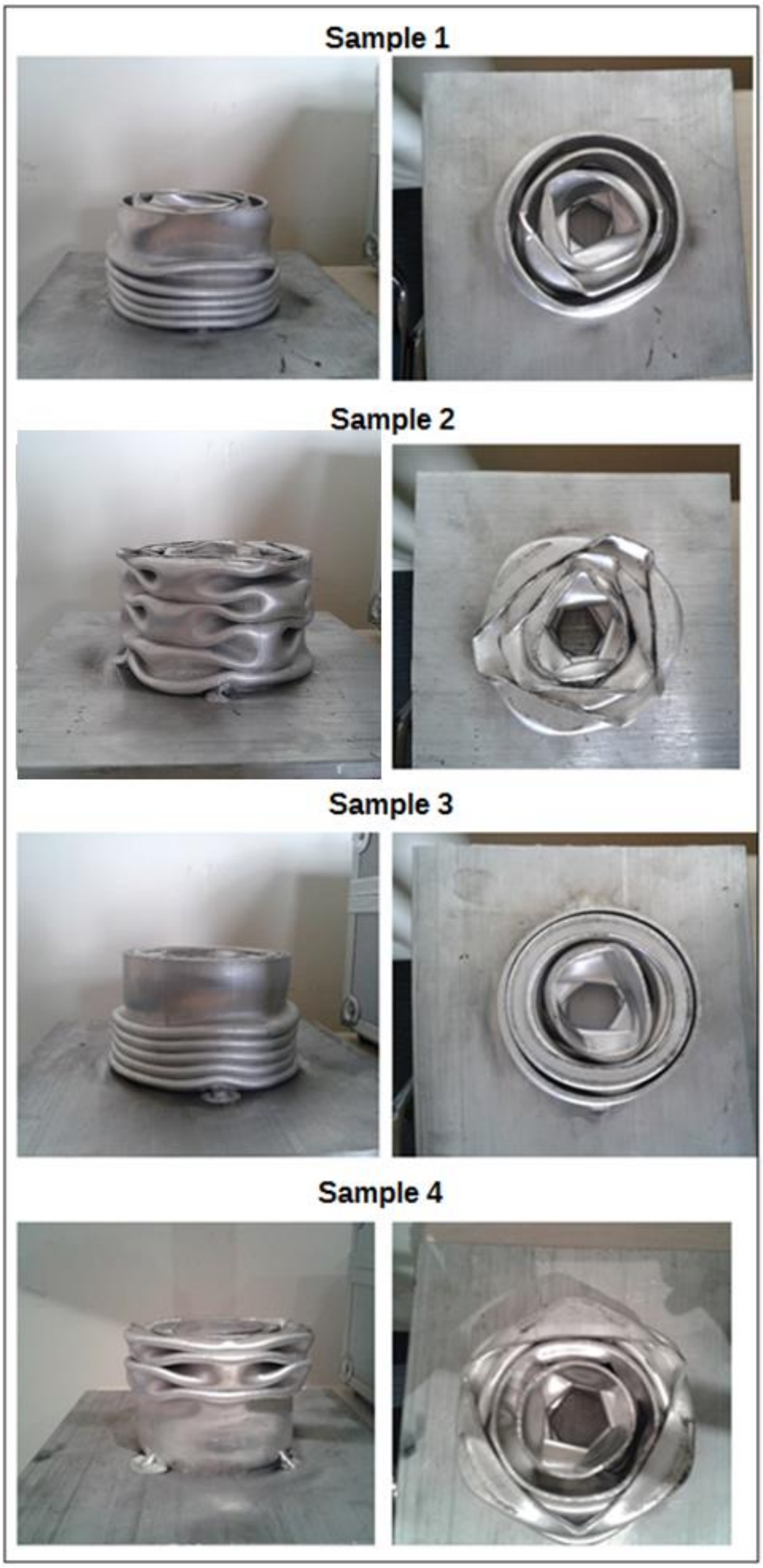

Figure 4.8 : Samples from front and side view after quasi-static tests.

Figure 4.9 : Deformation history of quasi-static tests.

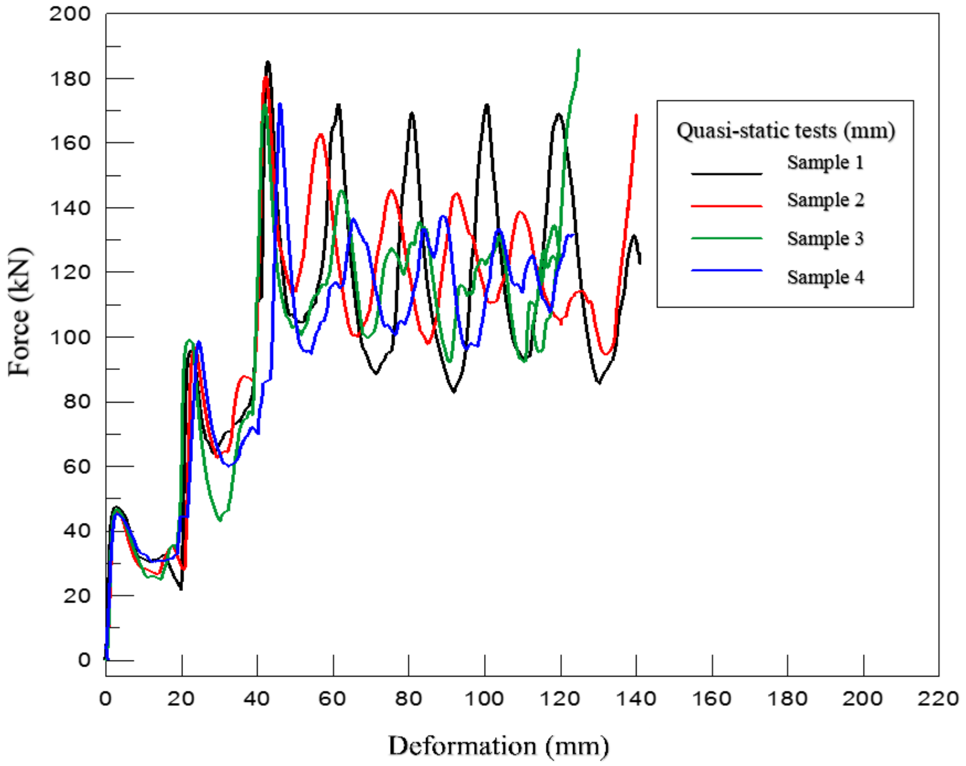

Figure 4.10 : Force –time curves of quasi static tests.

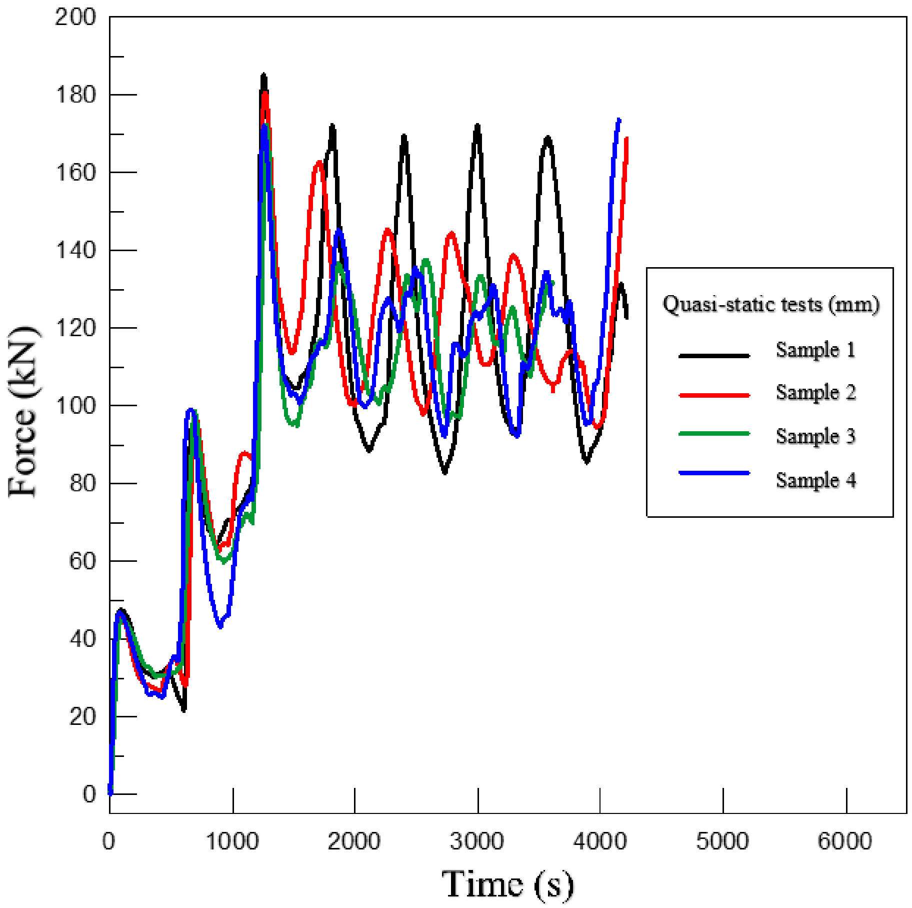

Figure 4.11 : Force –deflection curves of quasi static tests.

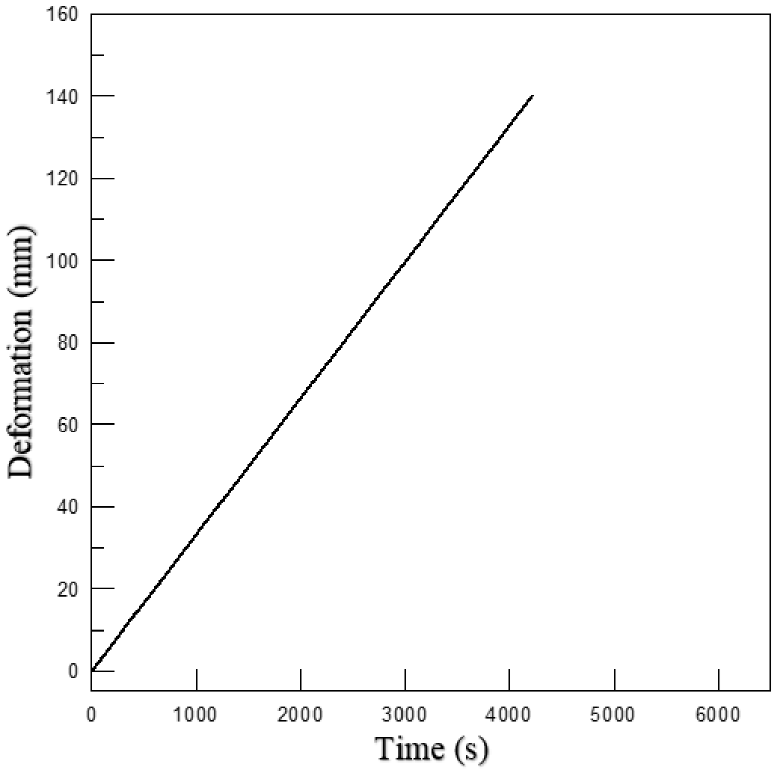

Figure 4.12 : Deformation–time curves of quasi static tests.

4.3 Dynamic Tests for Optimum Design

The dynamic tests for the optimum design were conducted at 4.22 m/s impact velocity. The images of before and after the experiments were given in the Figure 4.13. Deflection of first sample is 99 mm, second one is 100 mm. Force-time and energy-time curves were given in the Figure 4.14 and 4.15. Peak forces of the first sample are 68, 95, 160 kN; Second sample's are 59, 97, 157 kN.

Figure 4.13 : Optimum Design Samples Representations before and after the experiments.

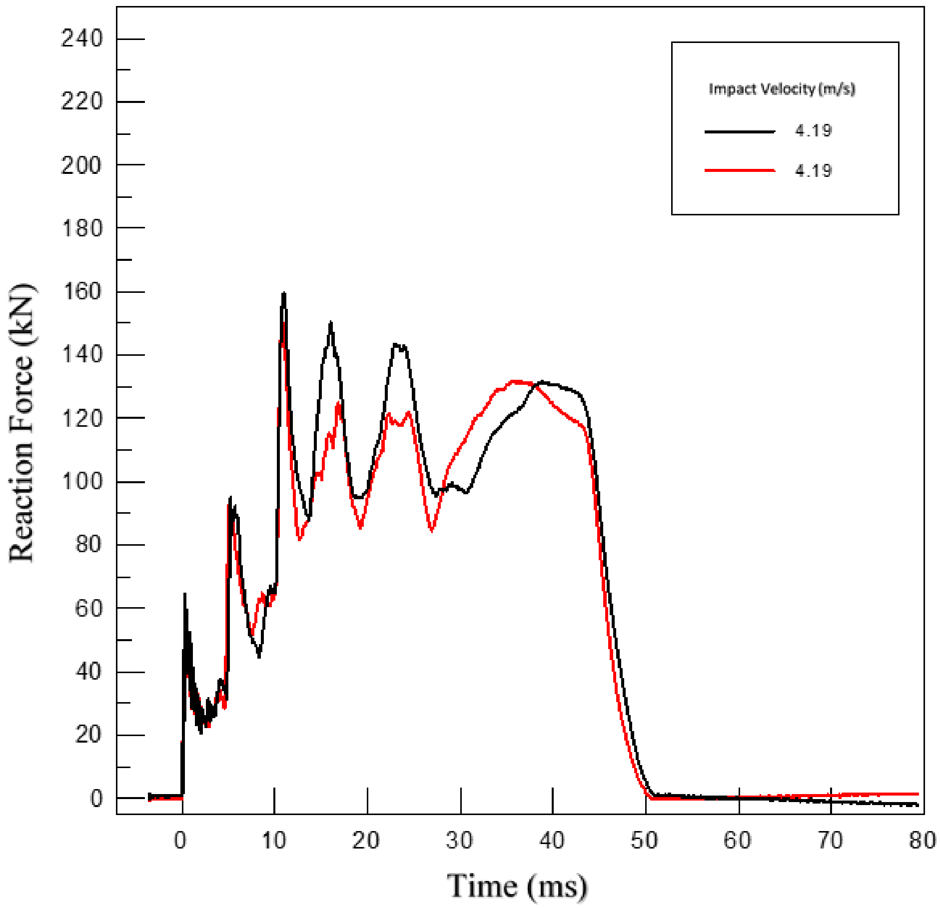

Figure 4.14 : Force-time curves of the optimum design consideration

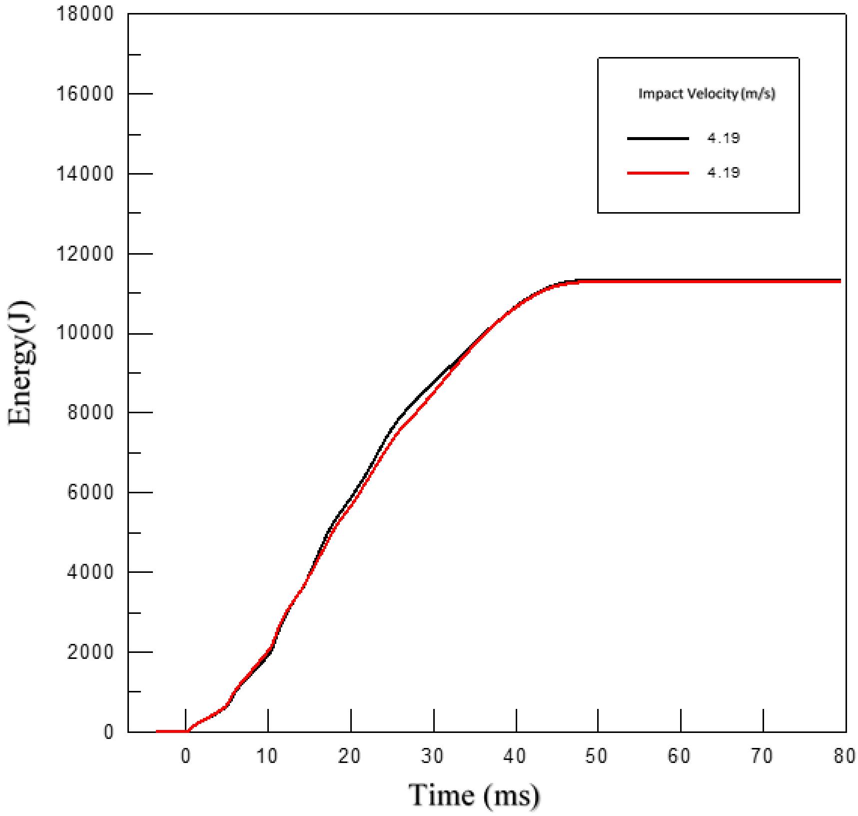

Figure 4.15 : Energy-time curves of the optimum design consideration

5 CONCLUSIONS AND RECOMMENDATIONS

In the thesis, explicit solvers were used to simulate the dynamic behaviour of axially impacted thin walled nested metal tubes . The aim was to show numerical modelling's efficiency against the experimental cases. For this purpose, Abaqus's and LS-DYNA's explicit solvers were used. To correlate the models, mostly known plastic stress-strain curves of materials were used. By using the material data, effect of cross section shape and sort of material were observed and commented. After that, tensile test results were used to run new analysis and the results were compared with the experiments. Via this process, capability of the non-linear finite element solvers were measured. As a first step, AL 6063 and Advanced High Strength Steel DP 600 were modeled and investigated to find efficiency of them. When the experimental procedure was started, market availability of steel was investigated and sort of steel was changed to the AISI 304 mild steel.

Two types of the tubes having square and circular cross sections, respectively and made of AL 6063 and AISI 304 Steel were constructed. These tubes systems were tested in dynamical and quasi-static conditions. Deflection, absorbed energy and peak forces of samples were investigated using outputs of experimantal studies. As a result of comparisons, tubes having square cross sections had delaceration and rupture differently from circular cross sections. The one of the predicted reason is that these regions have high stress concentration. Another reason is that interaction between the tubes causes disrupting folding of exterior tube progressively. This issue decreased the efficiency of the square tubes while there was no step down for circular tubes. Especially, nested AL 6063 tubes had folding in akerdeon which is a proper folding mechanism.

The peak force comparison between AL 6063 and St AISI 304 tubes showed that steel tubes had higher peak force levels. For instance, steel tube placed in the middle caused higher peak force difference between first and second peak levels but decreased peak levels second and third peak force levels.

It was observed that peak forces increased linearly for tubes having same material. The results from the experimental studies showed that mixed design considiration can provide better efficiency but as a result of wieght saving consideration circular aluminium tube system is mostly preffered.

In the metal market, there was no dual phase steel profile products so mild steel product were used but it has been seen that their effciency was lower than aluminium tubes. Dynamic tests were conducted at 2.69, 3.28, 3.77 and 4.22 m/s velocities. For the 2.69 m/s case, comparison for specific energy absorption amd crush force efficiency between samples showed that the system that its inner and outer tubes having square cross section and made of aluminium, middle tube having circular cross section is considered ideal one.

The nested AL 6063 tube systems having circular cross section were considered ideal one with the reason of that they had less system weight and the highest CFE. When the crash tests at 3.28, 3.77 and 4.22 m/s velocities were compared with each other, crush force efficiency and specific energy absorption were observed for all of them.

Dynamic and static crush tests' force behaviours were compared and it was inferred that because of the strain rate insensitivity of alumunium, force levels were in same level. The new design methodology has been applied succesfully. Moreover, it was calculated that steel and aluminium tube combinations can provide efficiency increase by comparing different parameters.

REFERENCES

Abaqus. (n.d.-a). 2.1.16 Progressive failure analysis of thin-wall aluminum extrusion under quasi-static and dynamic loads.

Abaqus. (n.d.-b). 29.4.28 Applying SAE filtering to an X–Y data object Use one of the SAE filtering functions to apply an SAE filtering operation to a previously saved. Retrieved December 20, 2015, from http://www.egr.msu.edu/software/abaqus/Documentation/docs/v6.7/books/usi/default.htm?startat=pt05ch29s03hlb26.html

Bathe, K.-J. (2007). Conserving energy and momentum in nonlinear dynamics: A simple implicit time integration scheme. *Computers & Structures*, *85*(7-8), 437–445. http://doi.org/10.1016/j.compstruc.2006.09.004

Chen, W., & Wierzbicki, T. (2001). Relative merits of single-cell, multi-cell and foam-filled thin-walled structures in energy absorption. *Thin-Walled Structures*, *39*(4), 287–306. http://doi.org/10.1016/S0263-8231(01)00006-4

Chiandussi, G., & Avalle, M. (2002). Maximisation of the crushing performance of a tubular device by shape optimisation. *Computers & Structures*, *80*(27-30), 2425–2432. http://doi.org/10.1016/S0045-7949(02)00247-X

Eren, Z., Usta, F., Kazancı, Z., Türkmen, H. S., & Mecitoğlu, Z. (2015). Axial Crash and Crush Response of Novel Nested Tube Designs. In *12th International Conference on the Mechanical Behaviour of Materials (ICM12), Karlsruhe, Germany*. http://doi.org/10.13140/RG.2.1.2267.3124

Fan, Z., Lu, G., & Liu, K. (2013). Quasi-static axial compression of thin-walled tubes with different cross-sectional shapes. *Engineering Structures*, *55*, 80–89. http://doi.org/10.1016/j.engstruct.2011.09.020

Ghamarian, A., Zarei, H. R., & Abadi, M. T. (2011). Experimental and numerical crashworthiness investigation of empty and foam-filled end-capped conical tubes. *Thin-Walled Structures*, *49*(10), 1312–1319. http://doi.org/10.1016/j.tws.2011.03.005

İnce, F., Türkmen, H. S., Mecitoğlu, Z., Uludağ, N., Durgun, İ., Altınok, E., & Örenel, H. (2011). A numerical and experimental study on the impact behavior of box structures. *Procedia Engineering*, *10*, 1736–1741. http://doi.org/10.1016/j.proeng.2011.04.289

Kazancı, Z., & Bathe, K.-J. (2012). Crushing and crashing of tubes with implicit time integration. *International Journal of Impact Engineering*, *42*, 80–88. http://doi.org/10.1016/j.ijimpeng.2011.10.003

Key to Metals AG. (2015). TotalMateria Material Database. Retrieved November 22, 2015, from http://www.totalmateria.com/

Kim, H.-S. (2002). New extruded multi-cell aluminum profile for maximum crash energy absorption and weight efficiency. *Thin-Walled Structures*, *40*(4), 311–327. http://doi.org/10.1016/S0263-8231(01)00069-6

Li, F., Sun, G., Huang, X., Rong, J., & Li, Q. (2015). Multiobjective robust optimization for crashworthiness design of foam filled thin-walled structures with random and interval uncertainties. *Engineering Structures*, *88*, 111–124. http://doi.org/10.1016/j.engstruct.2015.01.023

Liu, M., Zhang, L., Wang, P., & Chang, Y. (2015). Buckling behaviors of section aluminum alloy columns under axial compression. *Engineering Structures*, *95*, 127–137. http://doi.org/10.1016/j.engstruct.2015.03.064

Livermore Software Technology Corporation. (2006). LS-DYNA Theory Manual. Retrieved December 21, 2015, from http://www.lstc.com/pdf/ls-dyna_theory_manual_2006.pdf

Livermore Software Technology Corporation. (2015). LS-DYNA User Manuals. Retrieved December 21, 2015, from http://www.dynasupport.com/manuals

LS DYNA. (2015). LS DYNA Consistent Units. Retrieved November 21, 2015, from http://www.dynasupport.com/howtos/general/consistent-units

Marzbanrad, J., Mehdikhanlo, M., & Saeedi Pour, A. (2009). An energy absorption comparison of square, circular, and elliptic steel and aluminum tubes under impact loading. *Turkish Journal of Engineering and Environmental Sciences*, *33*(3), 159–166. http://doi.org/10.3906/muh-0904-11

Nagel, G. M., & Thambiratnam, D. P. (2005). Computer simulation and energy absorption of tapered thin-walled rectangular tubes. *Thin-Walled Structures*, *43*(8), 1225–1242. http://doi.org/10.1016/j.tws.2005.03.008

Nagel, G. M., & Thambiratnam, D. P. (2006). Dynamic simulation and energy absorption of tapered thin-walled tubes under oblique impact loading. *International Journal of Impact Engineering*, *32*(10), 1595–1620. http://doi.org/10.1016/j.ijimpeng.2005.01.002

Olabi, A. G., Morris, E., & Hashmi, M. S. J. (2007). Metallic tube type energy absorbers: A synopsis. *Thin-Walled Structures*, *45*(7-8), 706–726. http://doi.org/10.1016/j.tws.2007.05.003

Qiao, J. S., Chen, J. H., & Che, H. Y. (2006). Crashworthiness assessment of square aluminum extrusions considering the damage evolution. *Thin-Walled Structures*, *44*(6), 692–700. http://doi.org/10.1016/j.tws.2006.04.015

Tang, Z., Liu, S., & Zhang, Z. (2012). Energy absorption properties of non-convex multi-corner thin-walled columns. *Thin-Walled Structures*, *51*, 112–120. http://doi.org/10.1016/j.tws.2011.10.005

Usta, F., Eren, Z., Türkmen, H. S., Kazancı, Z., & Mecitoğlu, Z. (2015). Numerical investigation of stepped concentric crash tubes subjected to axial impact: The effects of number of tubes. *7th International Conference on Recent Advances in Space Technologies (RAST) (2015)*. Istanbul. http://doi.org/10.1109/RAST.2015.7208312

World Health Organization. (n.d.). Road traffic deaths. Retrieved December 10, 2015, from http://www.who.int/gho/road_safety/mortality/en/

Yamashita, M., Gotoh, M., & Sawairi, Y. (2003). Axial crush of hollow cylindrical structures with various polygonal cross-sections. *Journal of Materials Processing Technology*, *140*(1-3), 59–64. http://doi.org/10.1016/S0924-0136(03)00821-5

Zhang, X., Cheng, G., Wang, B., & Zhang, H. (2008). Optimum design for energy absorption of bitubal hexagonal columns with honeycomb core. *International Journal of Crashworthiness*, *13*(1), 99–107. http://doi.org/10.1080/13588260701731732

Zhang, X., Cheng, G., & Zhang, H. (2006). Theoretical prediction and numerical simulation of multi-cell square thin-walled structures. *Thin-Walled Structures*, *44*(11), 1185–1191. http://doi.org/10.1016/j.tws.2006.09.002

Zhang, Y., Sun, G., Li, G., Luo, Z., & Li, Q. (2012). Optimization of foam-filled bitubal structures for crashworthiness criteria. *Materials & Design*, *38*, 99–109. http://doi.org/10.1016/j.matdes.2012.01.028

CURRICULUM VITAE

Name Surname: Zana EREN

Place and Date of Birth: Erzurum, 20.09.1989

E-Mail: erenza@itu.edu.tr

EDUCATION:

B.Sc.: Istanbul Technical University, Astronautical Enginering

PUBLICATIONS, PRESENTATIONS AND PATENTS ON THE THESIS:

- Z. Eren, M. Nikbay, and A. R. Aslan, "Çok Fonksiyonlu Yapıların Küçük Uydularda Uygulanması," in *5. Ulusal Havacılık ve Uzay Konferansı*, 2014, no. 013.
- Z. Eren, F. Usta, Z. Kazancı, H. S. Türkmen, and Z. Mecitoğlu, "Axial Crash and Crush Response of Novel Nested Tube Designs," in *12th International Conference on the Mechanical Behaviour of Materials (ICM12), Karlsruhe, Germany*, 2015.
- F. Usta, Z. Eren, H. S. Türkmen, Z. Kazancı, and Z. Mecitoğlu, "Numerical investigation of stepped concentric crash tubes subjected to axial impact: The effects of number of tubes," *7th International Conference on Recent Advances in Space Technologies (RAST) (2015)*. Istanbul, pp. 39–43, 2015.
- Z. Eren, Z. Saleem, E. Gündüz. 2012. "An Integrated Circuit System For Multifunctional Nano And Pico Satellites," TR Patent 2012/07917, Patent Issued.
- Z. Eren, Z. Kazancı, F. Usta, H.S. Türkmen, Z. Mecitoğlu. 2015. "Araçlarda Pasif Güvenlik Bileşeni Olarak İçiçe Çarpışma Kutusu," TR Patent 2015/10333 Patent Pending.